AD-A097 327 MISSISSIPPI UNIV UNIVERSITY DEPT OF ELECTRICAL ENGIN--ETC F/G 20/3
NUMERICAL PROCEDURES FOR HANDLING STEPPED-RADIUS WIRE JUNCTIONS--ETC(U)
MAR 79 A W GLISSON, D R WILTON N66001-77-C-0156

UNCLASSIFIED NL

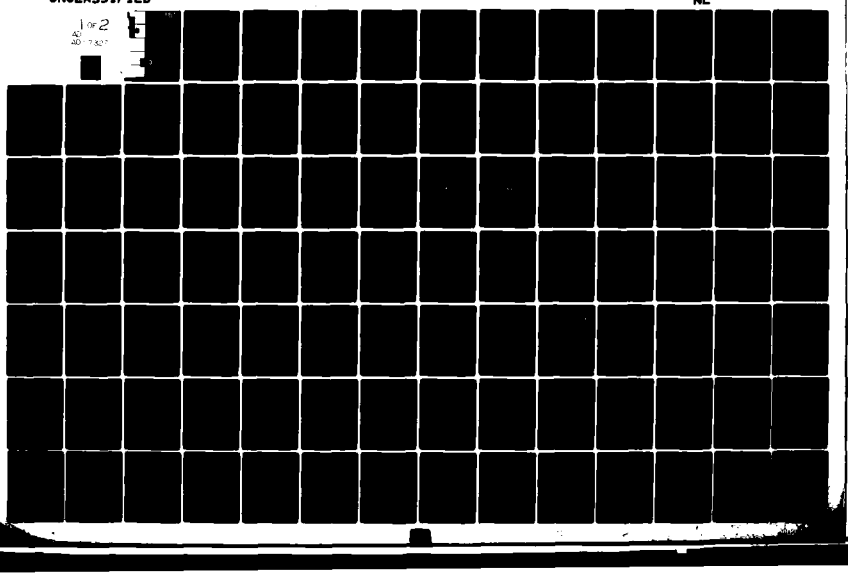

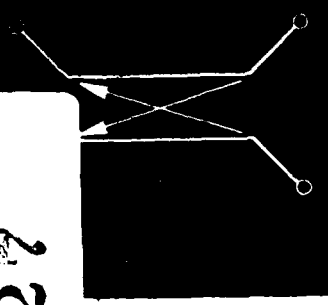

(1) LEVEL II

NUMERICAL PROCEDURES FOR HANDLING STEPPED-RADIUS WIRE JUNCTIONS

By

Allen W. Glisson
Donald R. Wilton

Department of Electrical Engineering
University of Mississippi
University, Mississippi 38677

For

Naval Ocean Systems Center
San Diego, California 92152

Contract No. N66001-77-C-0156

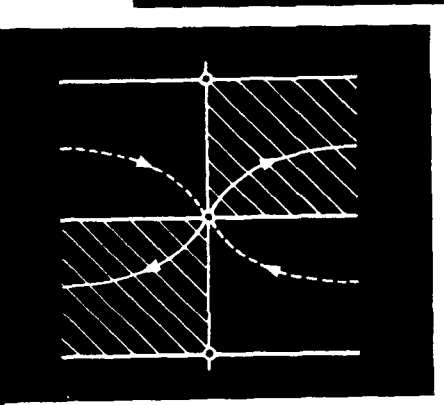

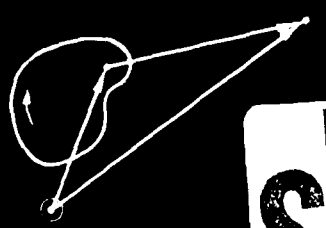

March, 1979

UNCLASSIFIED

SECURITY CLASSIFICATION OF THIS PAGE (When Data Entered)

REPORT DOCUMENTATION PAGE

READ INSTRUCTIONS BEFORE COMPLETING FORM

1. REPORT NUMBER

2. GOVT ACCESSION NO. AD-A097327

3. RECIPIENT'S CATALOG NUMBER

4. TITLE (and Subtitle)
NUMERICAL PROCEDURES FOR HANDLING STEPPED-RADIUS WIRE JUNCTIONS

5. TYPE OF REPORT & PERIOD COVERED
Final (6/1/77--11/30/78)

6. PERFORMING ORG. REPORT NUMBER

7. AUTHOR(s)
Allen W. Glisson
Donald R. Wilton

8. CONTRACT OR GRANT NUMBER(s)
N66001-77-C-0156

9. PERFORMING ORGANIZATION NAME AND ADDRESS
Department of Electrical Engineering
University of Mississippi
University, MS 38677

10. PROGRAM ELEMENT, PROJECT, TASK AREA & WORK UNIT NUMBERS
62762N
XF54585004

11. CONTROLLING OFFICE NAME AND ADDRESS
Naval Ocean Systems Center
San Diego, CA 92152

12. REPORT DATE
Mar[illegible]79

13. NUMBER OF PAGES
141

14. MONITORING AGENCY NAME & ADDRESS (if different from Controlling Office)
CNRRR, Atlanta Area Office
Georgia Institute of Technology
325 Hinman Research Building
Atlanta, GA 30332

15. SECURITY CLASS. (of this report)
UNCLASSIFIED

15a. DECLASSIFICATION/DOWNGRADING SCHEDULE

16. DISTRIBUTION STATEMENT (of this Report)
Approved for public release, distribution unlimited

17. DISTRIBUTION STATEMENT (of the abstract entered in Block 20, if different from Report)

18. SUPPLEMENTARY NOTES

19. KEY WORDS (Continue on reverse side if necessary and identify by block number)
Stepped-Radius Antenna
Wire Junctions
Numerical Techniques
Thin-Wire Theory
Induced Currents
Junction Conditions
Charge Jump Condition
Numerical Electromagnetics Code (NEC)

20. ABSTRACT (Continue on reverse side if necessary and identify by block number)
This report considers the numerical determination of the current and charge induced on stepped-radius wires by electromagnetic sources. A numerical technique is presented which provides an accurate solution for the current and charge on collinear stepped-radius wires. With this technique the detailed behavior of the current and charge in the vicinity of the step change in radius is also determined. A numerical technique employing the thin-wire theory approximations is also presented. This thin-wire approach

DD FORM 1 JAN 73 1473 EDITION OF 1 NOV 65 IS OBSOLETE

UNCLASSIFIED

SECURITY CLASSIFICATION OF THIS PAGE (When Data Entered)

requires no condition to be enforced on the charge at junctions of wires of dissimilar radius and yields accurate current and charge distributions away from the junction region. The concept of a "jump condition" for the charge on stepped-radius wires is discussed, and a numerical charge jump condition is computed and compared with the analytical expression of Wu and King. The use of a charge jump condition in other thin-wire theory approaches which require such a condition is discussed. In particular, the accuracy of the Numerical Electromagnetics Code (NEC), which explicitly enforces a charge jump condition at junctions of wires of dissimilar radii, is investigated. The effects on numerical current and charge distributions of the explicit enforcement of a charge jump condition and suggested limitations of the NEC code with regard to the modeling of stepped-radius wires are discussed.

NUMERICAL PROCEDURES FOR HANDLING STEPPED-RADIUS WIRE JUNCTIONS

by

Allen W. Glisson
Donald R. Wilton

Department of Electrical Engineering
University of Mississippi
University, Mississippi 38677

for

Naval Ocean Systems Center
San Diego, California 92152

Contract No. N66001-77-C-0156

March, 1979

ABSTRACT

This report considers the numerical determination of the current and charge induced on stepped-radius wires by electromagnetic sources. A numerical technique is presented which provides an accurate solution for the current and charge on collinear stepped-radius wires. With this technique the detailed behavior of the current and charge in the vicinity of the step change in radius is also determined. A numerical technique employing the thin-wire theory approximations is also presented. This thin-wire approach requires no condition to be enforced on the charge at junctions of wires of dissimilar radius and yields accurate current and charge distributions away from the junction region. The concept of a "jump condition" for the charge on stepped-radius wires is discussed, and a numerical charge jump condition is computed and compared with the analytical expression of Wu and King. The use of a charge jump condition in other thin-wire theory approaches which require such a condition is discussed. In particular, the accuracy of the Numerical Electromagnetics Code (NEC), which explicitly enforces a charge jump condition at junctions of wires of dissimilar radii, is investigated. The effects on numerical current and charge distributions of

the explicit enforcement of a charge jump condition and suggested limitations of the NEC code with regard to the modeling of stepped-radius wires are discussed.

TABLE OF CONTENTS

LIST OF FIGURES

SECTION I

INTRODUCTION

In recent years considerable effort has been expended developing general purpose computer codes capable of modeling complicated wire antenna structures via the method of moments. These codes have also been used, however, to model complex surfaces by means of grids of intersecting wires [1]. While the use of a wire grid to model surfaces is not entirely satisfactory, the simplicity and generality of the approach have led to its increasing usefulness as a tool for obtaining radar cross-sections and for assessing the performance of antennas attached to or located near such surfaces.

The power and flexibility of general purpose wire codes is largely due to the simplicity of wire problems, which in turn are simplified by the use of the so-called thin-wire approximations, one of which is that the current flowing on the surface of a wire is assumed to be circumferentially invariant on each wire. However, when this approximation is made, certain questions arise in the formulation as to the proper treatment of wire junctions, including junctions of wires of dissimilar radii. The usual procedures employed for treating thin wires require us to enforce certain conditions on the current and/or charge at the junction. From the

continuitv equation, one may show that Kirchoff's current law must be satisfied if it is assumed that no charge can accumulate at the junction. On the other hand, widely divergent opinions have existed as to what conditions the charge should satisfy at a wire junction. Indeed, several different charge junction conditions have been proposed [2-6] and considerable controversy has arisen as to which is correct [7-10]. In this report we attempt to provide somewhat more definitive answers concerning the need for and the validitv of charge jump conditions in thin wire codes.

In pursuit of the above goal, we are led to consider what might be called the canonical problem of two collinear wires with dissimilar radii which are joined to form a "stepped-radius" wire. Such a model might apply to a whip antenna mounted on a kingpost or other electrically thin cylinder which is collinear with the antenna but of a larger radius. To determine the current distribution on such a stepped-radius structure, it is necessary to include in the model the electrical influence of the step. However, it is neither practical nor desirable in most problems to actually determine the detailed nature of the current in the electrically small region around such a junction. Instead one would prefer to take an approach similar to that commonly used to treat trarsmission line discontinuities. In these problems, the transmission line voltages or currents are

first determined at some distance from the discontinuity and are then effectively extrapolated to the discontinuity. The discontinuity in the extrapolated voltage and/or current is then modeled by lumped circuit elements which enable one to ignore the detailed behavior of the fields near the line discontinuity (i.e., the fields which contain higher order non-transmission line modes), while preserving the electrical influence it has on remote portions of the structure. In this study, we have had a similar objective--either the development of new, or the verification of previously developed "lumped" boundary conditions on the extrapolated values of the current and/or charge at the radius discontinuity in the wire. The incorporation of such conditions into thin-wire codes should allow one to accurately compute the current and charge distribution away from the radius discontinuity without detailed knowledge of the charge and current in the junction region.

In order to determine the appropriate boundary conditions on the extrapolated current and charge at the radius discontinuity, we first accurately determine the current and charge distribution away from the junction region. To this end, we present in Section II a numerical technique which accurately determines the current and charge distribution on a collinear stepped-radius antenna, including a determination of the detailed behavior of the current and charge in the electrically small region around the junction. The

numerically determined current and charge distributions are then employed to obtain numerically extrapolated values of the current and charge at the junction, from which a charge "jump condition" may be computed and compared with the various derived conditions [2,3] - [6,7]. In Section II we also present numerical results based on a thin-wire technique which does not explicitly employ a charge jump condition but which nevertheless correctly predicts the current and charge distribution away from the junction region.

In Section III we compare results obtained via our accurate numerical model of the stepped-radius antenna with results obtained using the Numerical Electromagnetics Code (NEC) [11] which uses a very "smooth" basis set for the current representation and which enforces the charge jump condition of Wu and King [7] at discontinuities in wire radii. The accuracy of the code when structures involving junctions of wires of dissimilar radii are modeled is discussed. Conclusions and recommendations based on this study are presented in Section IV.

SECTION II

NUMERICAL INVESTIGATION OF THE STEPPED-RADIUS ANTENNA

In this section we examine with some care the problem of a stepped-radius antenna. A numerical technique is presented by which one may accurately determine the current and charge distributions, including the detailed behavior in the junction region, for the stepped-radius antenna. A body of revolution model is used to represent the antenna and the method of moments [12] is applied to solve for the unknown current distribution on the antenna. Since the method of moments is generally well-known, the numerical procedure is described only briefly, with particular emphasis on points which require special consideration for the present geometry. Numerical results for current and charge distributions are presented for several selected cases. Edge conditions for the current and charge in the vicinity of the radius change are also discussed and compared with the numerical results.

The stepped-radius antenna is also treated by a thin-wire theory approach in this section and results are compared with those obtained using the body of revolution model. Numerical results obtained by both approaches are used to calculate numerical "jump conditions" for the charge at the

radius discontinuity and these conditions are found to be in excellent agreement with the analytical jump condition of Wu and King [7]. Considerations in applying the charge jump condition and the appropriateness of the condition for junctions at bends and multiple wire junctions are also discussed.

2.1 Analysis of the Stepped-Radius Antenna as a Body of Revolution

Consider the stepped-radius antenna of Fig. 2.1 which is driven by a delta-gap voltage source. The dimensions of the antenna are specified by the three lengths L_1, L_2, and L_3, and by the two radii a_1 and a_2. The variable s in Fig. 2.1 denotes arc length along the surface of the antenna. At this point we stress the fact that for many of the cases considered in this report the scale of Fig. 2.1 is extremely deceptive. For example, if the radii shown in the figure were to remain unchanged and the total length of a typical antenna ($L_1 + L_2 + L_3$) were drawn to scale, the resultant antenna might well be several hundred meters long for thin antennas such that $a_1 \leq a_2 << L_1 + L_2 + L_3$. Thus, in order to represent the current and charge accurately in the junction region (i.e., to have several unknowns in the junction annulus region and within several radii of the junction) and still maintain a manageable number of unknowns for computer processing, the numerical technique must be capable of treating an enormous range of subdomain sizes. The first step in this investigation is therefore to briefly describe the

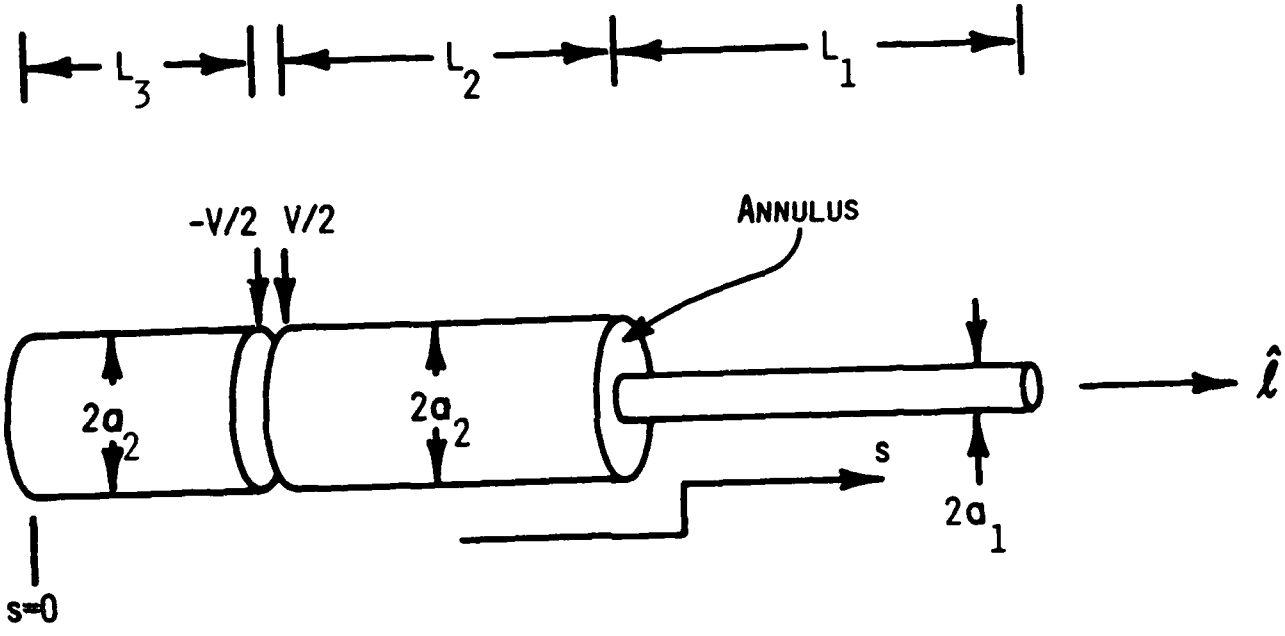

Figure 2.1. **Geometry of the stepped-radius antenna.**

numerical technique and verify that the computer code can indeed accommodate the required wide dynamic range of subdomain sizes.

In our analysis, the stepped-radius antenna is driven by a delta-gap voltage source which does not vary around the circumference of the wire. Hence, the surface current $\bar{J}(s)$ and the surface charge density $q_s(s)$ are functions of the arc length variable s only. Furthermore, these quantities may be converted to a "total" current $\bar{I}(s)$ and a linear charge density $q_\ell(s)$ simply by multiplication by $2\pi\rho(s)$, where $\rho(s)$ is the radius of the wire as a function of s. The current distribution on the stepped-radius antenna is calculated via a method of moments solution of the integro-differential equation

$$[-j\omega\bar{A}(\bar{r}) - \nabla\Phi(\bar{r})] \cdot \hat{s} = -\bar{E}^{inc}(\bar{r}) \cdot \hat{s}, \qquad \bar{r} \in S, \tag{2.1}$$

where

$$\bar{A}(\bar{r}) = \frac{\mu}{4\pi} \int_S \bar{J}(\bar{r}') \frac{e^{-jk|\bar{r} - \bar{r}'|}}{|\bar{r} - \bar{r}'|} \, dS', \tag{2.2a}$$

$$\Phi(\bar{r}) = \frac{1}{4\pi\varepsilon} \int_S q_s(\bar{r}') \frac{e^{-jk|\bar{r} - \bar{r}'|}}{|\bar{r} - \bar{r}'|} \, dS', \tag{2.2b}$$

and where $\bar{E}^{inc}(\bar{r})$ is the forcing function. The coordinate vectors $\bar{r}$ and $\bar{r}'$ locate the field and source points, respectively, with reference to an arbitrary coordinate origin.

For the numerical solution of (2.1), the unknown total current $\bar{I}(s)$ and the linear charge density $q_\ell(s)$ are expanded in a pulse basis set. The coefficients of the current expansion are treated as unknowns in the problem. The coefficients of the charge expansion are related to the coefficients of the current expansion via a finite difference approximation of the continuity equation

$$q_s = \frac{j}{\omega} \nabla \cdot \bar{J} \quad . \tag{2.3}$$

The current and charge expansions are represented schematically in Fig. 2.2. Notice that the current and charge pulses are shifted with respect to one another and that a half pulse of current (whose coefficient is zero) is used to represent the current at the end of the antenna where the current is zero.

When the expansions for the current and charge are substituted into (2.2) and the resulting equation (2.1) is "matched" at points in the center of the current subdomains, one obtains a set of simultaneous equations which may be solved to obtain values for the coefficients of the current expansion set. The coefficients of the expansion for the charge are then computed by a finite difference approximation of the continuity equation (2.3). More detailed explanations of this numerical procedure and its features are available in [13, 14].

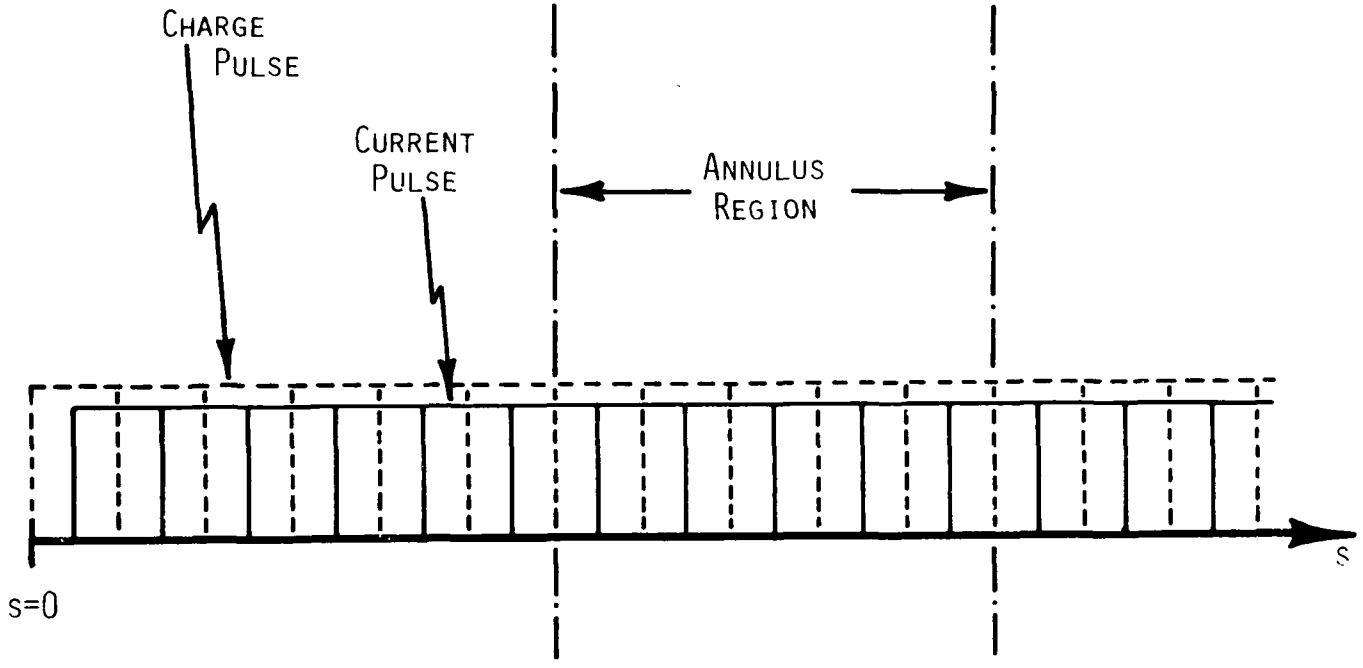

Figure 2.2. Schematic representation of the pulse basis sets for the current and charge on the stepped-radius antenna.

Implementation of the numerical techniques described in [13, 14] in a computer code is fairly straightforward. However, because the dimensions of the stepped-radius antenna require an extremely large dynamic range of subdomain sizes, some special precautions must be taken. First, one must insure that the integrations indicated in (2.2) are performed accurately, particularly when the field point is near the source region. Secondly, several significant digits may be lost in the specification of the subdomain locations alone due to the use of extremely small subdomain sizes such as occur near the junction region. Therefore if single precision arithmetic is used in the computations (as in this work), one must take special precautions to insure that no additional accuracy is lost in specifying the numerical integration quadrature points.

For this work, an existing general body of revolution computer code (DBR) [14] was modified to treat the stepped-radius antenna. This modified code, herein referred to as PECØ, was specialized to handle the large required dynamic range in subdomain sizes, to consider only a circumferentially independent current, and to calculate other special current-dependent quantities referred to later in this report. Verification that the code can indeed handle a very large range of subdomain sizes is obtained by considering a simple linear antenna without the step-radius discontinuity. Figs. 2.3 and 2.4 show the current and charge distributions,

respectively, for such an antenna with radius $ka_1 = ka_2 = 0.000125$ and lengths $k(L_1 + L_2) = 6.25$ and $kL_3 = 0.6$. An extremely small wire radius was chosen because the accuracy of the self term evaluation is more critical for smaller than for larger radii. For this case, 71 evenly spaced subdomains have been used to establish a well-converged base-line result. The results shown in the figures have been verified by comparison with other well-established wire codes. Figs. 2.5 and 2.6 show the current and charge distributions, respectively, obtained when unevenly spaced subdomains are used, such that the ratio of maximum to minimum subdomain size on the wire is 200,000 to 1. The subdomains are placed such that there are two small subdomains of width $k\Delta_{min} = 1.0 \times 10^{-6}$ located near $s/\lambda = 0.6$. Adjacent subdomains are progressively increased in width by a factor of 2.5 until the size reaches a maximum width of $k\Delta_{max} = 0.2$. Subdomains in the vicinity of the feed point are maintained at a constant width of $k\Delta = 0.1$. If one were to view the charge distribution shown in Fig. 2.6 on an extremely expanded scale, some very minor anomalous behavior would be noted, but this is not too surprising in view of the fact that the ratio indicated represents a dynamic range of 6 significant digits, while the computer on which the code runs maintains only 8 digit precision. One must also keep in mind that the charge is determined by a finite difference operation on the numerical current values.

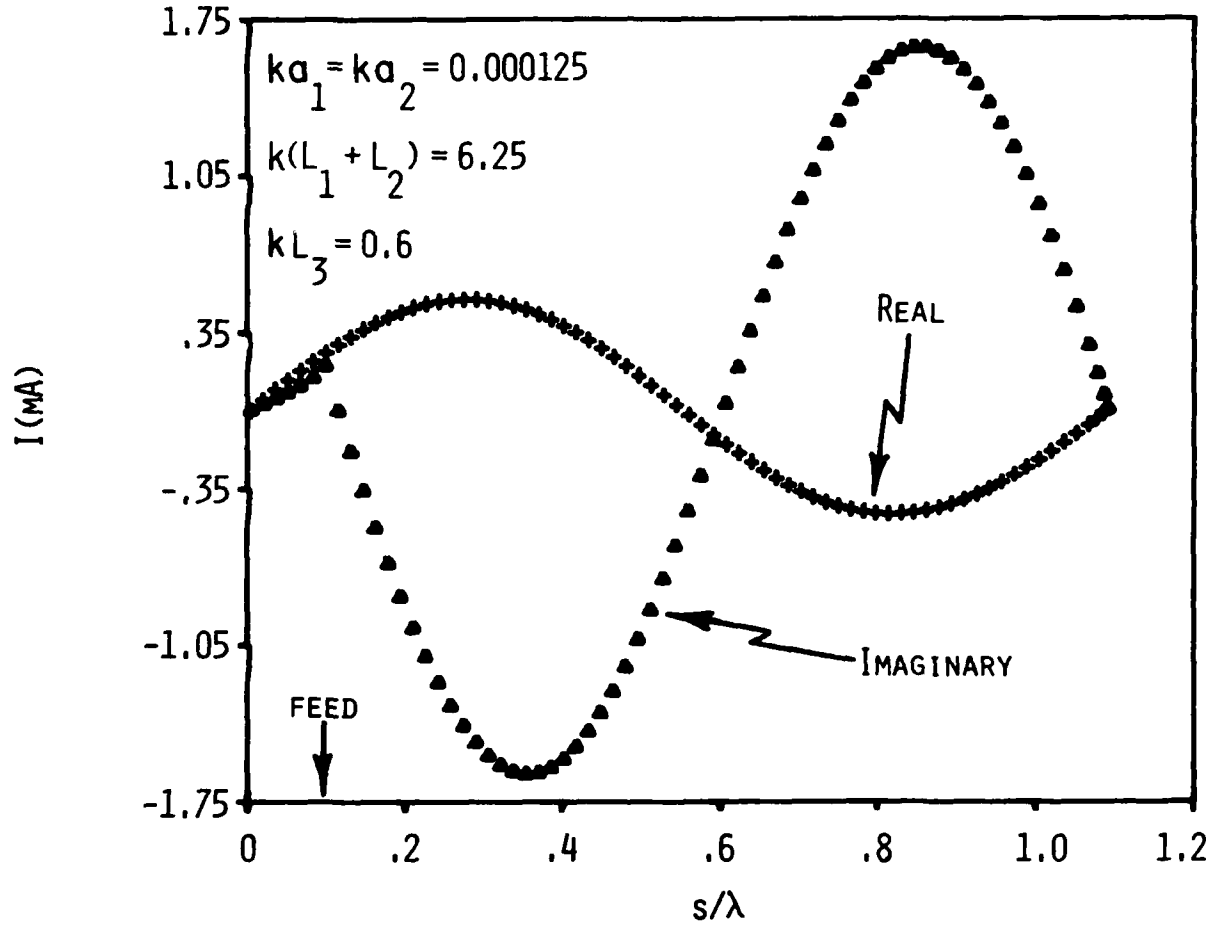

Figure 2.3. Current distribution on a thin linear antenna obtained with evenly spaced subdomains.

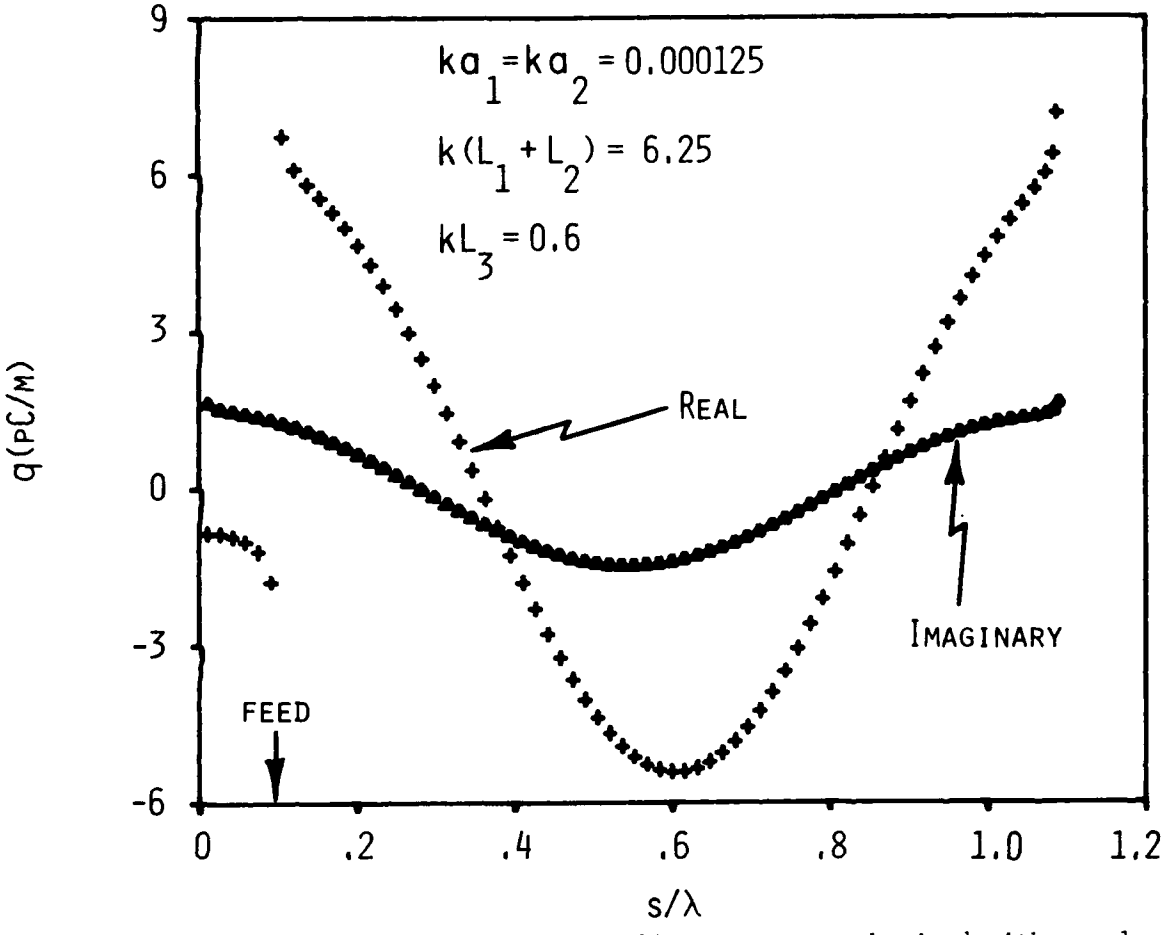

Figure 2.4. Charge distribution on a thin linear antenna obtained with evenly spaced subdomains.

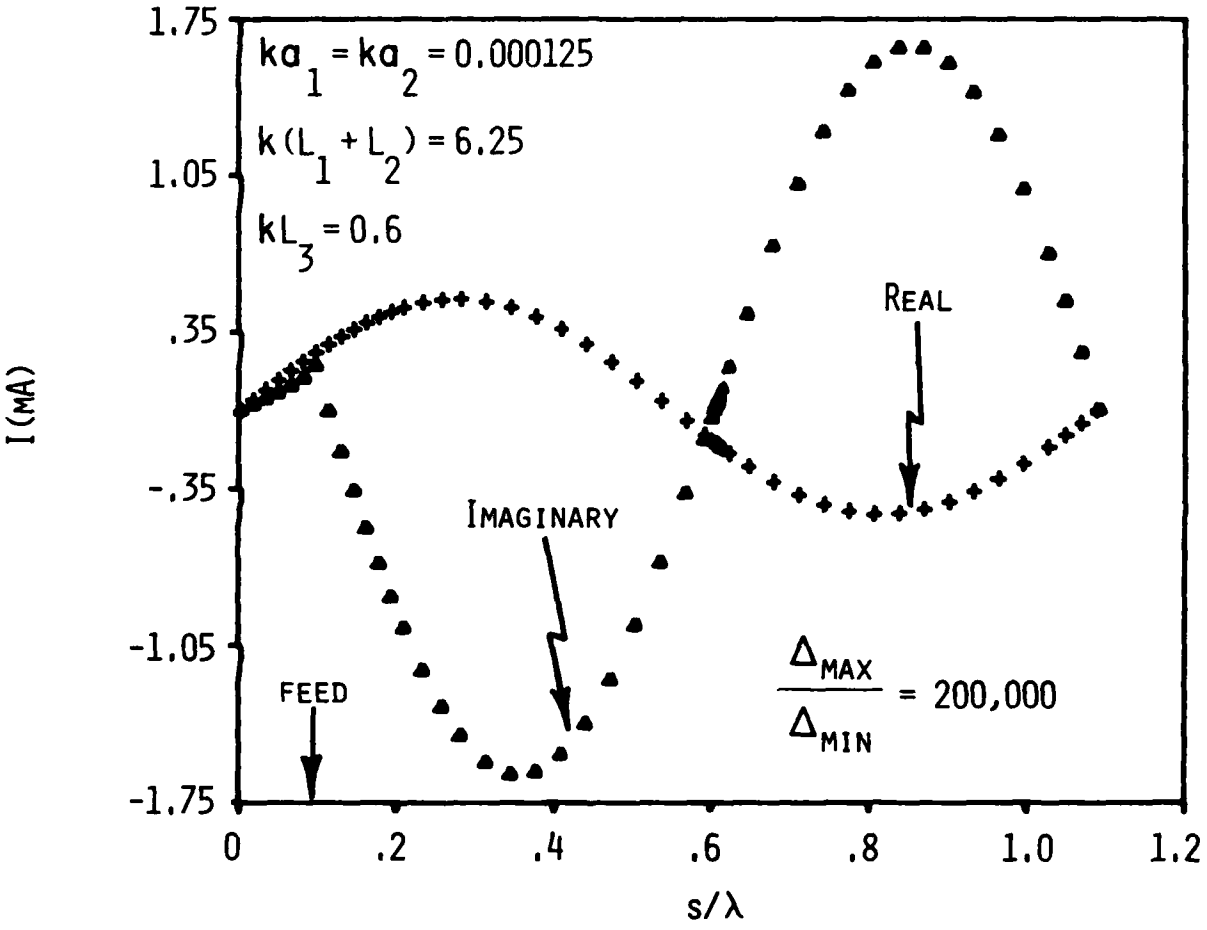

Figure 2.5. Current distribution on a thin linear antenna obtained with unevenly spaced subdomains.

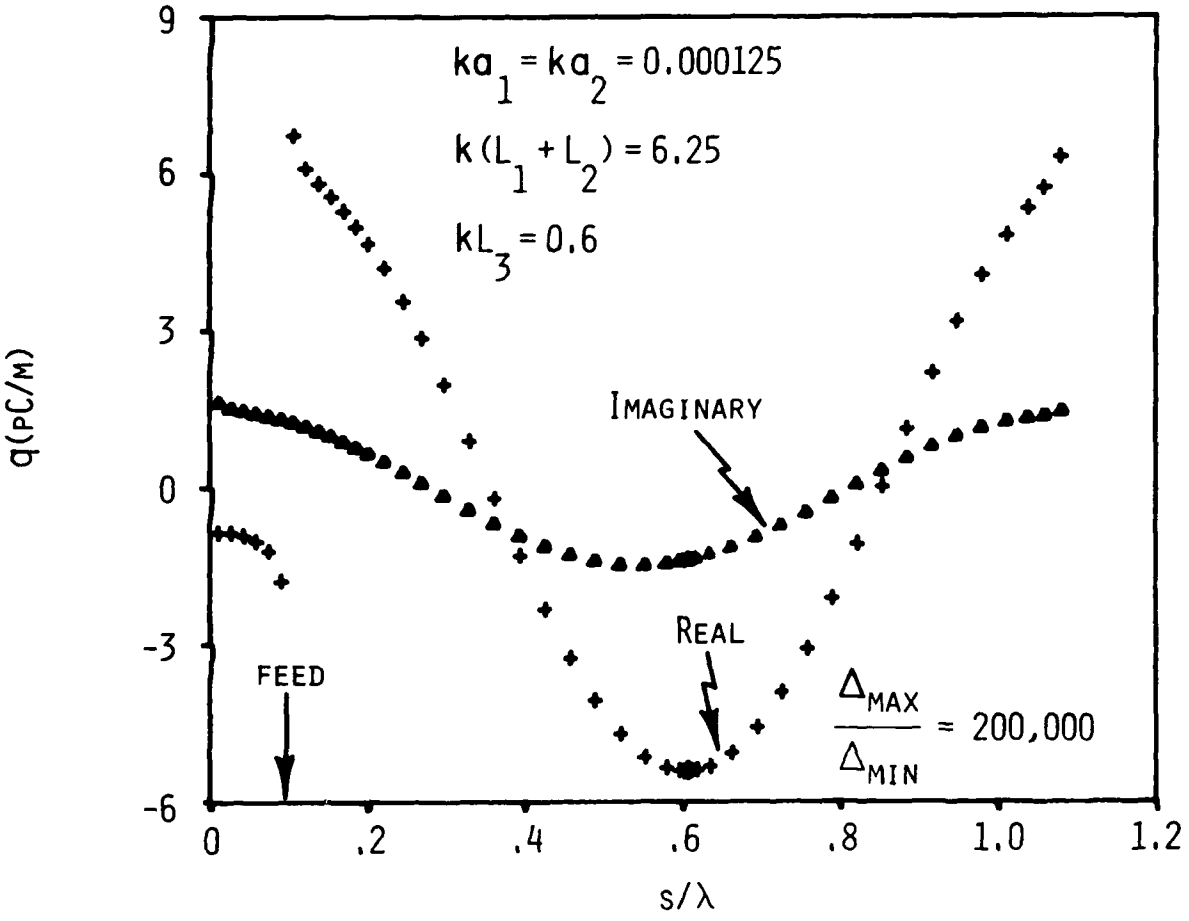

Figure 2.6. Charge distribution on a thin linear antenna obtained with unevenly spaced subdomains.

Other tests have been run to determine limitations of the code. For example, in one test case the wire was first divided into equally spaced segments and then ten small subdomains were added at a central point on the wire such that there was an abrupt change in subdomain size of ratio 1000 to 1. The current distribution obtained for this case was found to be virtually indistinguishable from that shown in Fig. 2.3. On the other hand, the charge distribution exhibited anomalous behavior, but only over the range of the ten small subdomains. Elsewhere, the charge distribution was essentially indistinguishable from that of Fig. 2.4. It is likely that such anomalous behavior is due to the fact that the current changes so slowly over the small region that the computation of the charge by finite difference procedures involves small differences and thus the resultant charge may be significantly in error. In general, however, the tests which have been performed lead to the conclusion that the computer code PECØ does provide accurate representations for both the current and charge when the subdomain size varies over an enormous dynamic range, as long as the changes in subdomain size are not too abrupt. In this study we have limited the ratio of the larger to the smaller subdomain widths of adjacent charge subdomains to be no greater than 2.5.

We now consider a sample result for a stepped-radius antenna. Figs. 2.7 and 2.8 illustrate the current and charge

distributions, respectively, on a stepped-radius antenna with the following dimensions: $ka_1 = 0.01$, $ka_2 = 0.02$, $kL_1 = 3.05$, $kL_2 = 3.2$, $kL_3 = 0.6$. In these figures the current and charge distributions are plotted as a function of the arc length variable s and thus show also the behavior of the current and charge in the annulus region of the junction. What appears to be a single dashed line in each of the figures is actually two dashed lines which delineate the extent of the annular junction region. The annulus is so small for this case, however, that the junction region is not visible in the plot. One observes that the overall distributions are much the same as illustrated in Figs. 2.3 and 2.4, except, of course, for the behavior of the charge in the vicinity of the junction. One notes upon inspection of Fig. 2.8, however, that the overall "level" of the charge distribution on each side of the junction is different if one ignores the junction region itself and merely extrapolates the sinusoidal-looking charge into the junction region. It thus becomes clear how the concept of a charge "jump condition" arises. One might, however, raise the question as to whether the computed behavior of the current and charge in the vicinity of the junction is correct, or if it represents some numerical anomaly which has affected the entire charge distribution. We note, however, that the approximate variation of the charge near the junction can be determined from edge conditions [15]. Accordingly, we propose the following

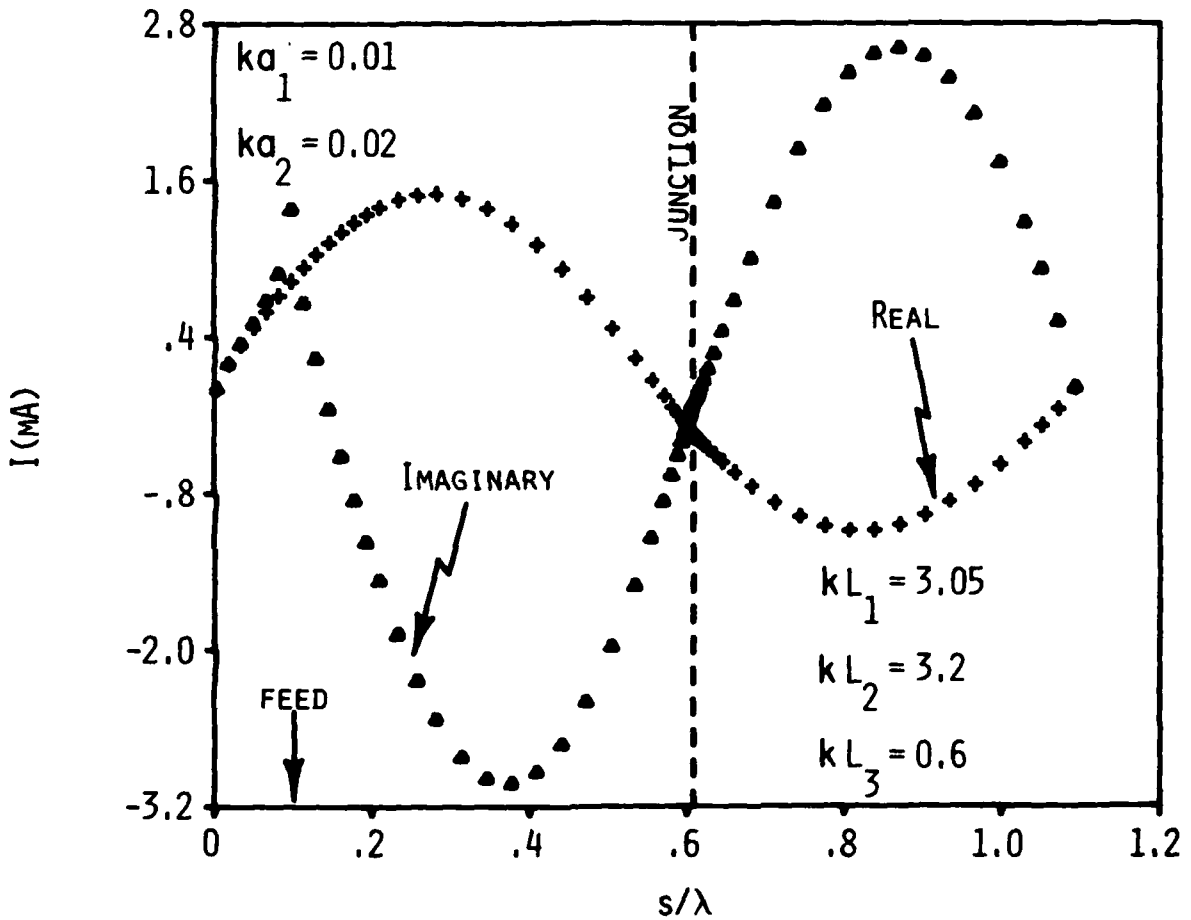

Figure 2.7. Current distribution on a stepped-radius antenna obtained by treating the wire as a body of revolution.

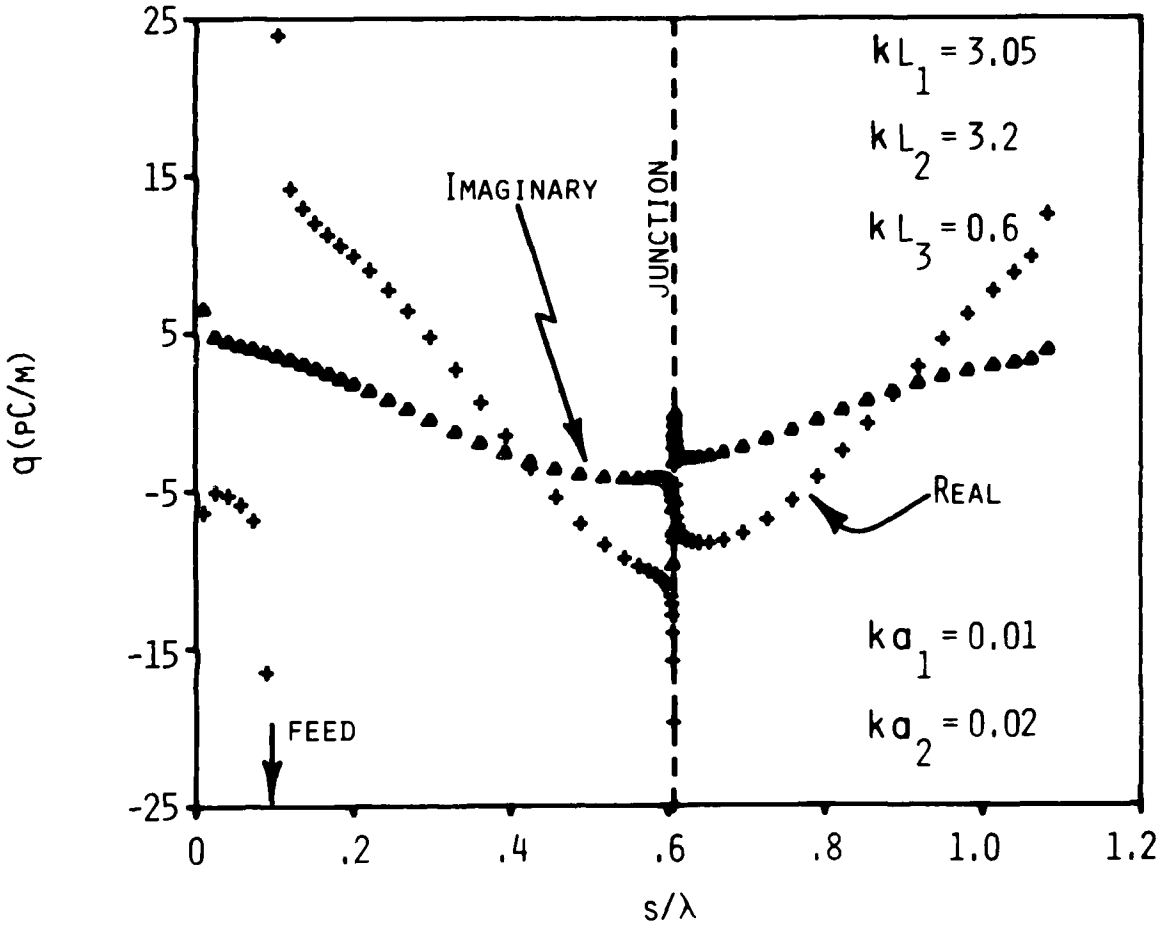

Figure 2.8. Charge distribution on a stepped-radius antenna obtained by treating the wire as a body of revolution.

approximate form for the linear charge density in the vicinity of the junction:

$$q(s) = \begin{cases} Ba_2(s_1 - s_2)(s_2 - s)^{-1/3} & , \ s \le s_2 \quad , \\ B\rho(s_1 - s)(s - s_2)^{-1/3} & , \ s_2 \le s \le s_1 \quad , \\ Ba_1(s - s_1)(s_1 - s_2)^{-1/3} & , \ s_1 \le s \quad , \end{cases} \tag{2.4}$$

where s is the arc length along the wire surface, ρ is the cylindrical coordinate variable on the annulus, s_2 is the value of the arc length variable at the outer edge of the annulus where $\rho = a_2$, s_1 is the value of the arc length variable at the inner edge of the annulus where $\rho = a_1$, and B is an unknown constant. In justifying (2.4), we note that edge conditions [15] require that for s near s_2, the surface charge density (proportional to the normal component of $\bar{E}$) must vary as $|s - s_2|^{-1/3}$, and for s near s_1, the charge density must vary as $|s - s_1|$. The <u>linear</u> charge density must therefore vary as $\rho|s - s_2|^{-1/3}$ and $\rho|s - s_1|$, respectively. There is one unknown constant associated with each region, but two of these may be eliminated by noting that the edge conditions require the charge density near s_1 and s_2 to vary in the same manner on either side of the points s_1 and s_2, thus yielding (2.4). Furthermore, the linear charge density is related to the total current by

$$q(s) = \frac{1}{\omega} \frac{dI(s)}{ds} \ , \tag{2.5}$$

so that one may determine the corresponding variation of the current by simple integration in each region. Three additional constants are introduced by the integration, but two of these may be eliminated by enforcing continuity of the current at the points s_1 and s_2. The resulting expression for the current follows:

$$I(s) = \begin{cases} C - \dfrac{3j\omega B a_2}{2}(s_1 - s_2)(s_2 - s)^{2/3}, & s \le s_2 \\ C - j\omega B\left[\dfrac{3a_1}{2}(s_1 - s)(s - s_2)^{2/3} + \dfrac{9a_1}{10}(s - s_2)^{5/3} + \dfrac{3}{2}(s_1 - s)^2(s - s_2)^{2/3} + \dfrac{9}{5}(s_1 - s)(s - s_2)^{5/3} + \dfrac{27}{40}(s - s_2)^{8/3}\right], & s_2 \le s \le s_1 \\ C - j\omega B\left[\dfrac{9a_1}{10}(s_1 - s_2)^{5/3} + \dfrac{27}{40}(s_1 - s_2)^{8/3} + \dfrac{a_1}{2}(s - s_1)^2(s_1 - s_2)^{-1/3}\right], & s_1 \le s \end{cases} \tag{2.6}$$

Figs. 2.9 and 2.10 show the charge and current distributions, respectively, in the vicinity of the junction for the case considered in Figs. 2.7 and 2.8 but with an expanded scale. The numerically obtained values are compared with the expected variation, as given by (2.4) and (2.6). To obtain the comparison for the charge (Fig. 2.9) the expression (2.4) must be "matched" to the numerical data at one point in order to determine the unknown constant B. For the current (Fig. 2.10), the same value of B is used and the numerical data are matched at one other point to determine the unknown constant C of (2.6). While the data-fitting procedure does not assure that the magnitudes (i.e., the undetermined constants) of the computed values are correct, the excellent agreement in the variation of the charge and current verifies that the numerical values indeed satisfy the edge conditions and hence, in all likelihood, are correct.

Some measured data is also available for two stepped-radius monopole structures fed at the ground plane [8]. PECØ is also capable of treating the stepped-radius monopole as a center driven dipole with two step changes in radius and thus comparison with the measured data is possible. The geometry may be visualized by referring to Fig. 2.1, from which a monopole with its image is obtained simply by eliminating segment 3 and reflecting segments 1 and 2 about the feed point. Both monopole structures have three fixed dimensions: $ka_2 = 0.05$, $ka_1 = 0.02$, and $L_2 = \lambda/4$. In all of the measurements, the length of segment 1 was fixed at

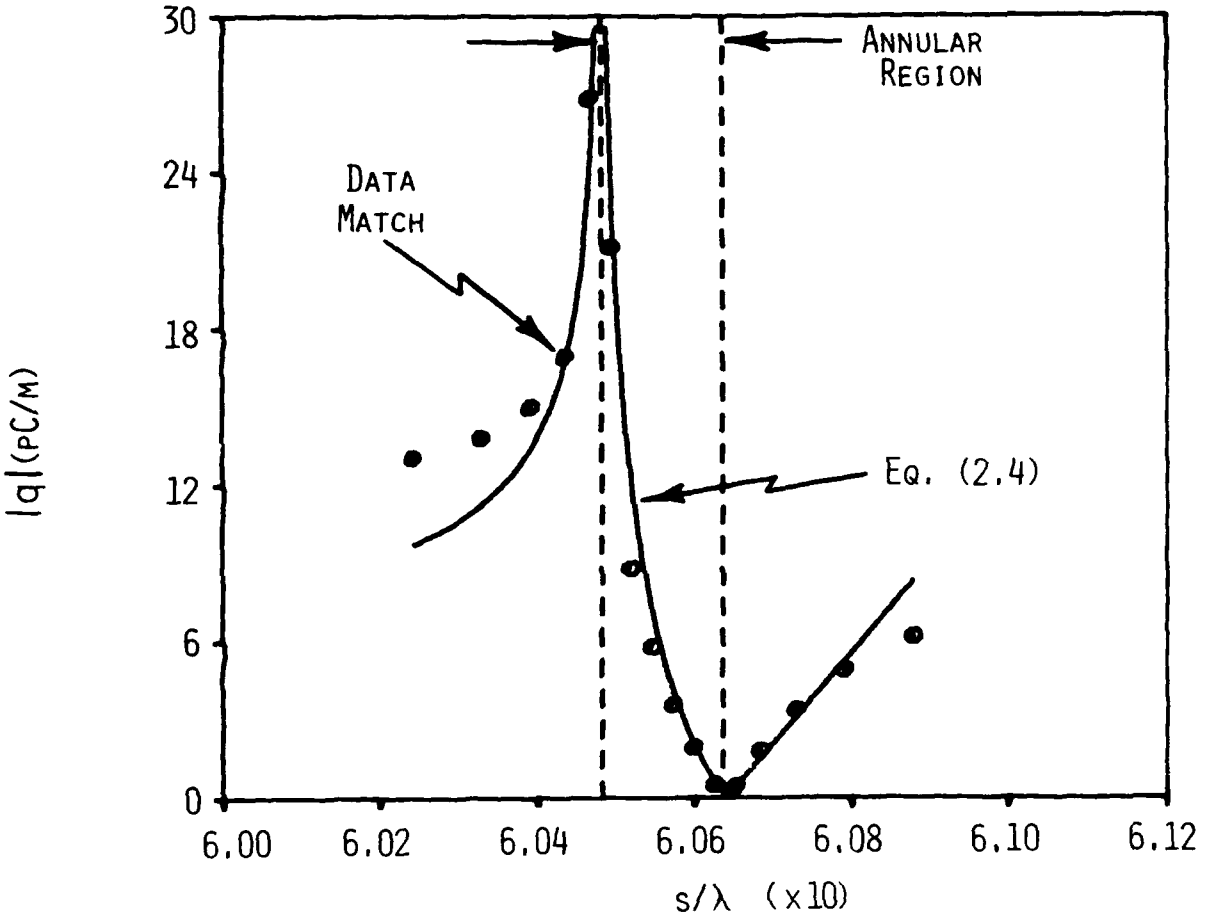

Figure 2.9. Comparison of the computed charge distribution in the vicinity of the junction with the approximate distribution based on edge conditions.

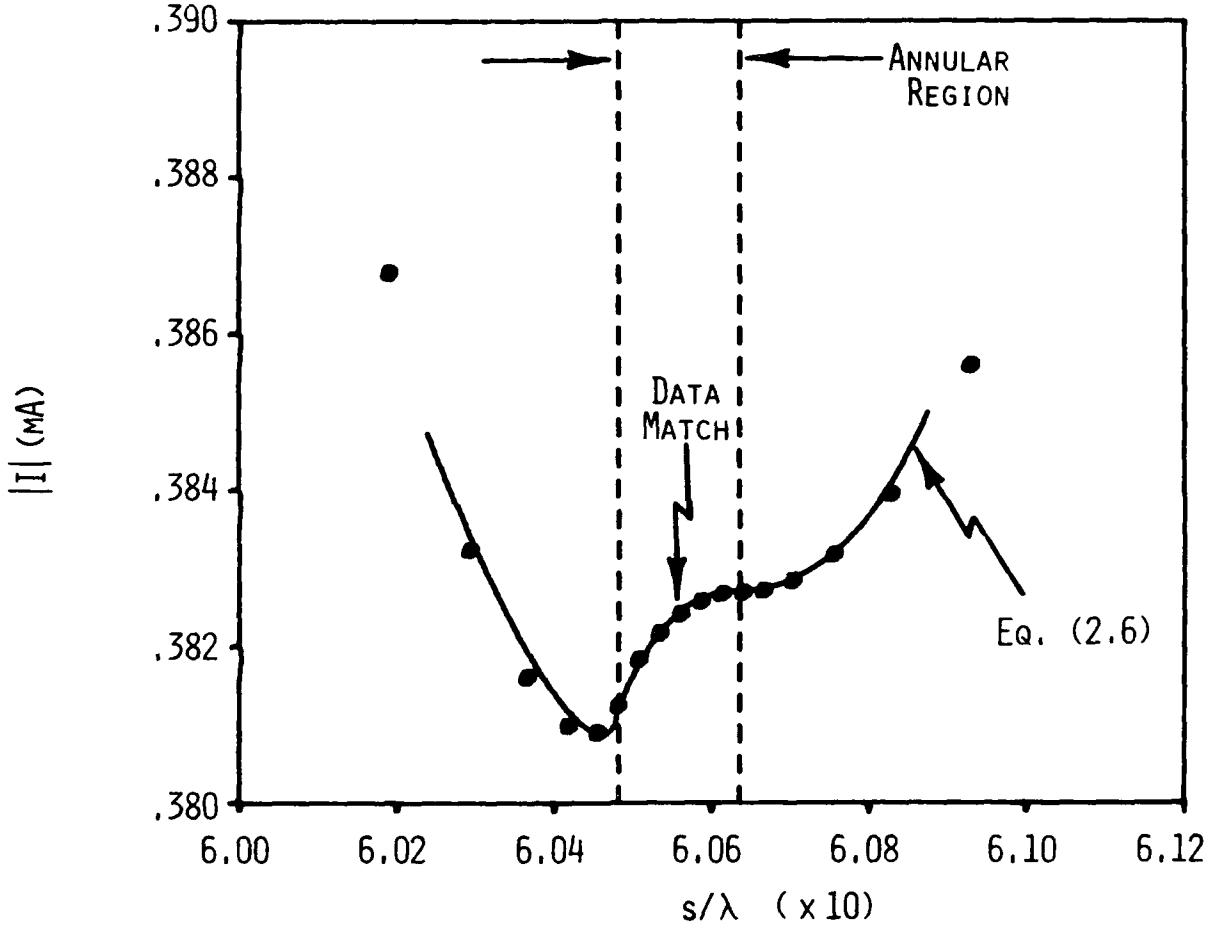

Figure 2.10. Comparison of the computed current distribution in the vicinity of the junction with the approximate distribution based on edge conditions.

either $L_1 = \lambda/4$ or $L_1 = \lambda/2$. Figs. 2.11 and 2.12 compare the measured data with current and charge distributions, respectively, calculated by PECØ for the case $L_1 = \lambda/4$. Figs. 2.13 and 2.14 illustrate the comparison for the case $L_1 = \lambda/2$. For both cases the calculated and measured current distributions agree in shape. The magnitudes, however, disagree by a factor of nearly 1.25 but in opposite directions in the two cases. On the other hand, the calculated and measured charge distributions are in excellent agreement for both cases. No definitive explanation for the magnitude differences in the calculated and measured current is offered at this time. However, there is a strong possibility that the differences arise due to the difficulty in determining an accurate calibration factor for the measurement probes [16]. Further data is presented in [8], however, which demonstrates agreement between calculated and measured data for the case when $L_1 = \lambda/4$. This comparison is given in Fig. 2.15 which shows that results obtained with PECØ are in excellent agreement with the measurements. However, the measured data in Figs. 2.11 and 2.15 supposedly apply to the same case, so that an inconsistency appears in the measured data. Furthermore, since the measured charge agrees with the computed charge and since the current can be obtained from the charge by integration, beginning from the end of the monopole where the current is known to vanish, the charge and current measurements shown in Figs. 2.11-2.15 are also inconsistent. It is

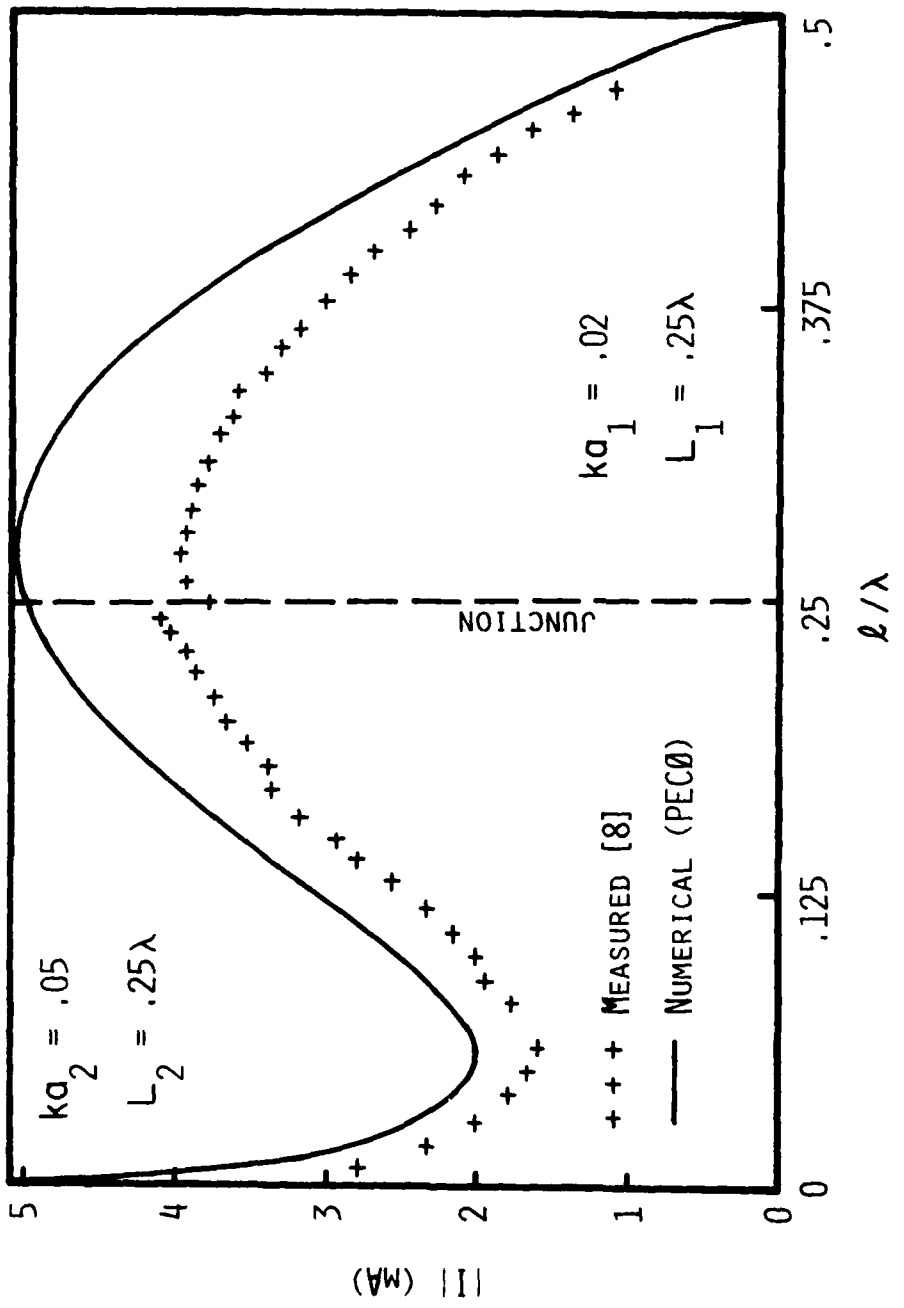

Figure 2.11. Comparison of calculated current distribution with measured data for a stepped-radius monopole of height $L_1+L_2 = \lambda/2$.

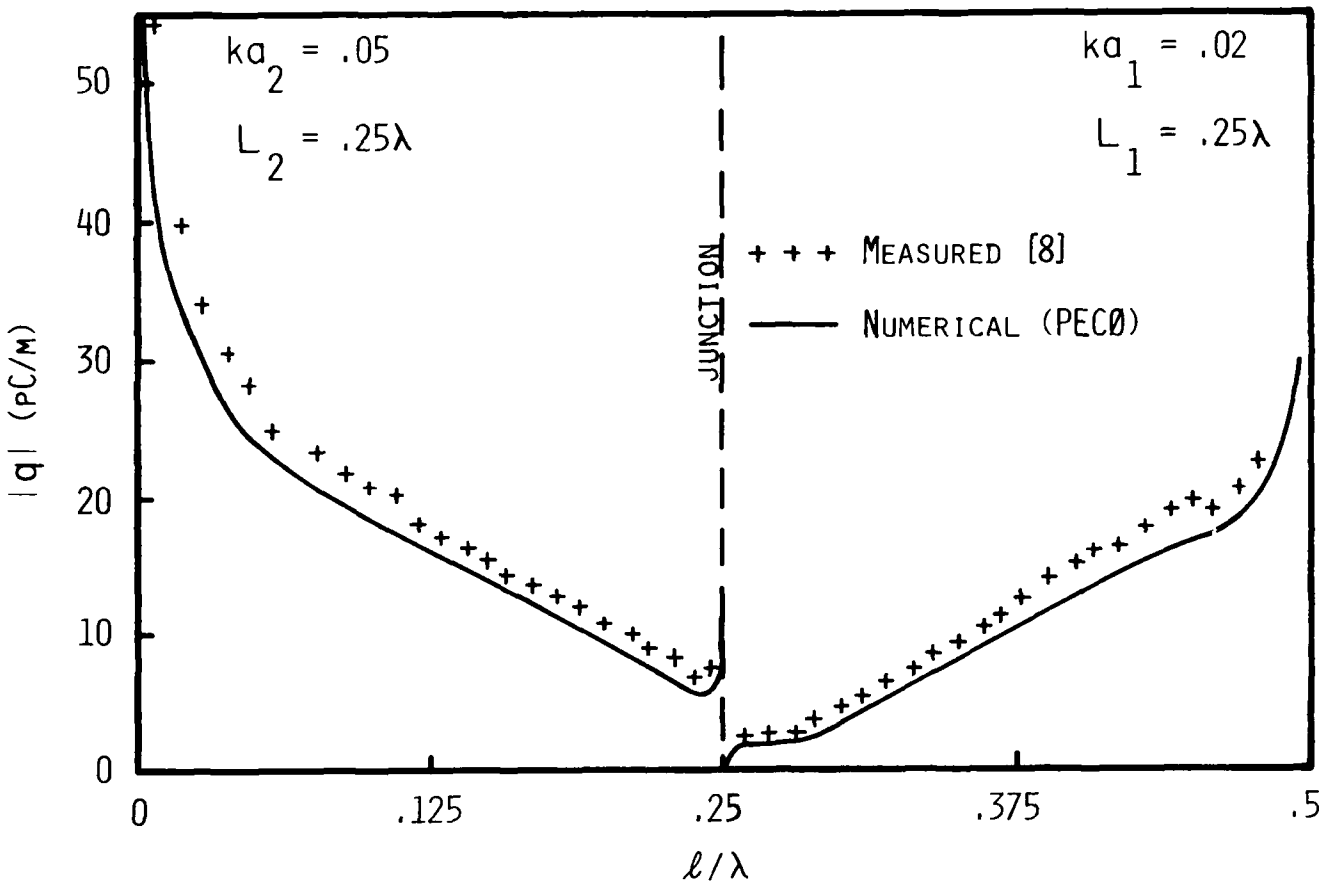

Figure 2.12. Comparison of calculated charge distribution with measured data for a stepped-radius monopole of height $L_1+L_2 = \lambda/2$.

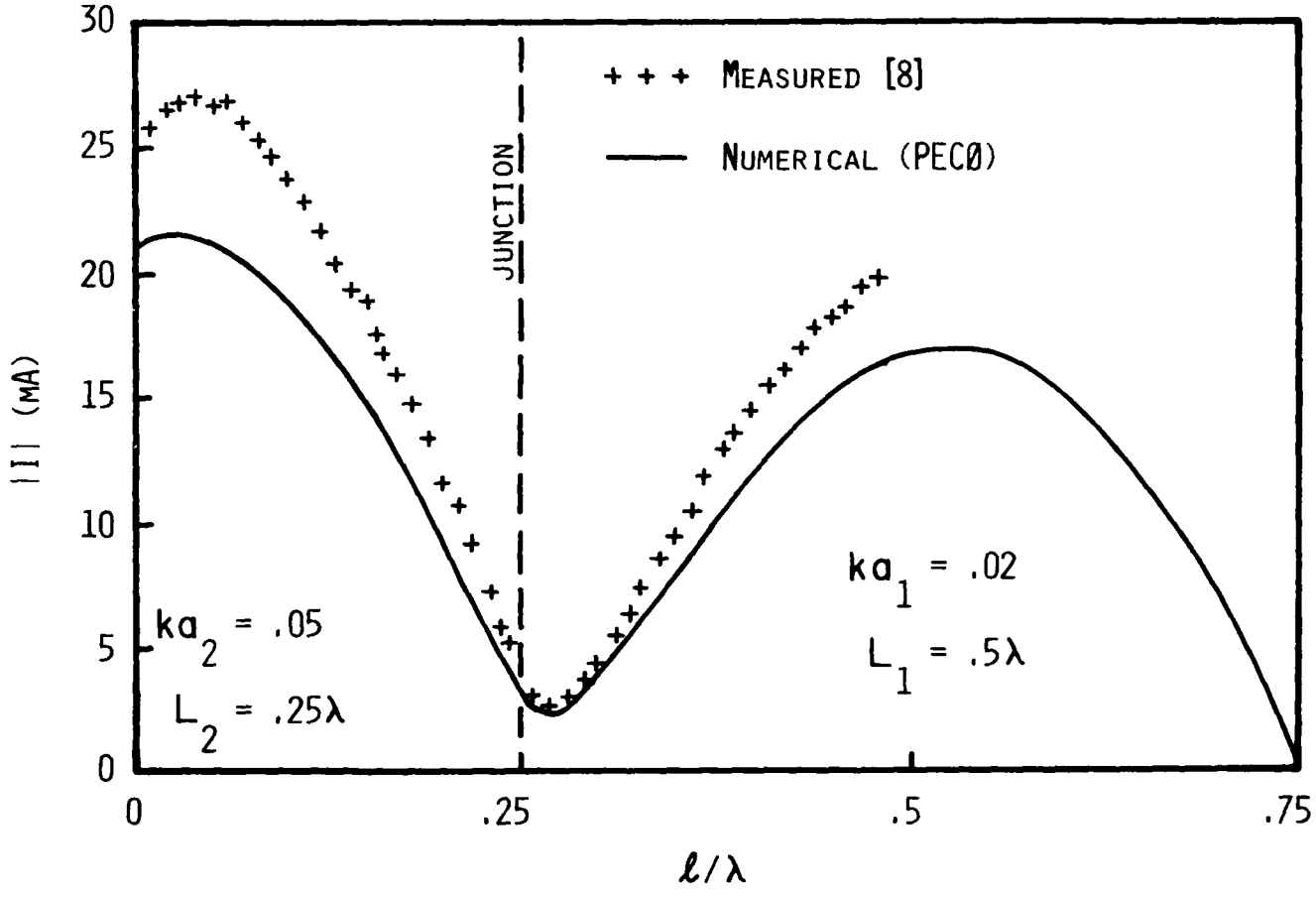

Figure 2.13. Comparison of calculated current distribution with measured data for a stepped-radius monopole of height $L_1+L_2 = 0.75\lambda$.

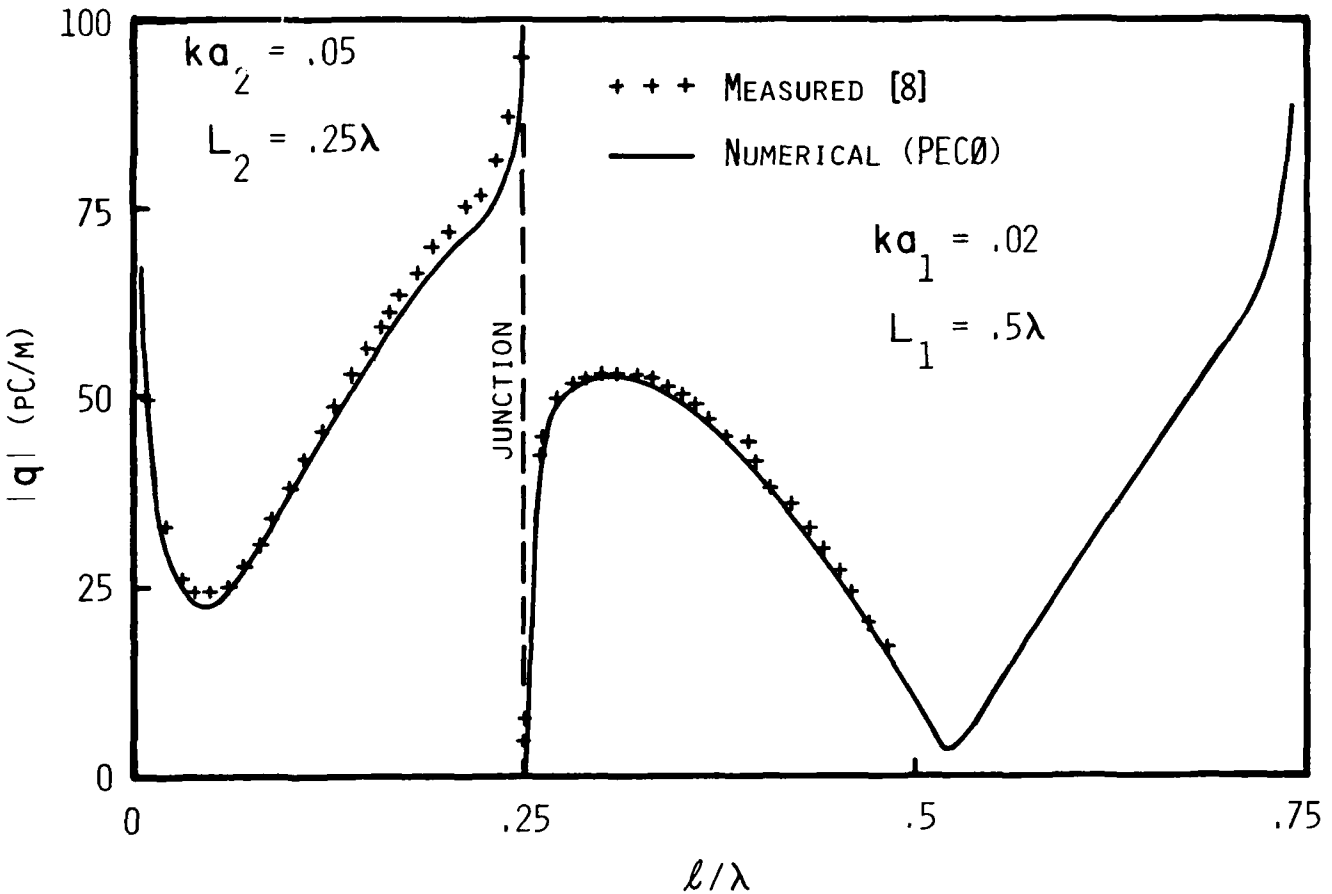

Figure 2.14. Comparison of calculated charge distribution with measured data for a stepped-radius monopole of height $L_1+L_2 = 0.75\lambda$.

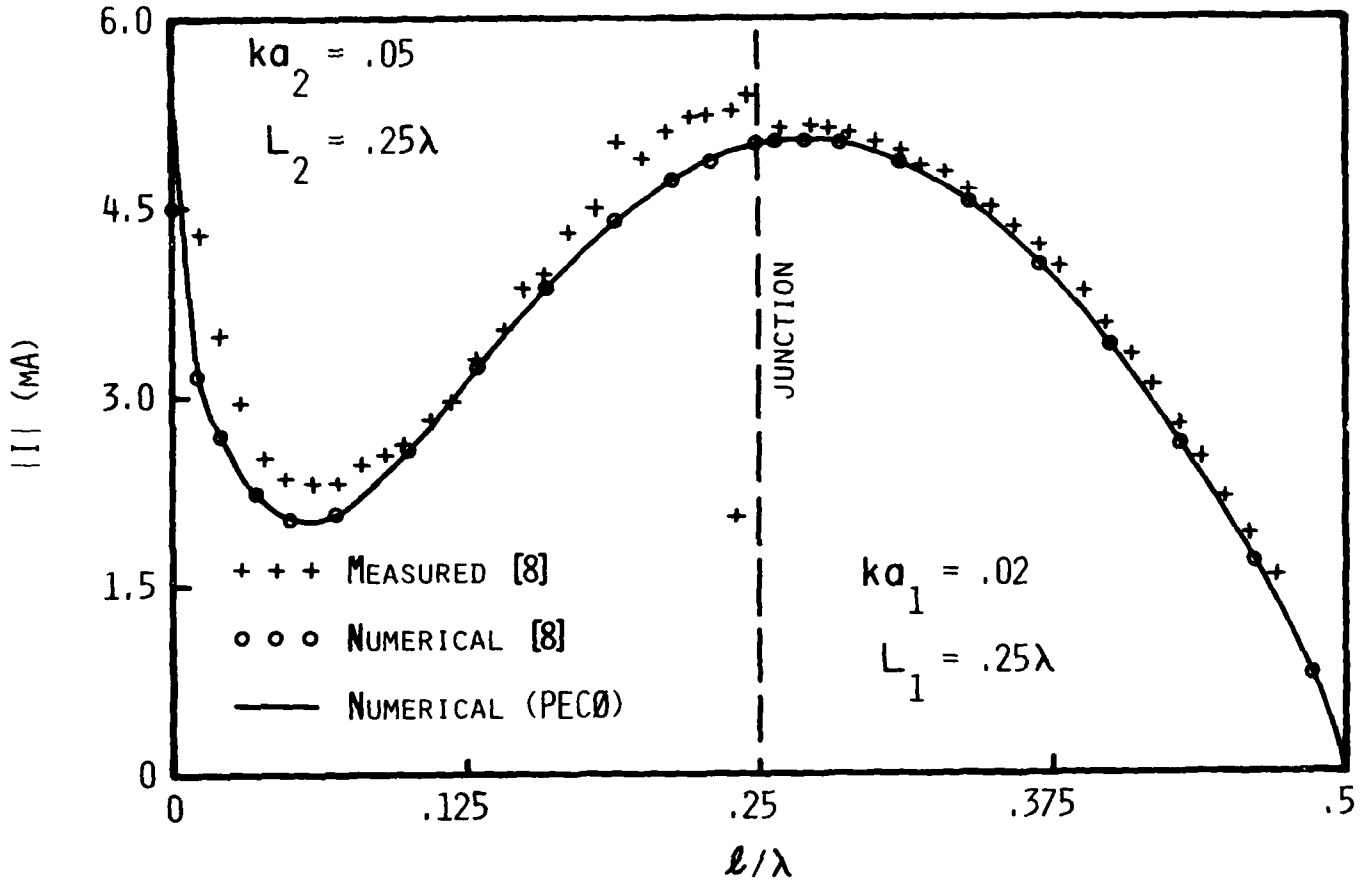

Figure 2.15. Current distribution on a stepped-radius monopole of height $L_1+L_2 = \lambda/2$.

possible that the measured data shown in Fig. 2.15 have been scaled to demonstrate the agreement in shape between the measured and the numerical data available at that time [16]. Unfortunately, if this is the case, mention of the data scaling was omitted from the text of [8]. We conclude, however, based on the excellent agreement between the computed and measured charge and on other evidence presented in this section, that the computer code PECØ does indeed provide accurate current and charge distributions on stepped-radius antenna structures--including showing the detailed behavior of the current and charge in the junction region.

2.2 Thin-Wire Analysis of the Stepped-Radius Antenna

The analysis of the stepped-radius antenna by means of thin-wire theory differs from the body of revolution analysis in two respects. First, the current and charge on the annular region of the junction are completely ignored and secondly, the so-called reduced kernel is employed in the integral equation. The reduced kernel is obtained by approximating

$$\int_0^{2\pi} \frac{e^{-jk|\bar{r} - \bar{r}'|}}{|\bar{r} - \bar{r}'|} \, d\phi \tag{2.7}$$

as

$$\frac{e^{-jk[(\ell - \ell')^2 + a^2]^{\frac{1}{2}}}}{[(\ell - \ell')^2 + a^2]^{\frac{1}{2}}} \, . \tag{2.8}$$

where ℓ is defined in Fig. 2.1 and a is the radius of the wire. For the stepped-radius wire, however, the radius a has two distinct values, and one might ask whether the value of a to be used is the radius at the "match point" or the radius associated with the source region. The answer depends on the physical interpretation of (2.8). One common approach is to interpret (2.8) as effectively replacing the wire by a filament of current flowing down the axis of the wire with the match point placed on the wire surface. With this interpretation, one should obviously use the radius of the wire at the match point. On the other hand, one may also view the problem in an extended boundary condition sense [17]. This approach would imply that the match point is on the wire axis, while the current flows along the wire surface. The appropriate radius to use in (2.8) in this case would therefore be the radius associated with the source region. The extended boundary condition argument and approach is used in the analysis presented here to avoid an ambiguity in the choice of the match point location at the junction.

As we have said, in a thin-wire analysis the charge and current on the annular region are ignored. One may visualize the placement of the subdomains in the thin-wire analysis then, simply by letting the width of the annulus region in Fig. 2.2 be equal to zero. Thus a single current subdomain is split at the junction while full pulses of charge are placed on each side of the step. The current subdomain split

by the junction has associated with it a single unknown coefficient while the full pulses of charge residing on each side of the radius change are completely independent of one another. Note that the two portions of the current pulse split across the junction are associated with different radii according to which section of the wire they reside on. Also note that we need not explicitly enforce any condition on the charge at the junction, the only condition explicitly enforced at the junction being that of current continuity. We note, however, that the testing procedure, which in this approach requires that the average tangential electric field vanish over each current subdomain, effectively (in the limit of decreasing subdomain size) enforces continuity of the scalar potential at the junction. We emphasize that this condition is, in reality, the "correct junction condition" and hence we should anticipate reasonable performance with the thin-wire code.

The resultant current and charge distributions computed with 27 unknowns by this method for the same stepped-radius antenna as that of Fig. 2.7 are shown in Figs. 2.16 and 2.17, respectively. The current distribution is virtually identical to that obtained from the body of revolution computer code PECØ (Fig. 2.7). Note that owing to the sparseness of the sample points in the neighborhood of the junction, the charge distribution shown in Fig. 2.17 does indeed appear to have a jump discontinuity there. The computed values, however, are

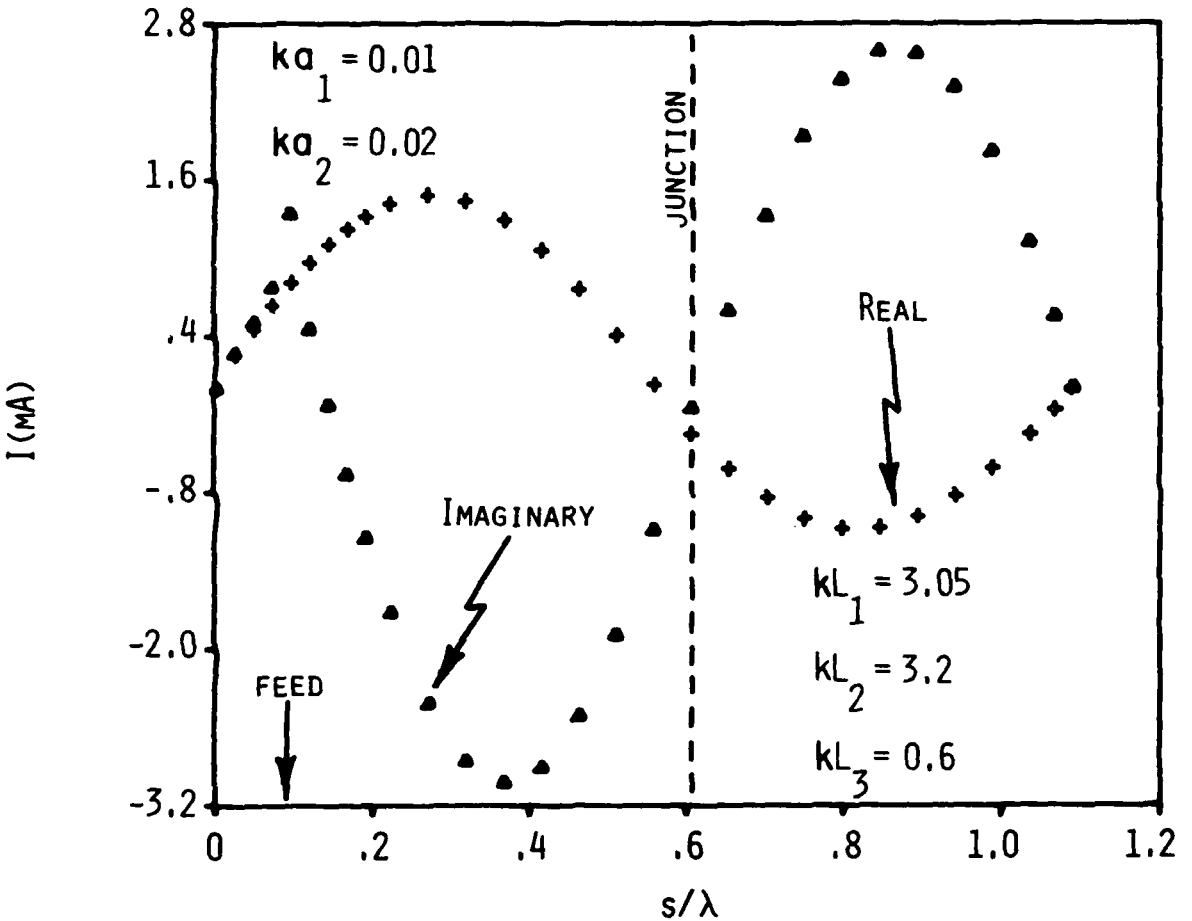

Figure 2.16. Current distribution on a stepped-radius antenna computed by thin-wire analysis.

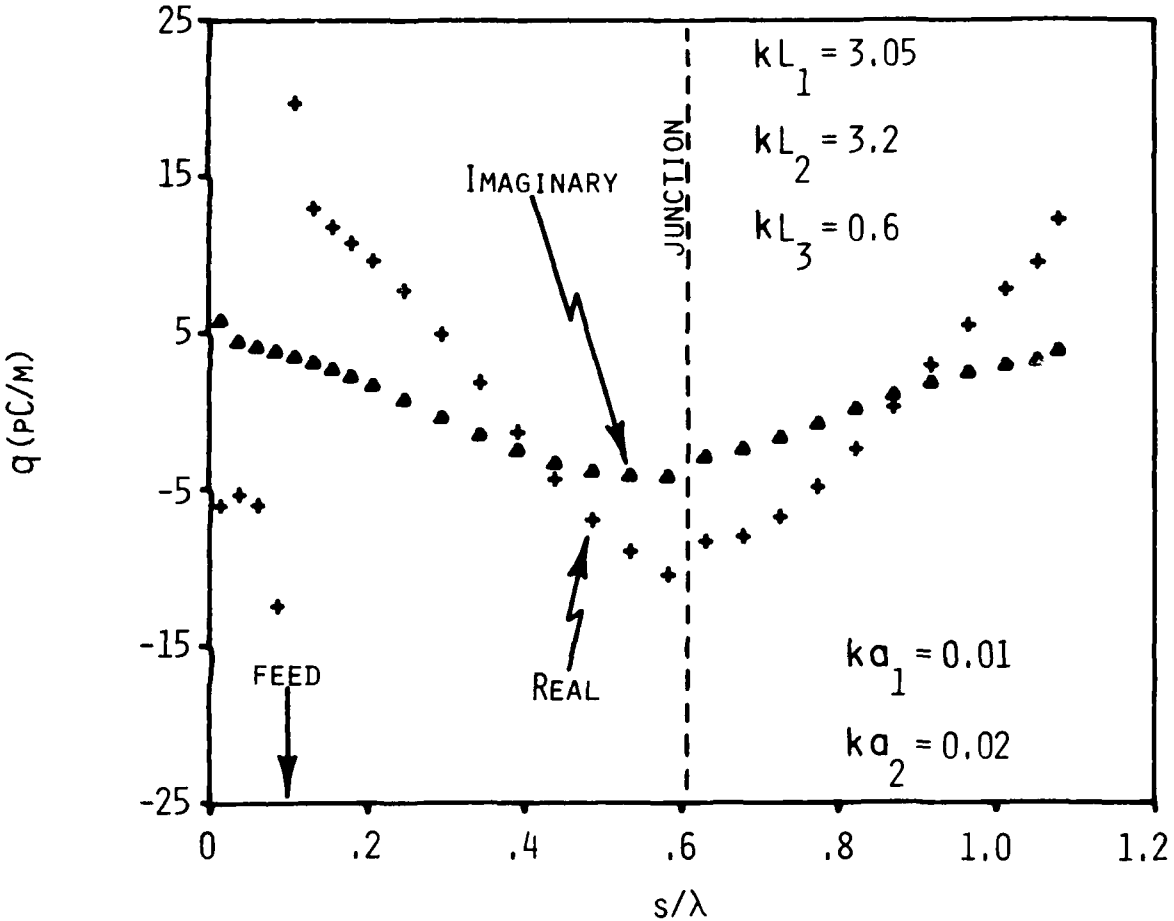

Figure 2.17. Charge distribution on a stepped-radius antenna computed by thin-wire analysis.

virtually identical with the charge distribution computed with the body of revolution code (Fig. 2.8).

Consider next a stepped-radius antenna with the following dimensions: $ka_1 = 0.001$, $ka_2 = 0.05$, $kL_1 = 3.05$, $kL_2 = 3.2$, and $kL_3 = 0.6$. Note that the structure has a radius discontinuity of ratio 50 to 1. The current and charge distributions obtained using PECØ are presented in Figs. 2.18 and 2.19, respectively. Figs. 2.20 and 2.21 show the current and charge distributions obtained using the thin-wire theory approach with 26 unknowns. A comparison of the appropriate figures shows that the results for the current are in excellent agreement. The charge distributions also agree very well. In Figs. 2.22 and 2.23 the number of unknowns used in the thin-wire approach has been increased to 43. The current and charge distributions obtained are essentially the same as shown in Figs. 2.18 and 2.19. In Fig. 2.23, however, one notes that the charge in the vicinity of the junction tends to show the proper edge behavior (compare with Fig. 2.19) even though the annulus region has been completely ignored in the thin-wire approach. This behavior has been verified for many different wire radii and radius jump ratios, and is further demonstrated in Section III. Thus, Figures 2.18 through 2.23 demonstrate that the thin-wire approach presented in this section can be used to treat wires with step changes in radius--even very large changes--without the explicit enforcement of any conditions on the charge at the junction.

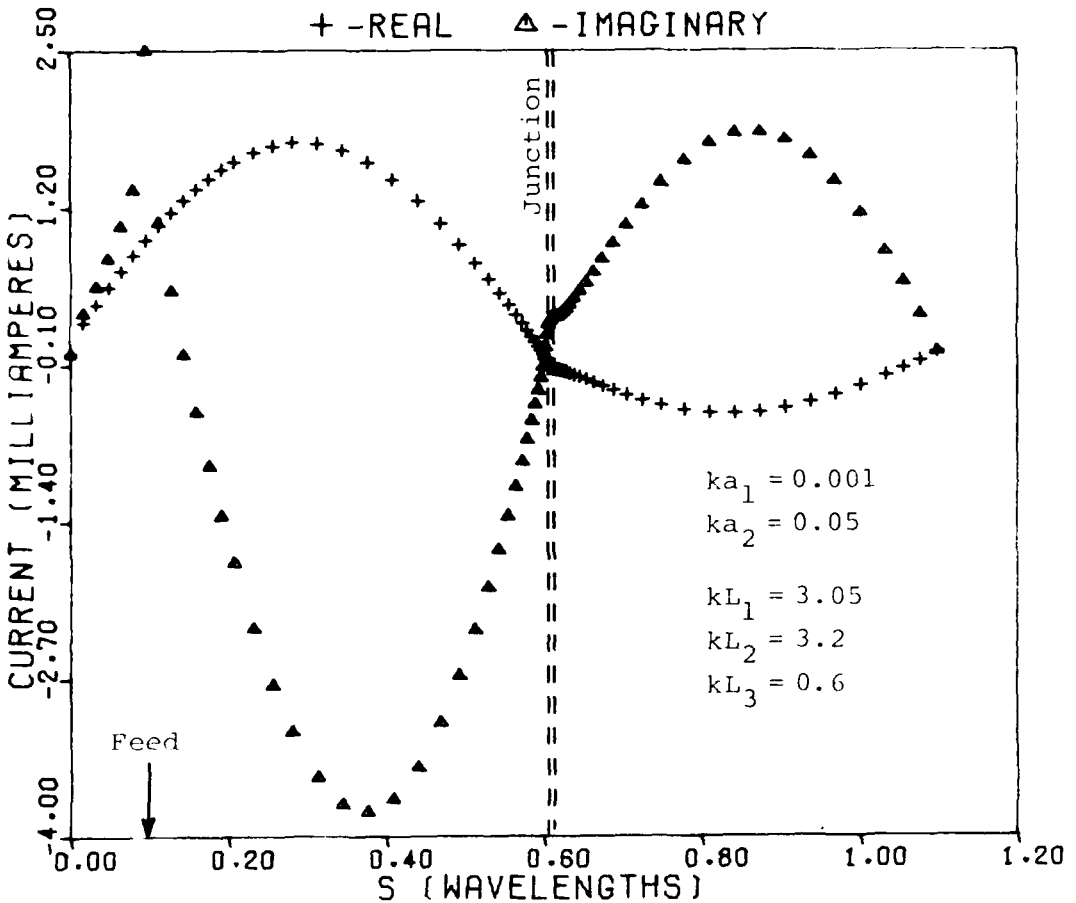

Figure 2.18. Current distribution (PECØ) on a stepped-radius antenna with a 50 to 1 change in radius.

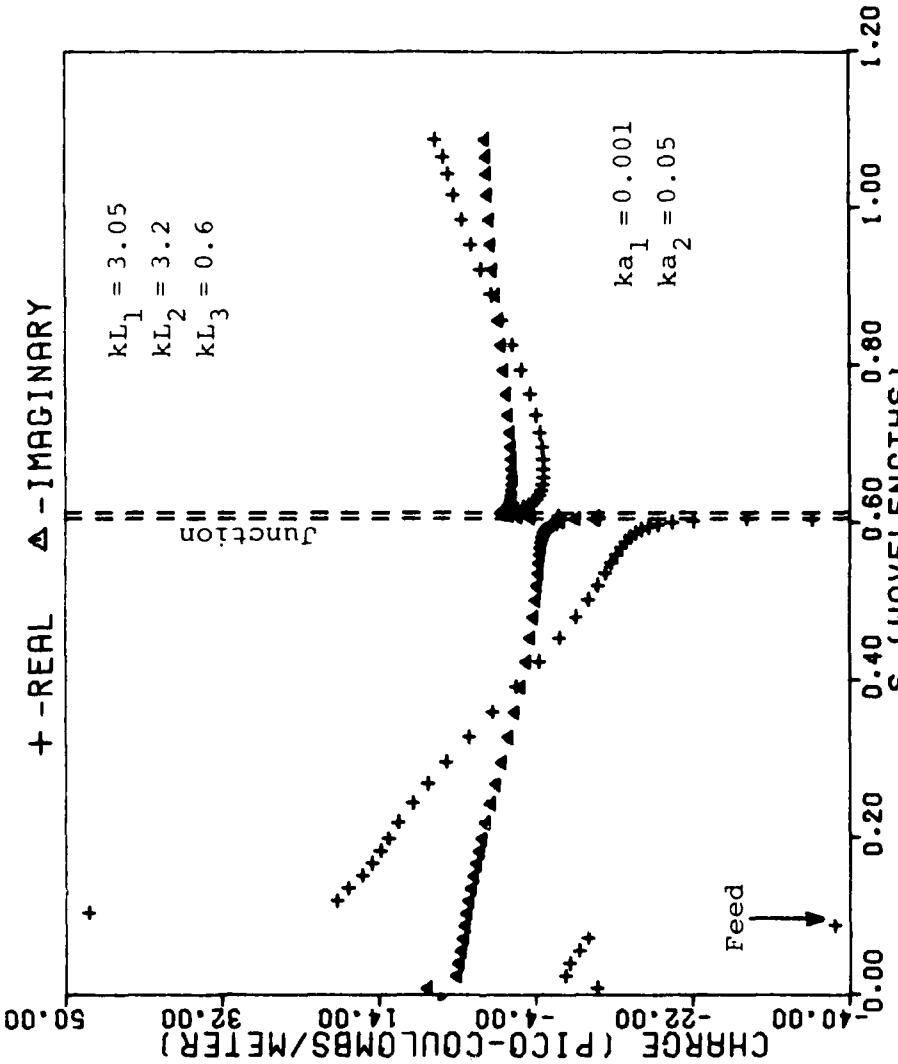

Figure 2.19. Charge distribution (PECØ) on a stepped-radius antenna with a 50 to 1 change in radius.

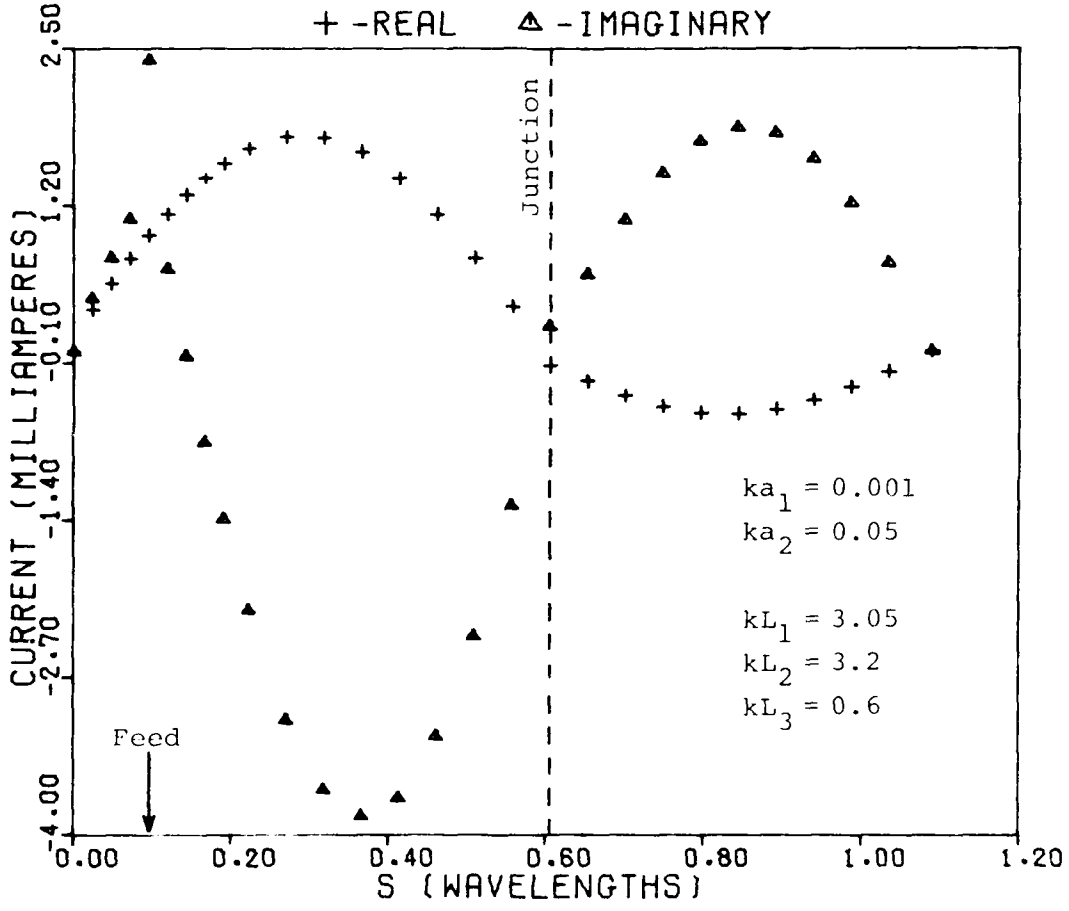

Figure 2.20. Current distribution (thin-wire approach) on a stepped-radius antenna with a 50 to 1 change in radius.

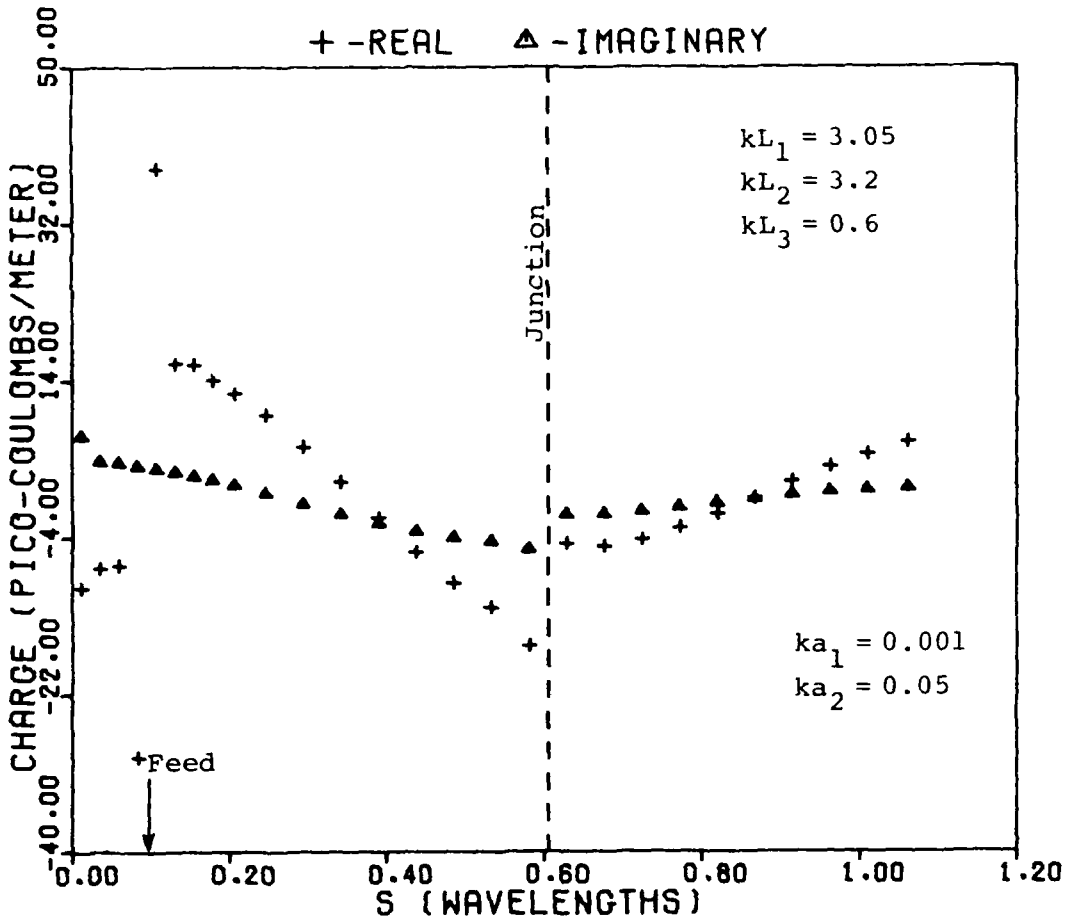

Figure 2.21. Charge distribution (thin-wire approach) on a stepped-radius antenna with a 50 to 1 change in radius.

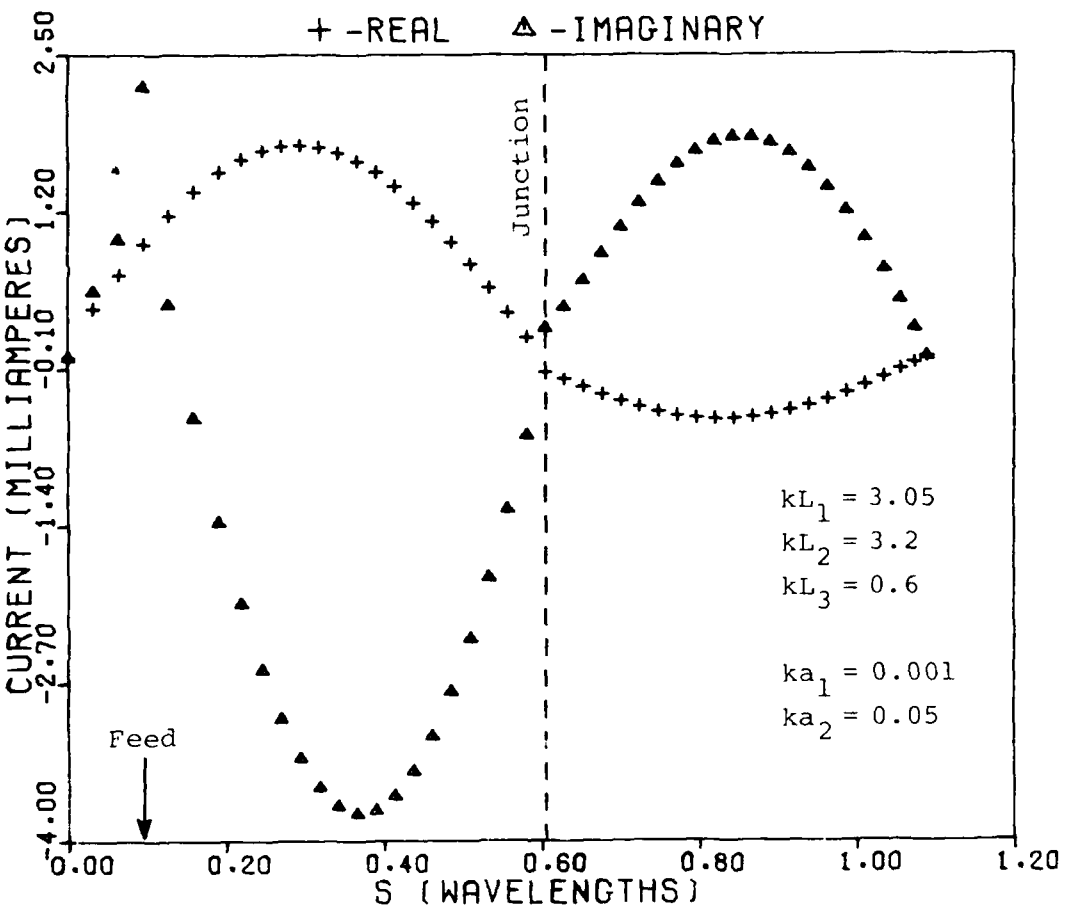

Figure 2.22. Current distribution (thin-wire approach; increased number of unknowns) on a stepped-radius antenna with a 50 to 1 change in radius.

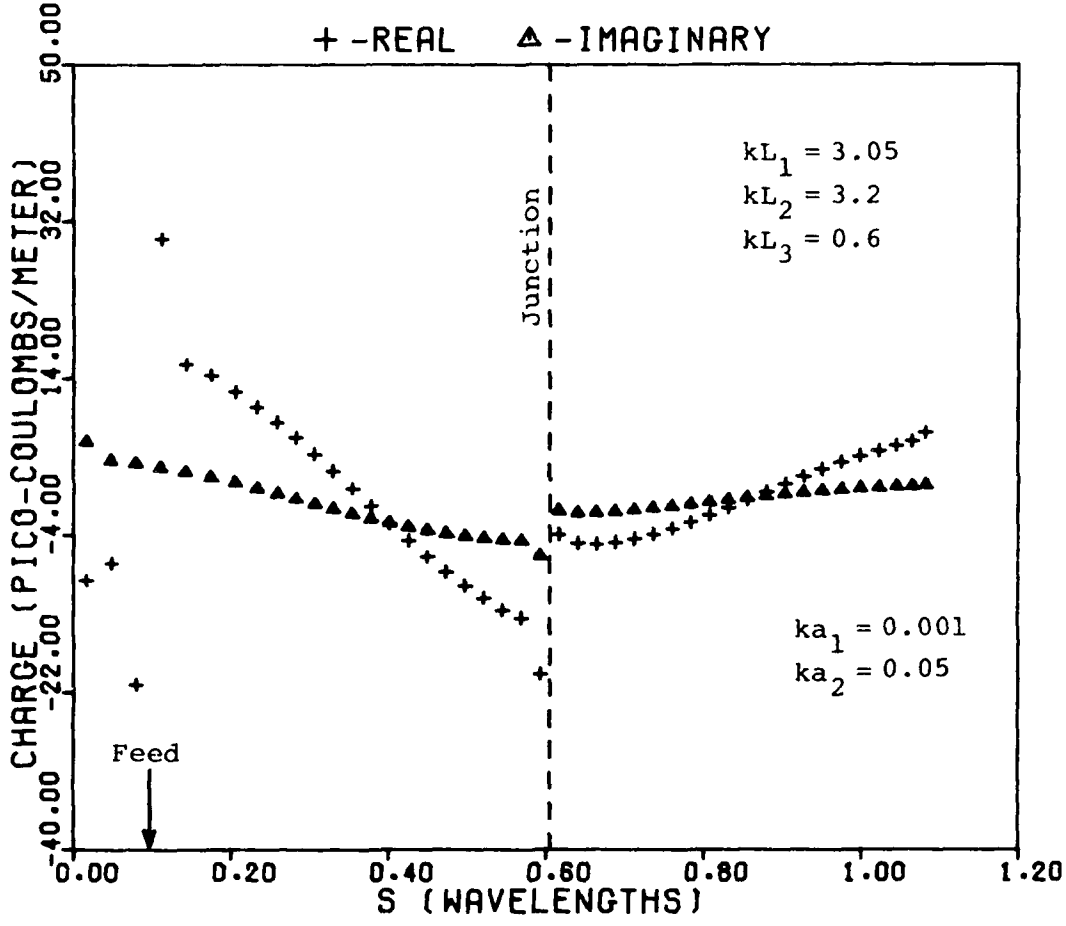

Figure 2.23. Charge distribution (thin-wire approach; increased number of unknowns) on a stepped-radius antenna with a 50 to 1 change in radius.

2.3 Computation of the Charge "Jump Condition"

In this section numerically derived charge jump conditions are computed for various wire radii and changes in radii and are compared with the analytical jump conditon of Wu and King. We compute the charge jump condition for a specific structure by ignoring the actual behavior of the charge in the junction region and instead extrapolate to the junction using values of current and charge computed on both sides of the junction at some distance away from it. This process is analogous to that of determining an equivalent circuit for a discontinuity at a terminal plane in a single mode waveguide--from measurements of standing waves away from the discontinuity, we deduce the reflection coefficient (and hence the discontinuity of the modal coefficients) at the terminal plane, thus determining the equivalent circuit. This mode alone, however, would not be useful for describing the true fields in the region of the discontinuity because of the presence of higher order modes in the terminal plane region.

We calculate charge jump conditions using charge distributions obtained with both the body of revolution code PECØ and with the thin-wire approach described in the previous section. Calculation of the charge jump condition from the thin-wire approach can be used to further validate the thin-wire approach over a wide range of wire sizes and jump ratios.

The calculation of the jump condition relies on the fact that away from the junction region (and also from wire ends

and feed points) both the current and the charge on the antenna are essentially sinusoidal. If the sinusoidal variation is independently determined on each side of the junction and the resulting variation is extrapolated to the junction region, one obtains a total current distribution which has a slope discontinuity at the junction and hence a charge distribution which exhibits a step function jump there. The extrapolated charge variation in the vicinity of the junction may therefore be expressed as

$$q(s) = \begin{cases} A_1\cos(ks) + B_1\sin(ks) & , \ s_1 < s \\ A_2\cos(ks) + B_2\sin(ks) & , \ s < s_2 \end{cases} , \qquad (2.9)$$

where k is the free space wavenumber, s, s_1, and s_2 are defined as in Section 2.1, and A_1, A_2, B_1, and B_2 are unknown constants. To determine the constants in (2.9) it is necessary to find a region on each side of and away from the junction, over which the computed current (and hence the charge) is essentially sinusoidal. These regions are located by considering the expression

$$P = 100 \frac{\left| \left(k^2 + \frac{d^2}{ds^2} \right) I(s) \right|}{|k^2 I|_{max}} . \qquad (2.10)$$

The quantity P may be used as a gauge of the percentage deviation from sinusoidal. The current is known only as numerical values, so a finite difference approximation may

be used to calculate the derivatives in (2.10). $|I|_{max}$ represents the largest value of the current magnitude on the structure, ignoring the region near the feed point. The points from which the charge is extrapolated are found by assuming a very small value for a quantity P_{max} and then searching for the points nearest the junction for which $P < P_{max}$. The value of P_{max} is increased progressively until such points can be found. In practice, such regions are generally found for $P_{max} \leq 15$ (per cent). The numerical charge distribution is then equated to the appropriate representation in (2.9) at two points in each region to determine the constants. The extrapolated ch rge at the junction is then found to be

$$q_1 = A_1\cos(ks_1) + B_1\sin(ks_1) \qquad (2.11a)$$

$$q_2 = A_2\cos(ks_2) + B_2\sin(ks_2) \quad , \qquad (2.11b)$$

where q_1 and q_2 represent the charge at the junction on the wire of smaller radius and larger radius, respectively.

An example of the results this extrapolation procedure is illustrated in Fig. 2.24 for the charge distribution shown in Fig. 2.19. The figure shows an expanded plot of the numerically computed values in the junction region. The solid lines represent the linear charge density (2.9) after the constants have been computed by "matching" the data at two points on each side of the junction. The points at which the solid lines intersect the two dashed lines

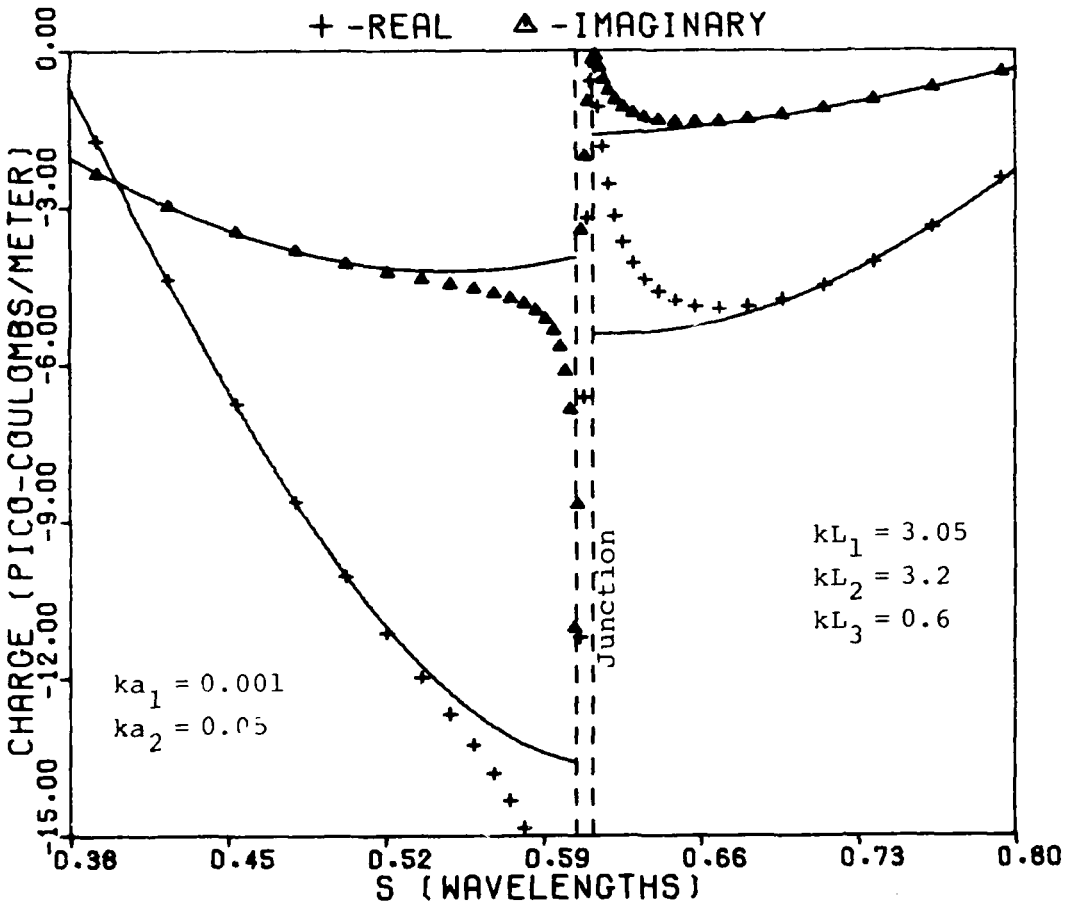

Figure 2.24. Charge distribution (PECØ) in the vicinity of the junction on a stepped-radius antenna with a 50 to 1 change in radius. The solid lines represent the "extrapolated" charge.

(delineating the annulus region) represent the real and imaginary parts of q_2 and q_1 as defined by (2.11). A number of similar calcualtions have been made and the resulting ratio q_1/q_2 is compared with the formula of Wu and King [7] in Fig. 2.25 for several wire radii and various ratios of radii at the discontinuity. For reference, the formula of Wu and King is given as

$$\frac{q_1}{q_2} = \frac{\ell n \left(\frac{2}{ka_2}\right) - \gamma}{\ell n \left(\frac{2}{ka_1}\right) - \gamma} \quad , \tag{2.12}$$

where $\gamma \doteq 0.5772$ is Euler's constant. One observes from Fig. 2.25 that the numerical computations of both the body of revolution code and the thin-wire code are in very good agreement with the formula of Wu and King. The only exception appears on the curve for $ka_1 = 0.01$, where it is noted that for $a_1/a_2 = 0.02$, the point computed by thin-wire analysis is significantly in error. However, in this case, the radius of the thicker wire ($ka_2 = 0.5$) is well beyond the limit for which thin-wire theory is applicable. We comment that all data were obtained for the wire length dimensions $kL_1 = 3.05$, $kL_2 = 3.2$, and $kL_3 = 0.6$, since this results in an approximate charge maximum in the vicinity of the junction, thus improving the sensitivity of the computations. Results obtained for several other wire lengths,

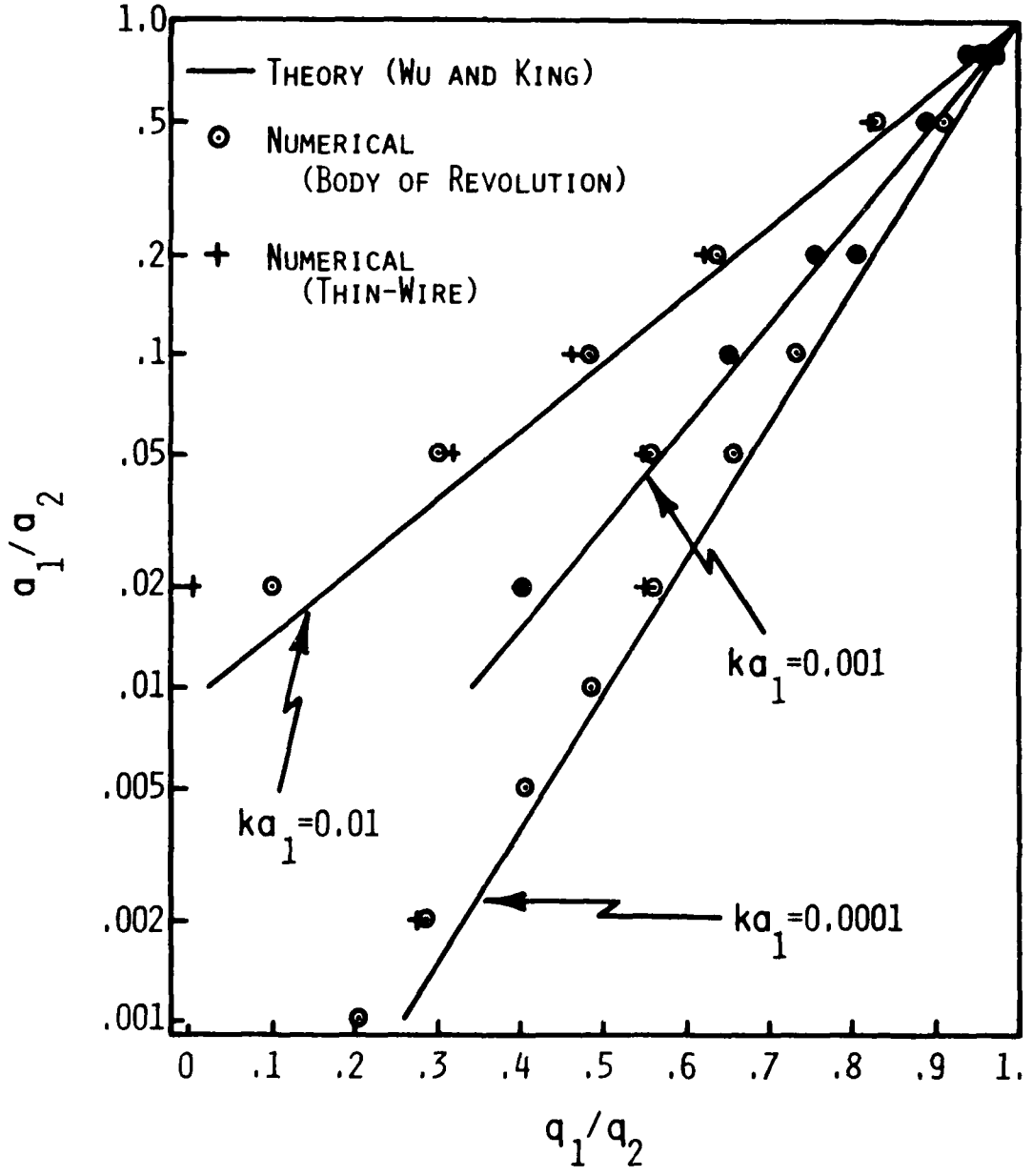

Figure 2.25. Comparison of numerically computed charge "jump condition" for stepped-radius wires with theory of Wu and King.

however, where a charge maximum does not occur near the junction, have also confirmed agreement of the computations with the formula of Wu and King. We mention briefly that a similar procedure to that above for extrapolating the charge, has been used to verify that the extrapolated current is continuous at the junction in both the body of revolution and in the thin-wire theory approach.

These computations verify that the charge jump condition of Wu and King is correct for the stepped-radius structure illustrated in Fig. 2.1. Time and resources have not permitted us to attempt to calculate charge jump conditions for more complex dissimilar radii wire structures such as multiple wire junctions or wires bent at a radius discontinuity. However, it can easily be shown (see Appendix) that the Wu-King condition is approximately equivalent to requiring continuity of scalar potential at a junction. Hence establishing the accuracy of the condition for the stepped-radius cylinder lends a great deal of support to its applicability to these more general junctions where, again, the correct junction conditions are that (1) Kirchoff's current law be satisfied and that (2) scalar potential be continuous at each junction.

Because of the difficulty involved, it is not likely that a detailed investigation of bent wire junctions or multiple wire junctions at the detail we have considered here will be carried out in the near future. Nevertheless, the

success of our thin-wire code in modeling the stepped-radius junction, leads us to suggest a less ambitious investigation--that of establishing whether or not the thin-wire approach described here yields results satisfying the Wu-King condition on such structures. In applying the thin-wire approach, Kirchoff's current law would be enforced at the junction, but no condition on the charge would be required. Our conjecture is that the proposed thin-wire approach would yield charge distributions in good agreement with the Wu-King condition because both approaches employ an approximate enforcement of continuity of scalar potential at the junction. Such agreement would, in our opinion, lend substantial credence to the use of both thin-wire theory and the Wu-King condition to handle such configurations.

SECTION III

APPLICATION OF THE NUMERICAL ELECTROMAGNETICS COMPUTER CODE TO STEPPED-RADIUS JUNCTIONS

The Numerical Electromagnetics Code (NEC) is a general purpose computer code capable of performing a variety of tasks related to electromagnetic radiation and scattering problems [11]. NEC is based on a method of moments solution [12] of integral equations for the currents induced on a structure (or structures) by electromagnetic sources or incident fields. The code is capable of treating wire structures and/or smooth surfaces (by wire-grid modeling or the Magnetic Field Integral Equation). In this report we concern ourselves only with a particular aspect of the code--the modeling of junctions of wires of dissimilar radii. This single aspect is of interest because NEC explicitly employs the charge jump condition (2.12) of Wu and King [7] at wire junctions. In Section II, we have numerically verified that this charge jump condition is indeed a "correct" condition to enforce at the junction of two collinear wires and thus we expect NEC to provide accurate results. On the other hand, some aspects of thin-wire modeling indicated in the previous section lead one to expect that the explicit enforcement of (2.12) might, under some conditions, result in

erroneous solutions. Specifically, we refer to the fact that the current and charge obtained via the thin-wire approach of Section II tend to show the true edge behavior--not the extrapolated behavior--as the number of unknowns is increased in the junction region.

In this section we address the question of whether the explicit enforcement by NEC of the charge jump condition (2.12) at junctions of collinear wires leads to accurate solutions for the current and charge away from the junction region. A very brief description of the wire modeling technique used in NEC is first presented as background (for further details, one should see [11]). Numerical results obtained with NEC are then compared with results obtained using PECØ for various structures and the data are discussed.

3.1 Wire Modeling in NEC

The NEC program models arbitrary wire structures as a set of straight wire segments. For each of these wire segments one of three thin-wire approximations for the kernel of the integral equation is used. For most cases a reduced kernel corresponding to (2.8) is used, where the current is assumed to be a filamentary current flowing along the axis of each segment and the match point is assumed to reside on the wire surface. For thick wires an extended thin-wire kernel [11] can be selected by the user. In this case the current is assumed to flow on the surface of the wire and the integral (2.7) is approximated by a two term series.

Finally, whenever wire segments are separated by large distances, fields are calculated by treating the current segment as an infinitesimal current element with the appropriate dipole moment. The current element in this case is located at the center of the source segment.

The method of moments is applied by choosing an appropriate set of testing functions and basis functions for the current on the wire segments. Substitution into the integral equation for the structure under consideration results in a set of simultaneous equations which can be solved to determine the coefficients of the current basis functions. In the development of the NEC program, the basis functions used to represent the current on wires were chosen so as to yield a highly efficient and accurate solution. Since the current distribution on wire structures is smooth (except at junctions), a very "smooth" set of basis functions was chosen for NEC. Furthermore, because of the accuracy with which these smooth basis functions can represent a smoothly-varying current, a set of delta functions could be used for the testing functions, resulting in a collocation or point-matching solution technique. The use of very smooth basis functions generally results in improved convergence over pulse or piecewise linear current expansions and, indeed, we have found the NEC program to be a highly efficient and accurate code. It is, however, the use of smooth basis functions which necessitates the use of an equivalent charge

jump condition to replace the actual non-smooth (in fact, singular) variation of the charge at a junction.

The current expansion in NEC consists of three terms defined on each segment--a constant, a sine, and a cosine term. The trigonometric terms have the form of standing waves employing the free space propagation constant. The total current on each segment thus takes the form

$$I_i(\ell) = A_i + B_i \sin [k(\ell - \ell_i)] + C_i \cos [k(\ell - \ell_i)], \quad (3.1)$$

$$|\ell - \ell_i| \leq \Delta_i/2,$$

where ℓ is defined in Fig. 2.1, ℓ_i is the value of ℓ at the center of segment i, and Δ_i is the length of segment i. There are three unknown constants (A_i, B_i, C_i) associated with the current expansion. One of these constants is eliminated by requiring that Kirchoff's current law be satisfied at junctions. (Between two adjacent wire segments, the requirement simply reduces to a continuity of current requirement.) A second constant is eliminated by requiring a condition on the charge to be satisfied at junctions. The condition used in NEC is the Wu-King charge jump condition given by (2.12). For two adjacent segments of the same radii, this condition corresponds simply to enforcement of continuity of charge at the junction. The actual implementation of these two conditions in NEC is somewhat involved for

general wire structures and the details can be found in [11]. The final result of applying the current and charge conditions, however, is that only one unknown constant related to the current amplitude on each segment remains to be evaluated via the method of moments. With this brief background, we now proceed to discuss the results obtained using NEC.

3.2 Numerical Results and Discussion

In this section we wish to determine if NEC's explicit enforcement of the charge jump condition (2.12) yields accurate current and charge distributions away from junction regions. The most reliable way to accomplish this appears to be to make direct graphical comparisons of results computed using NEC and using the baseline code PECØ. Simpler comparisons such as of the input admittance computed by both codes, have been found to be less reliable because the differences between the codes in numerical modeling of the source result in slightly different admittance values. Following the presentations of the graphical comparisons, an attempt is made to reduce the principal results of the data to a more compact form.

First, we describe the format of the data presented in this section. For all of the figures illustrating current and charge distributions, results obtained using NEC are plotted with different symbols for the real and imaginary parts. Results obtained using the baseline code PECØ are plotted as a solid line. In general, the number of unknowns

used in NEC is not specified, but this can be easily determined from the figures since each symbol represents the value of the current at the center of a subdomain. Of more importance is the subdomain width in terms of wire radii, which may be different on opposite sides of the junction. This information is given in most plots as $\Delta_i = Ca_i$, where Δ_i is the subdomain size and a_i is the radius of the i^{th} wire (Fig. 2.1) and C is the proportionality factor relating them. We note that the subdomain sizes indicated in the figures refer only to the two subdomains on either side of the junction.

We begin our comparisons by investigating stepped-radius antennas with various radii and ratios of radii, but with fixed lengths. The lengths of the structure considered are (c.f. Fig. 2.1) $kL_1 = 3.05$, $kL_2 = 3.2$, and $kL_3 = 0.6$, chosen so as to keep the source away from the junction region and to result in a charge maximum in the neighborhood of the junction. We first consider several cases for which the radius of the smaller wire (section 1) is $ka_1 = 0.0001$. Figs. 3.1 and 3.2 show, respectively, the current and charge distributions on such an antenna with $ka_2 = 0.000125$. The radius change in this case is very small and the agreement between PECØ and NEC is excellent. Figs. 3.3 and 3.4. show, respectively, the current and charge distributions with ka_2 increased to 0.001, representing a 10 to 1 change in radius. We note that there is a small difference in the current on

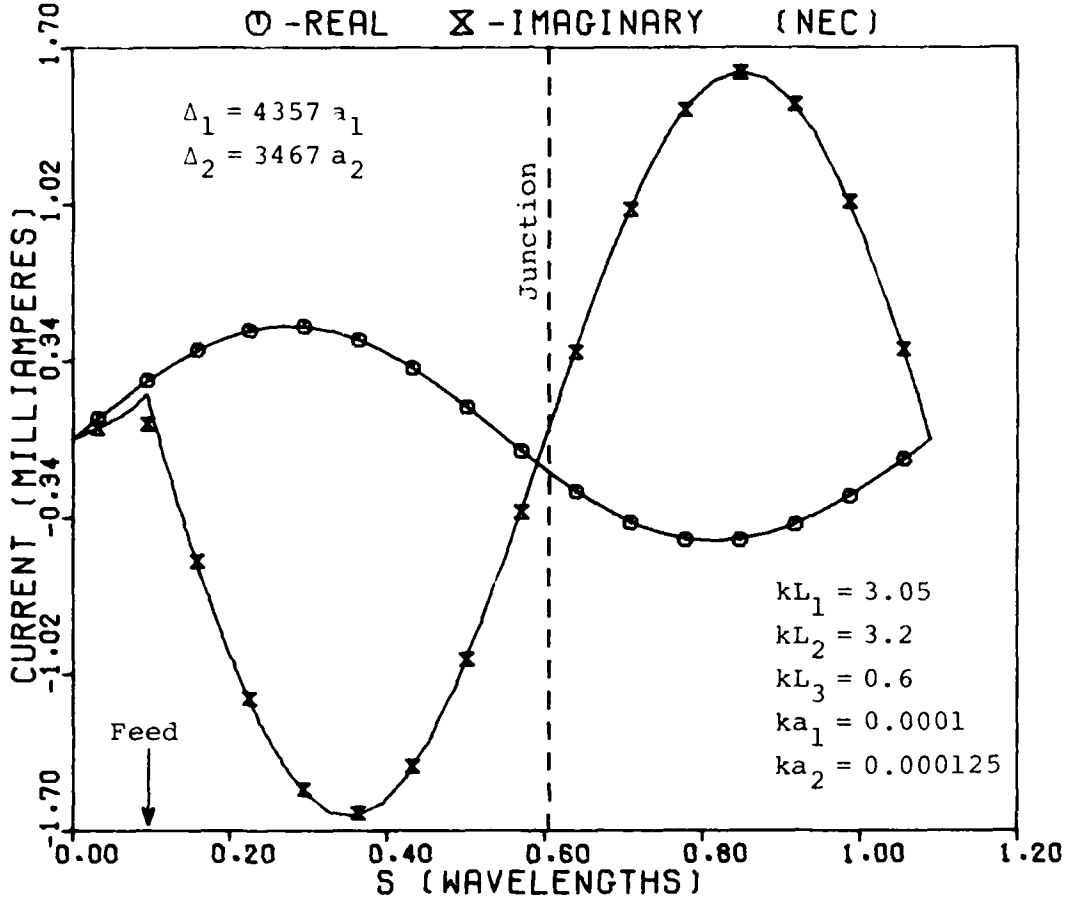

Figure 3.1. Comparison of calculated current distribution (NEC) with baseline code results for a very thin antenna having a radius change of ratio 1.25 to 1.0.

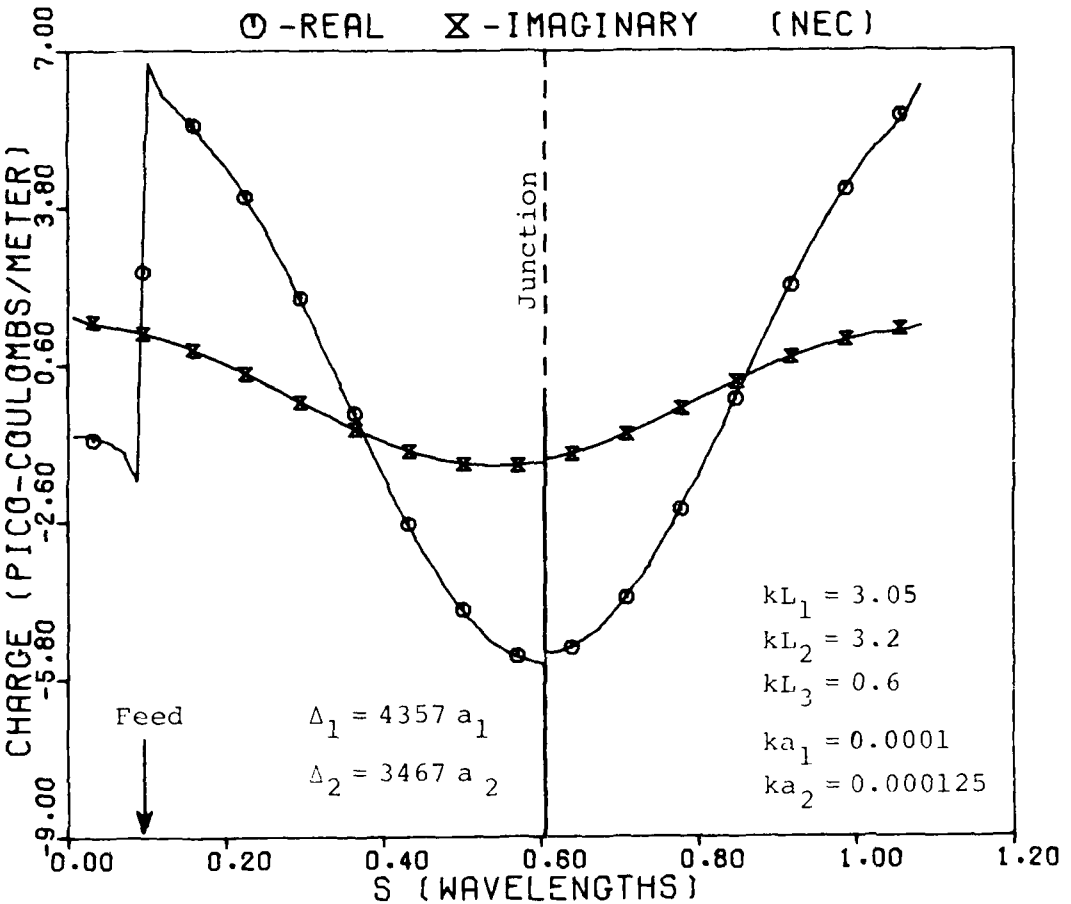

Figure 3.2. Comparison of calculated charge distribution (NEC) with baseline code results for a very thin antenna having a radius change of ratio 1.25 to 1.0.

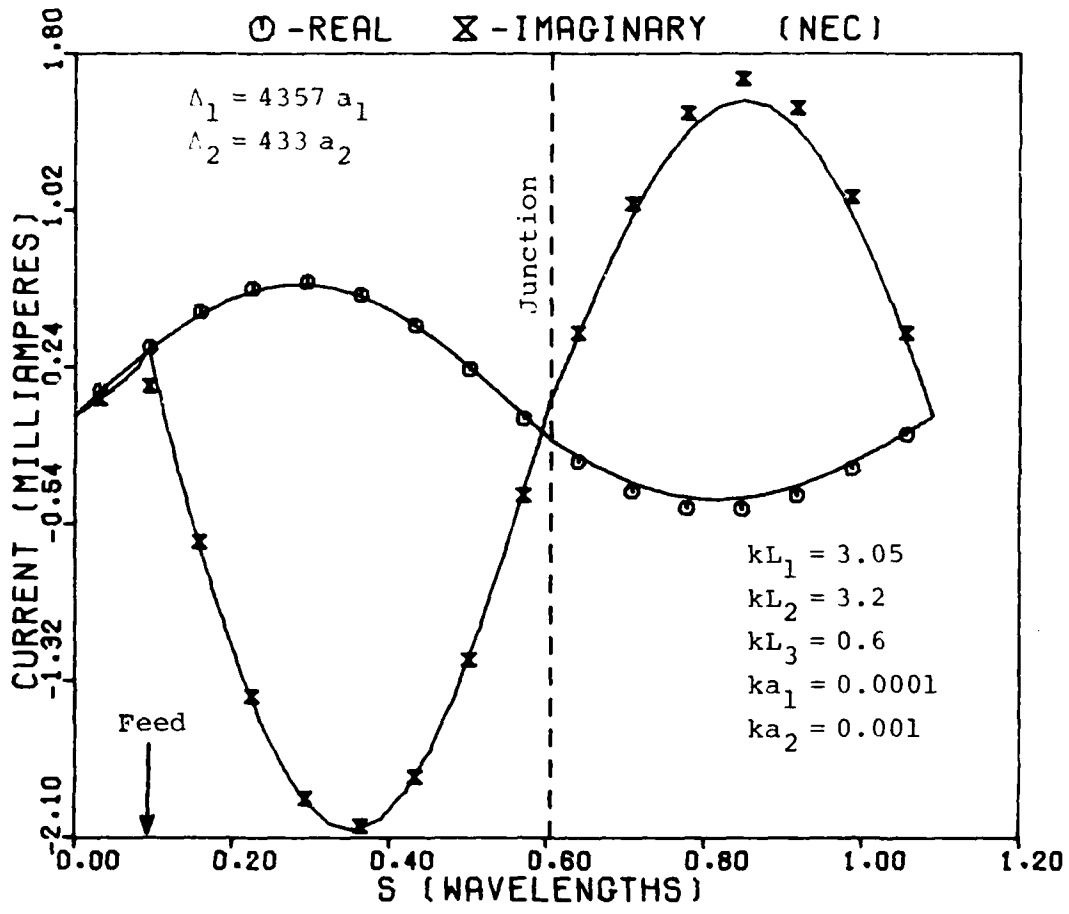

Figure 3.3. Comparison of calculated current distribution (NEC) with baseline code results for a very thin antenna having a radius change of ratio 10 to 1.

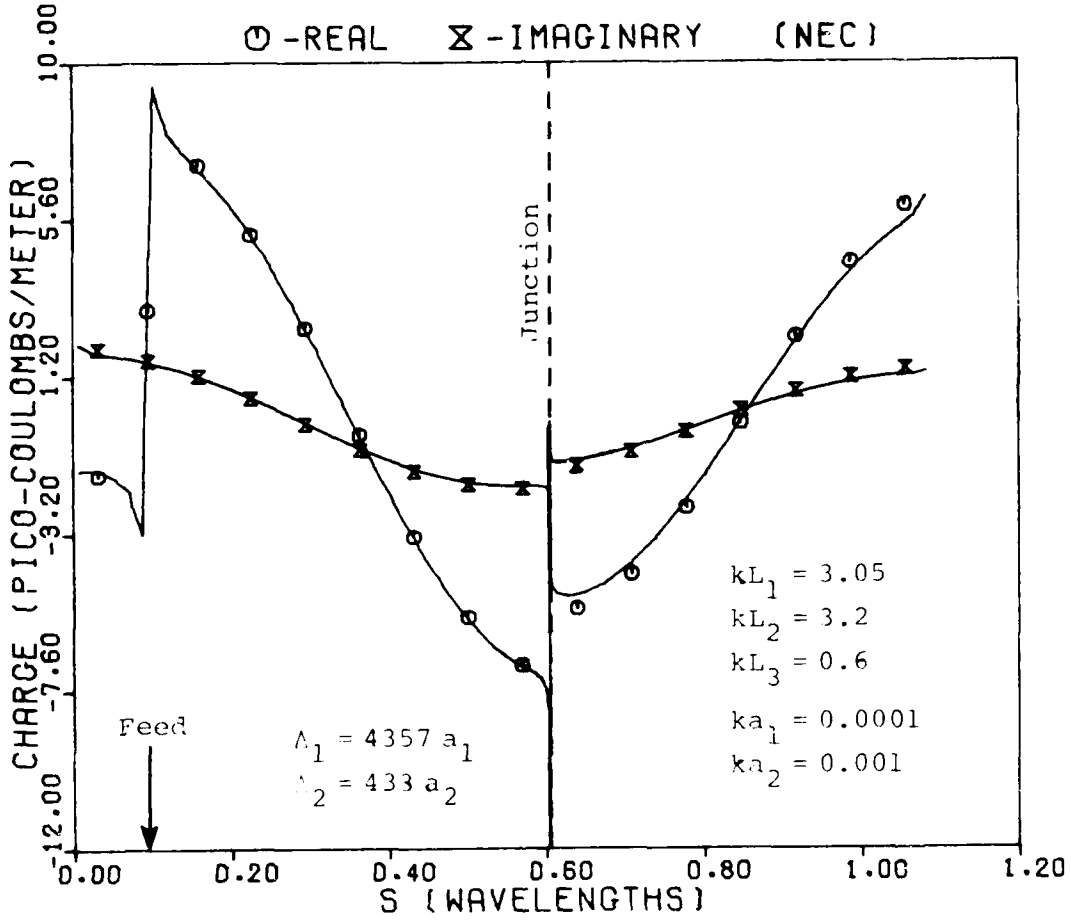

Figure 3.4. Comparison of calculated charge distribution (NEC) with baseline code results for a very thin antenna having a radius change of ratio 10 to 1.

the wire of smaller radius, whereas the current computed by NEC on the larger radius wire is in excellent agreement with that obtained from PECØ. The charge distribution on the wire with the smaller radius also shows a slight difference. Figs. 3.5 and 3.6 show the computed current and charge distributions which result when the radius of the larger wire is increased to $ka_2 = 0.01$. There is now a significant difference in the current on the section of the wire with smaller radius, but on the section with larger radius (which contains the source) the agreement is still excellent. (Note that although an input admittance comparison alone might show the methods to be in excellent agreement, comparison of the current and charge distributions shows that they are not.) Figs. 3.7 and 3.8 show current and charge distributions for the same structure calculated with NEC when a very large number of unknowns (48) is used. The differences between results calculated by NEC and PECØ are even greater in these figures. The use of so many unknowns is, of course, impractical on such a short antenna under normal conditions but here serves to illustrate a point. Upon close inspection of the charge distribution calculated by NEC (Fig. 3.8), one observes the same type of behavior in the junction region as was observed with our thin-wire approach in Section II; namely, the charge seems to attempt to satisfy the true edge behavior at the junction. On the other hand, the Wu-King charge jump condition has also been enforced and the two conditions are incompatible. One

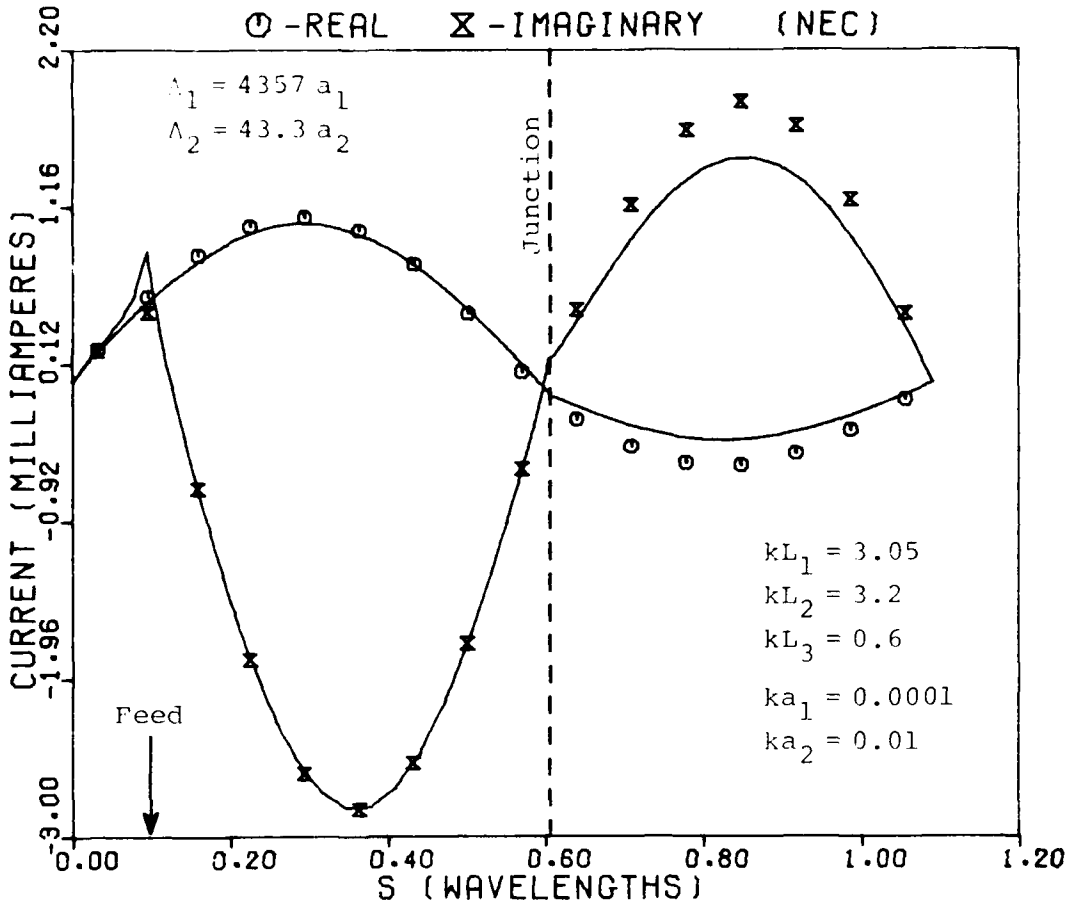

Figure 3.5. Comparison of calculated current distribution (NEC) with baseline code results for a thin wire having a radius change of ratio 100 to 1.

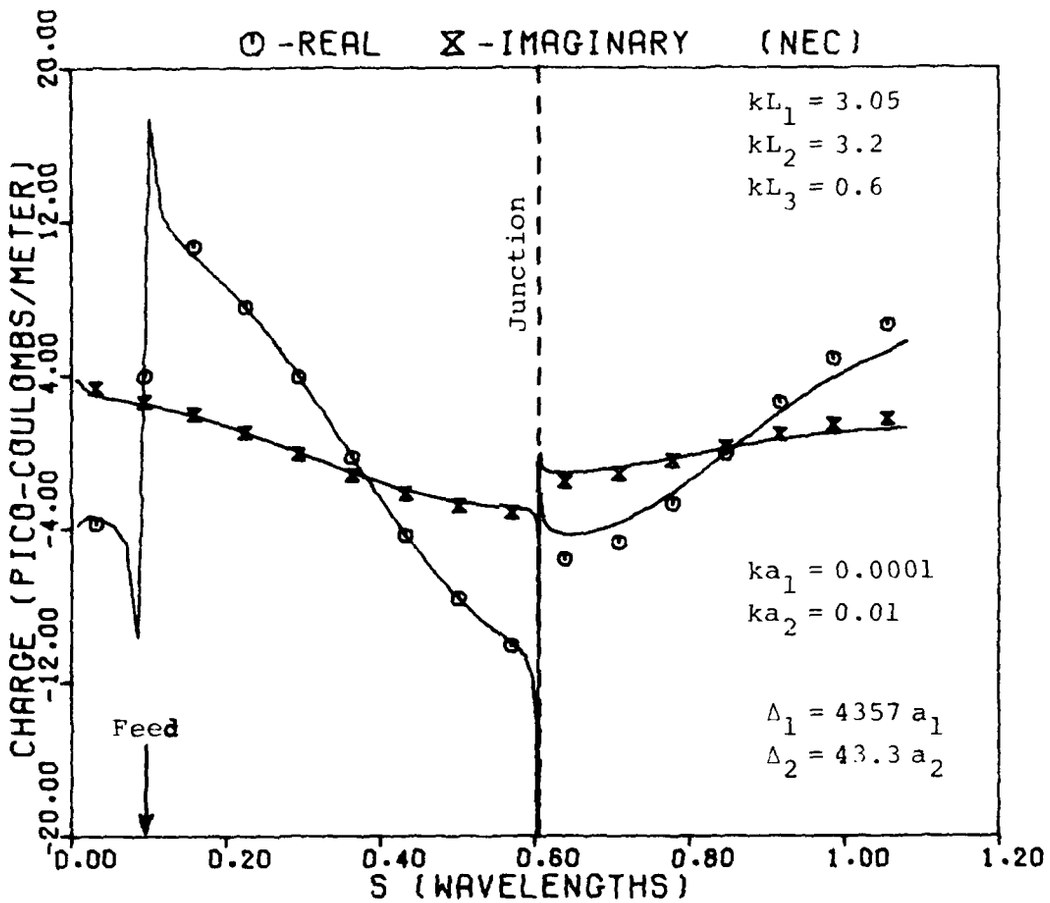

Figure 3.6. Comparison of calculated charge distribution (NEC) with baseline code results for a thin wire having a radius change of ratio 100 to 1.

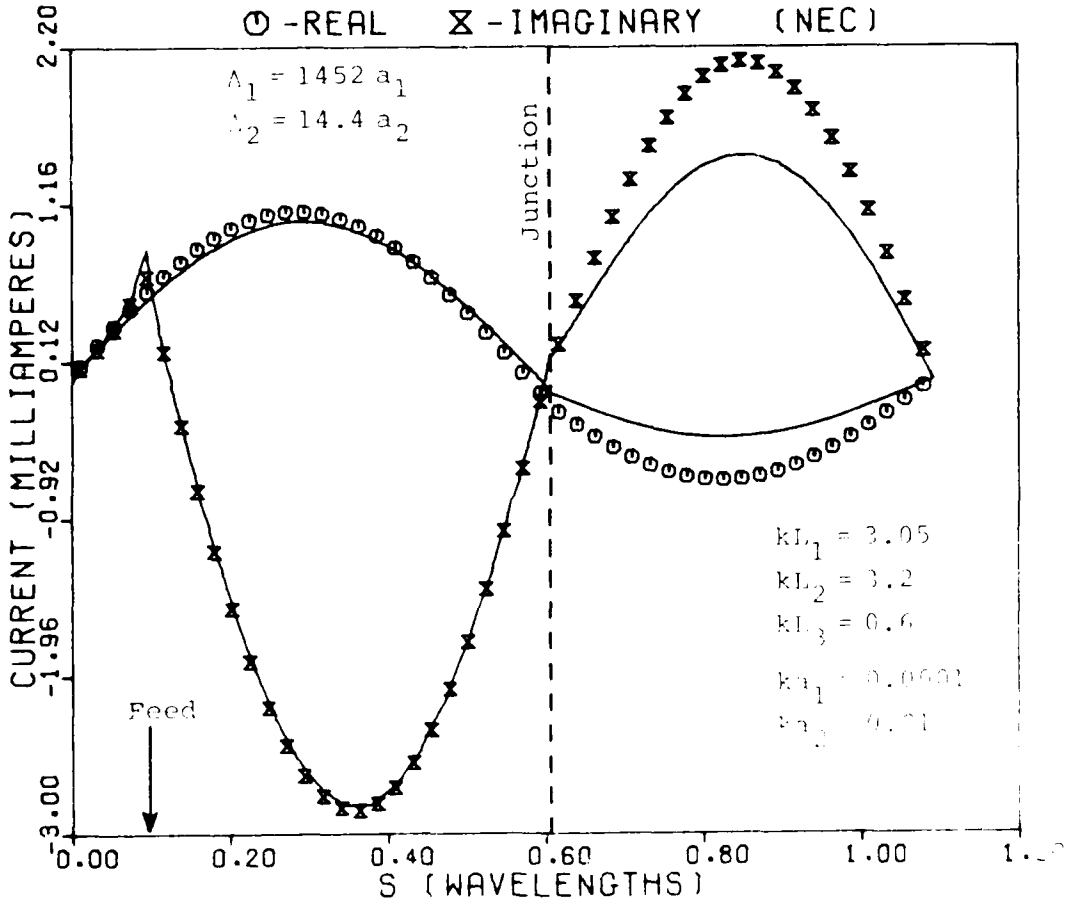

Figure 3.7. Comparison of calculated current distribution (NEC; increased number of unknowns) with baseline code results for a thin wire having a radius change of ratio 100 to 1.

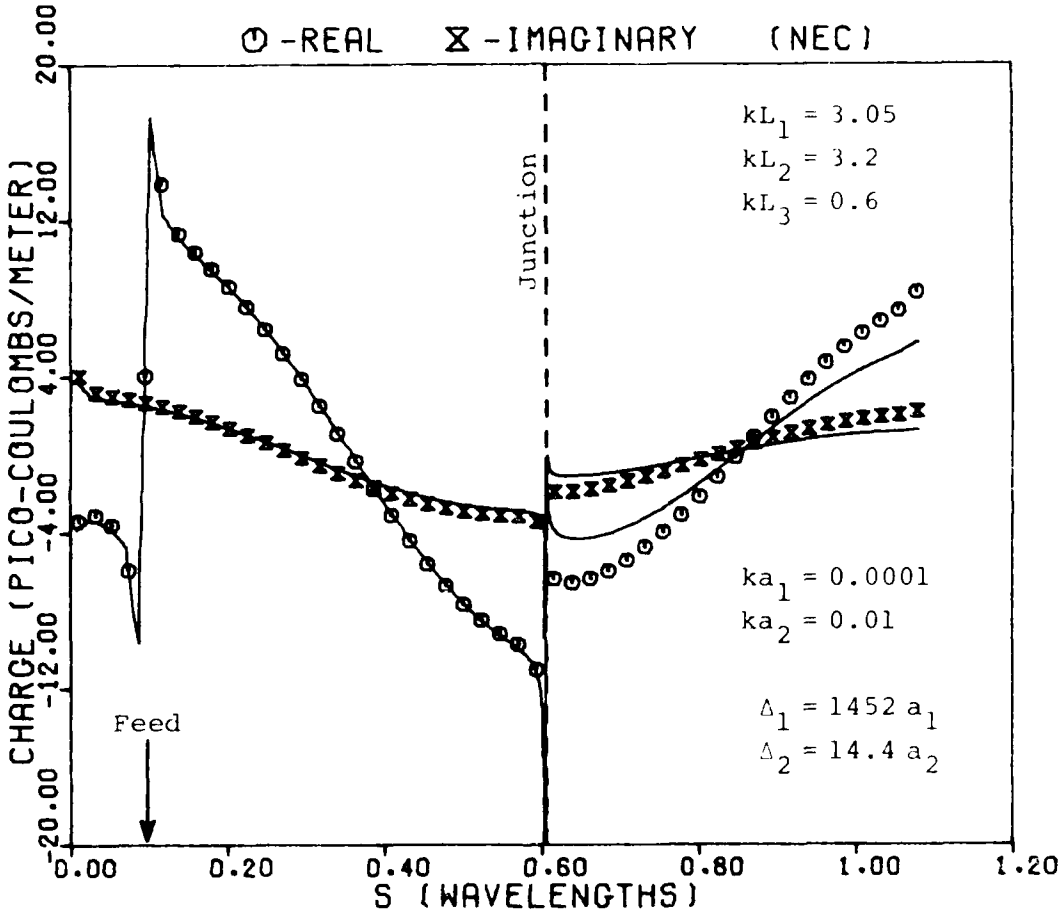

Figure 3.8. Comparison of calculated charge distribution (NEC; increased number of unknowns) with baseline code results for a thin wire having a radius change of ratio of 100 to 1.

would normally expect that these inconsistencies would manifest themselves as erroneous currents whenever matchpoints for NEC were located within a few radii (e.g., five times the radius of the larger wire) from the junction. Unfortunately, as reference to Figs. 3.3 and 3.4 shows, the region in which effects of the junction (edge conditions) on the current and charge seem to come into play can be much greater that this. Observation of a great deal of data has indicated to us that the actual distance from the junction at which such effects become negligible seems to depend on a number of factors such as the wire lengths, wire radii and their ratio. Broadly speaking, however, at a charge maximum the extent of the edge effects region appears to be a maximum as well. A comment is in order concerning the appearance of the error only on the thinner wire in these and subsequent figures.

The difference in the current distributions obtained by NEC and PECØ in Figs. 3.5 and 3.7 may be thought of as arising from an effective voltage source located at the junction. The strength of this effective source could be determined by calculating and taking the difference of the voltage appearing across the junction in the two numerical approaches. Because we must also take the differences of sources, the original delta-gap sources cancel (assuming equivalent modeling of the gap). We would then expect the resulting difference or "error" current distribution produced by the effective source at the junction to be a complicated function of the radii a_1 and a_2 and the two wire lengths, L_1 and

$L_2 + L_3$. We attribute the appearance of the "error" current only on the thinner wire in Figs. 3.5-3.8 and in many of the subsequent figures merely to our choice of a half-wavelength length ($kL_1 = 3.05$) for the thinner wire.

Next, let us consider two cases for which the radius of the smaller wire is increased to $ka_1 = 0.001$. Figs. 3.9 and 3.10 show the current and charge distributions on a structure with $ka_2 = 0.00125$, representing very small change in radius. The agreement between PECØ and NEC is again excellent. Figs. 3.11 and 3.12 compare results when the radius of the larger wire is increased to $ka_2 = 0.01$. For this 10 to 1 change in radius, the current distribution calculated using NEC begins to differ significantly from that of the baseline code on the segment with the smaller radius. (Note again that agreement is excellent on the segment with the larger radius.)

The above results are typical of a large number of observed cases. One might expect that for thicker wires, less radical changes in radii can be made before edge effects contaminate NEC current distributions. Figs. 3.13 and 3.14 show current and charge distributions on a rather thick wire for a very small change in radius: $ka_1 = 0.01$, $ka_2 = 0.0125$. The agreement between NEC and PECØ is excellent. However, when the radius of the thicker segment is increased to $ka_2 = 0.05$, one obtains the poorly agreeing distributions shown in Figs. 3.15 and 3.16. Thus on thicker wires, erroneous currents appear with NEC for less severe radius changes.

Consider next the same wire as in Fig. 3.11 but with the radius of the thicker wire increased to $ka_2 = 0.05$ (i.e.,

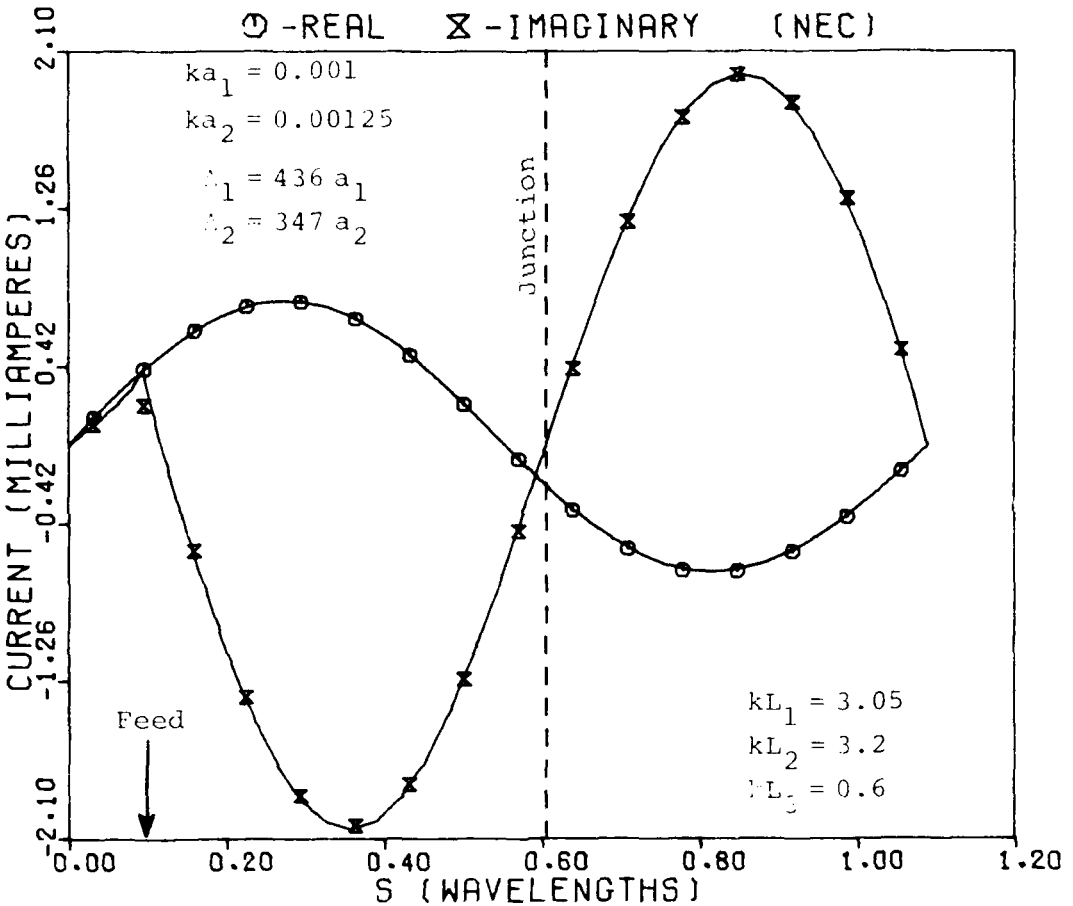

Figure 3.9. Comparison of calculated current distribution (NEC) with baseline code results for a thin wire having a radius change of ratio 1.25 to 1.

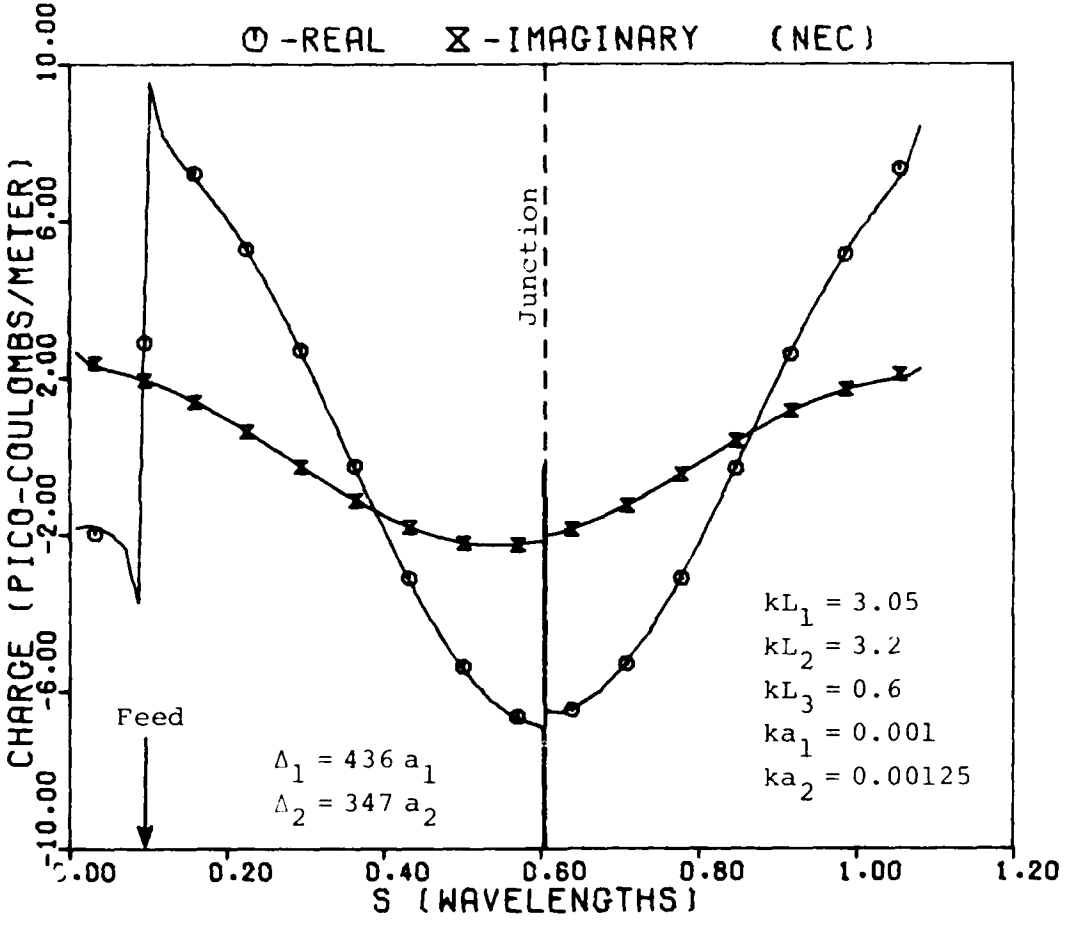

Figure 3.10. Comparison of calculated charge distribution (NEC) with baseline code results for a thin wire having a radius change of ratio 1.25 to 1.

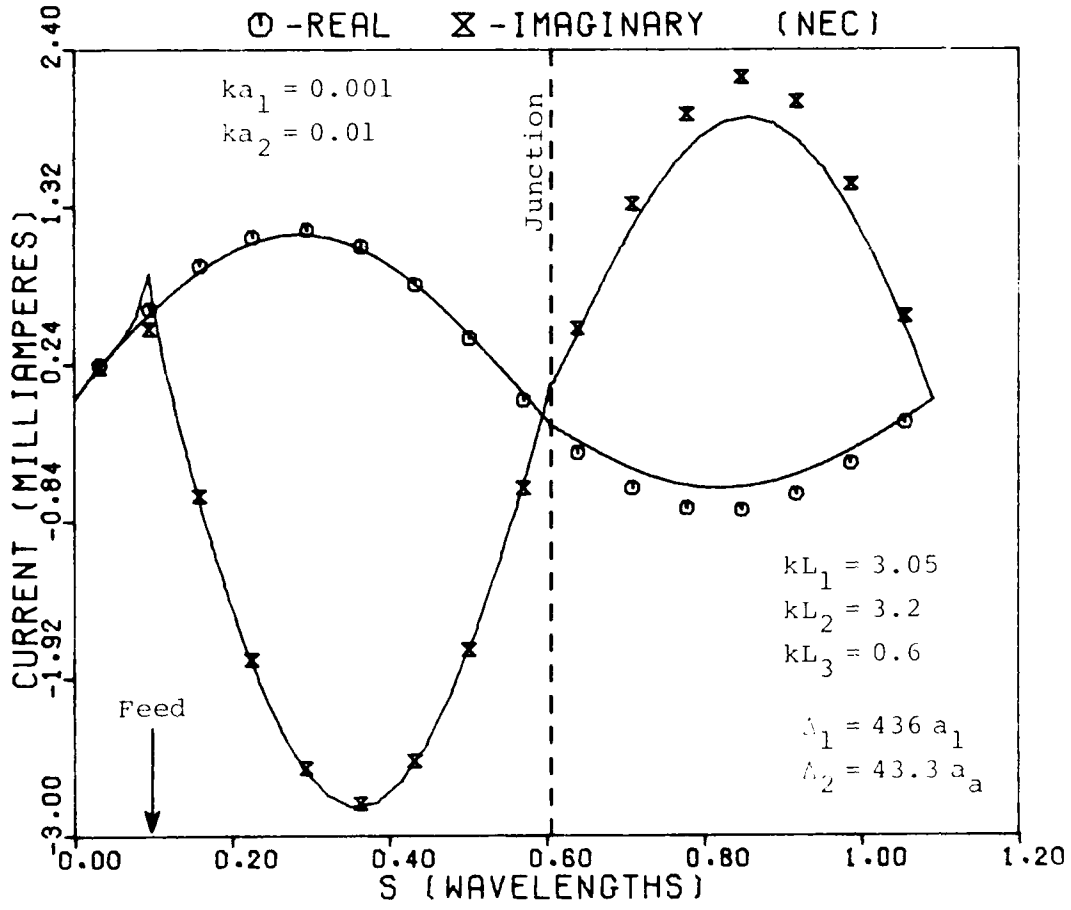

Figure 3.11. Comparison of calculated current distribution (NEC) with baseline code results for a thin wire having a radius change of ratio 10 to 1.

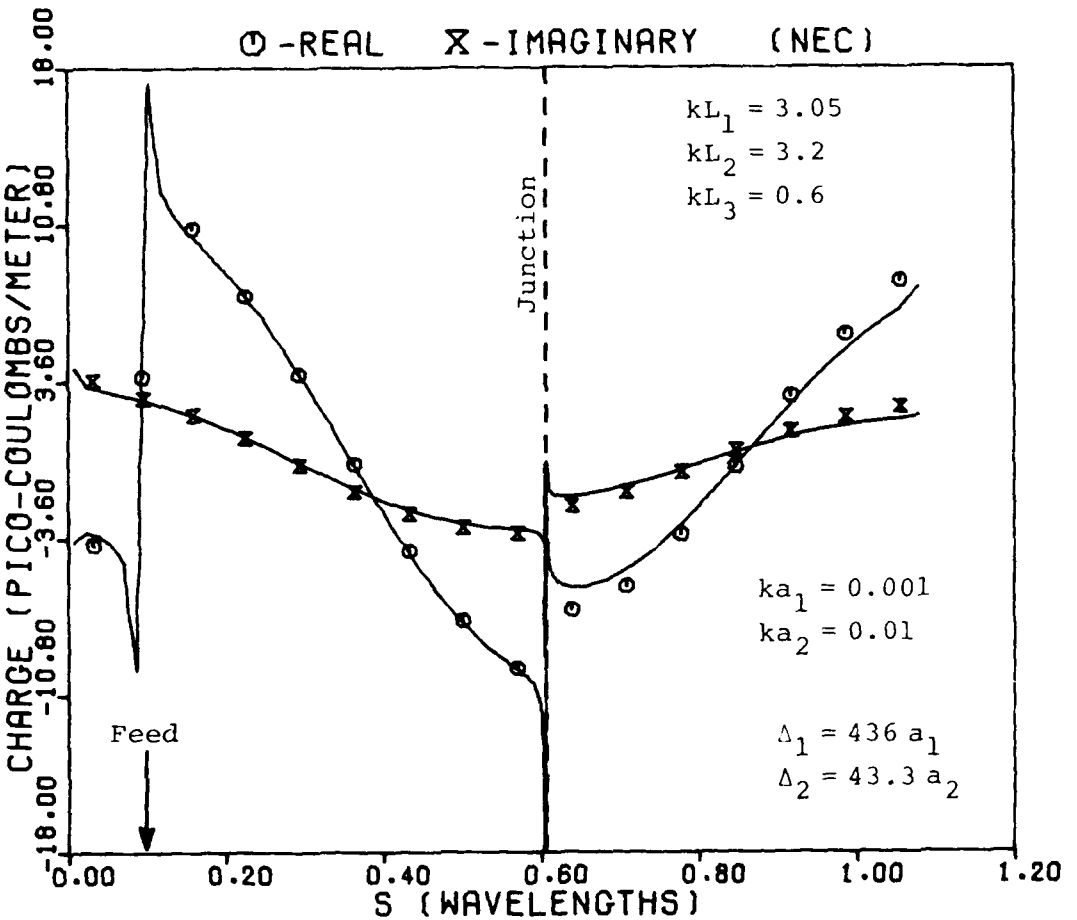

Figure 3.12. Comparison of calculated charge distribution (NEC) with baseline code results for a thin wire having a radius change of ratio 10 to 1.

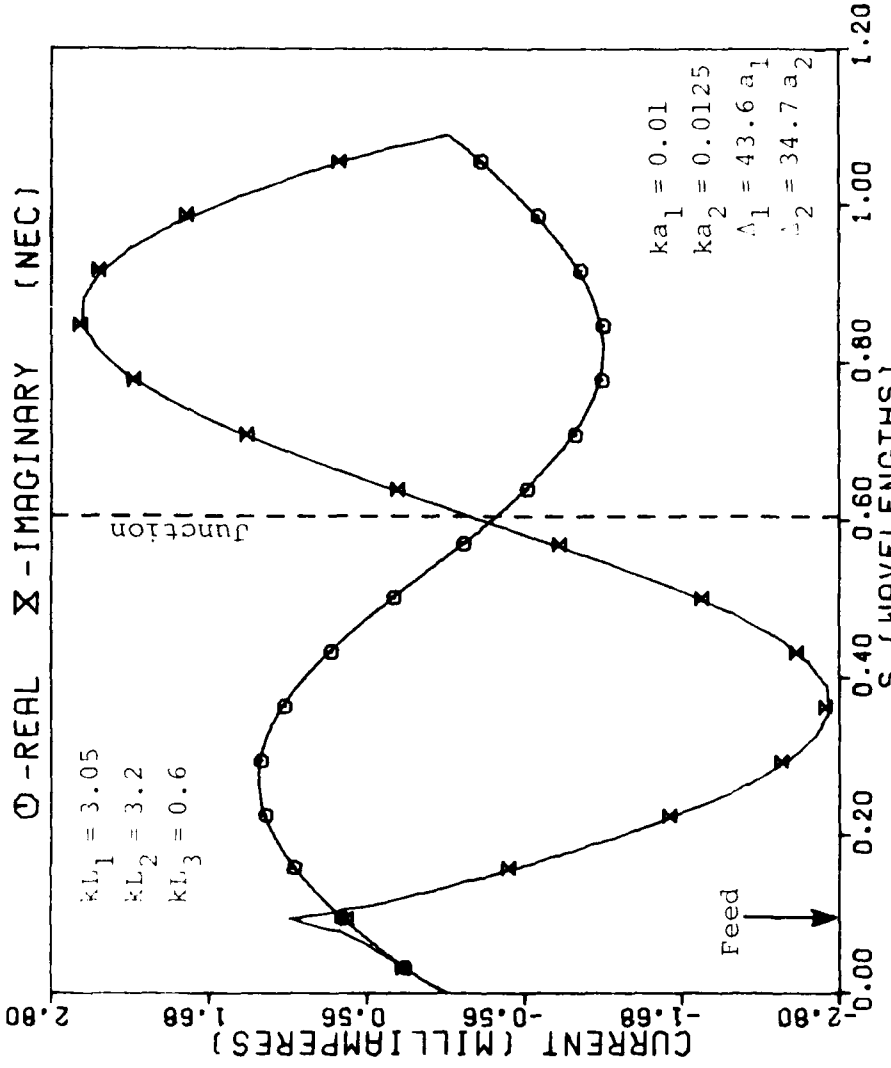

Figure 3.13. Comparison of calculated current distribution (NEC) with baseline code results for a fairly thick wire having a radius change of ratio 1.25 to 1.

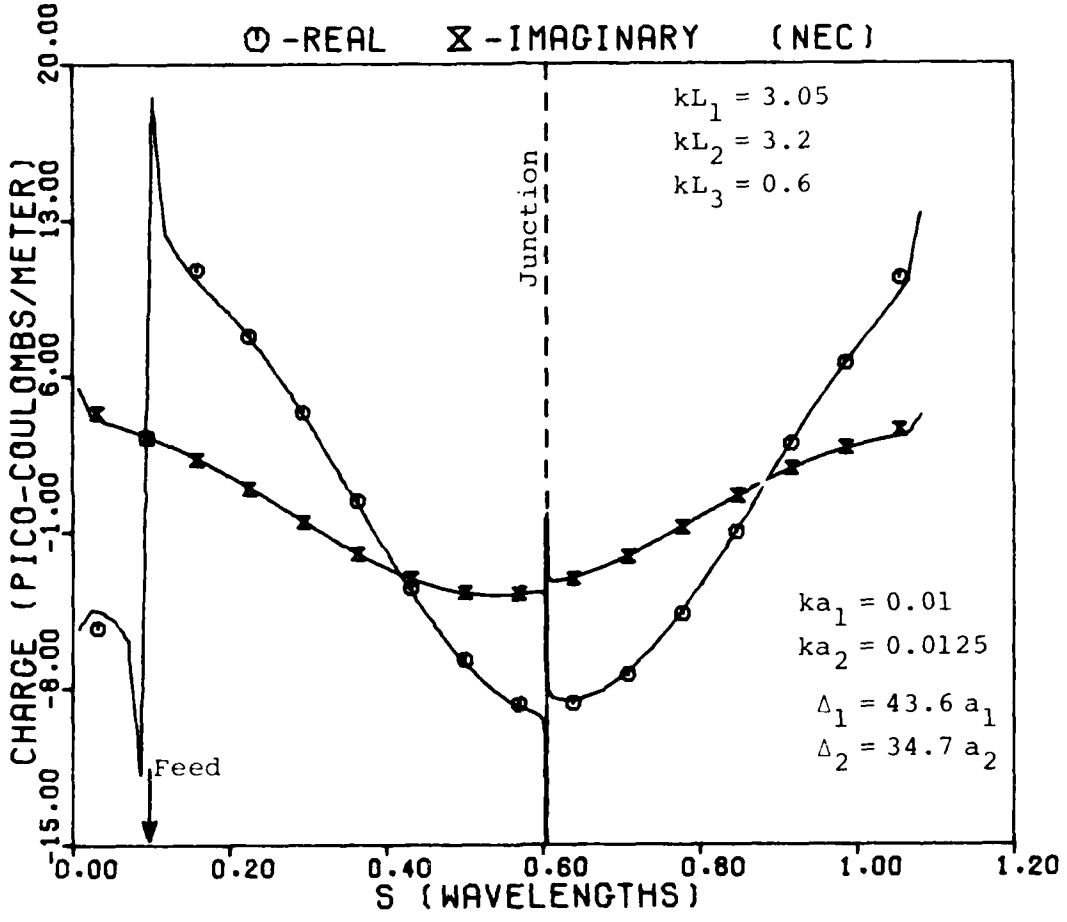

Figure 3.14. Comparison of calculated charge distribution (NEC) with baseline code results for a fairly thick wire having a radius change of ratio 1.25 to 1.

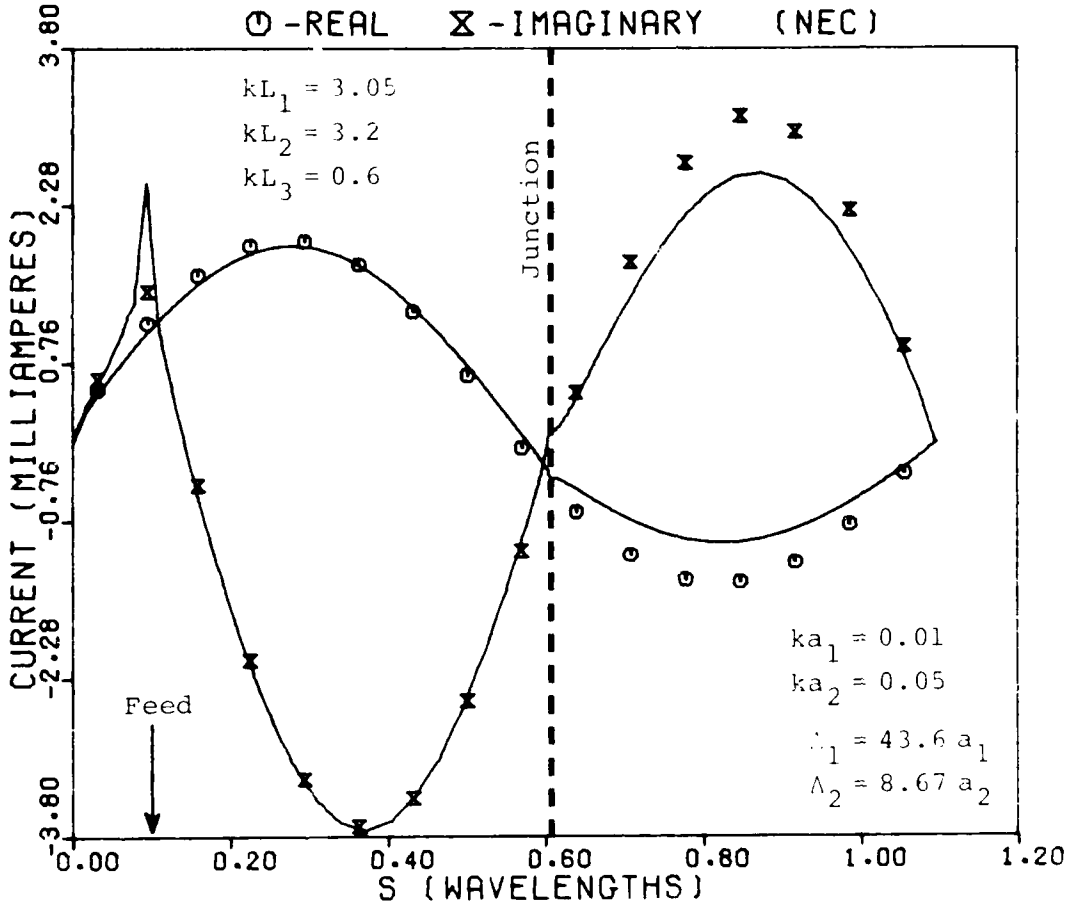

Figure 3.15. Comparison of calculated current distribution (NEC) with baseline code results for a fairly thick wire having a radius change of ratio 5 to 1.

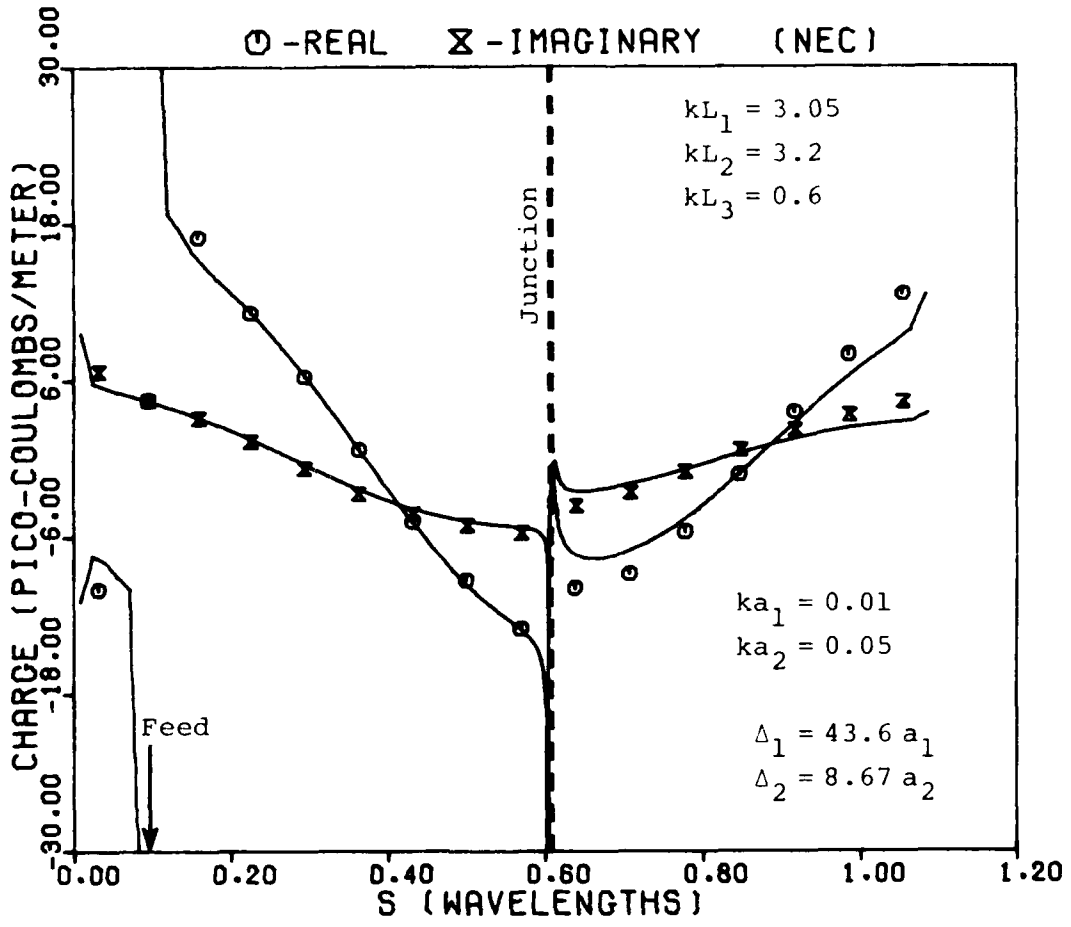

Figure 3.16. Comparison of calculated charge distribution (NEC) with baseline code results for a fairly thick wire having a radius change of ratio 5 to 1.

the radius change at the junction is a ratio of 50 to 1). Figs. 3.17 and 3.18 show the current and charge distributions obtained for this case. As we have seen before currents in Fig. 3.17 are significantly in error (≈ 50% error) on the segment of wire with the smaller radius, but again agree well with the baseline code results on the segment of larger radius (which contains the feed point). If the values of the wire radii are simply reversed, i.e. the driven segment becomes the thin wire ($ka_2 = 0.001$) and the undriven segment becomes the thick wire ($ka_1 = 0.05$), the current and charge distributions of Figs. 3.19 and 3.20 result. In the figures, one observes that the current calculated with NEC on the segment with the larger radius differs significantly from that predicted by the baseline code. On the segment having the smaller radius the real part of the current calculated by NEC agrees well with the baseline code result, while the imaginary part shows a slight shift toward the source region. Thus it is not true, as one might be led to suspect from the previous results, that the error tends to be localized on the thinner wire. As we have noted earlier, the error current distribution probably depends on the radii and lengths of the two segments as well as the source location.

For all the cases considered thus far, the junction has been located such that a charge maximum occurs at or near the junction region (discounting the region very near the junction where an infinite charge occurs). We have purposely

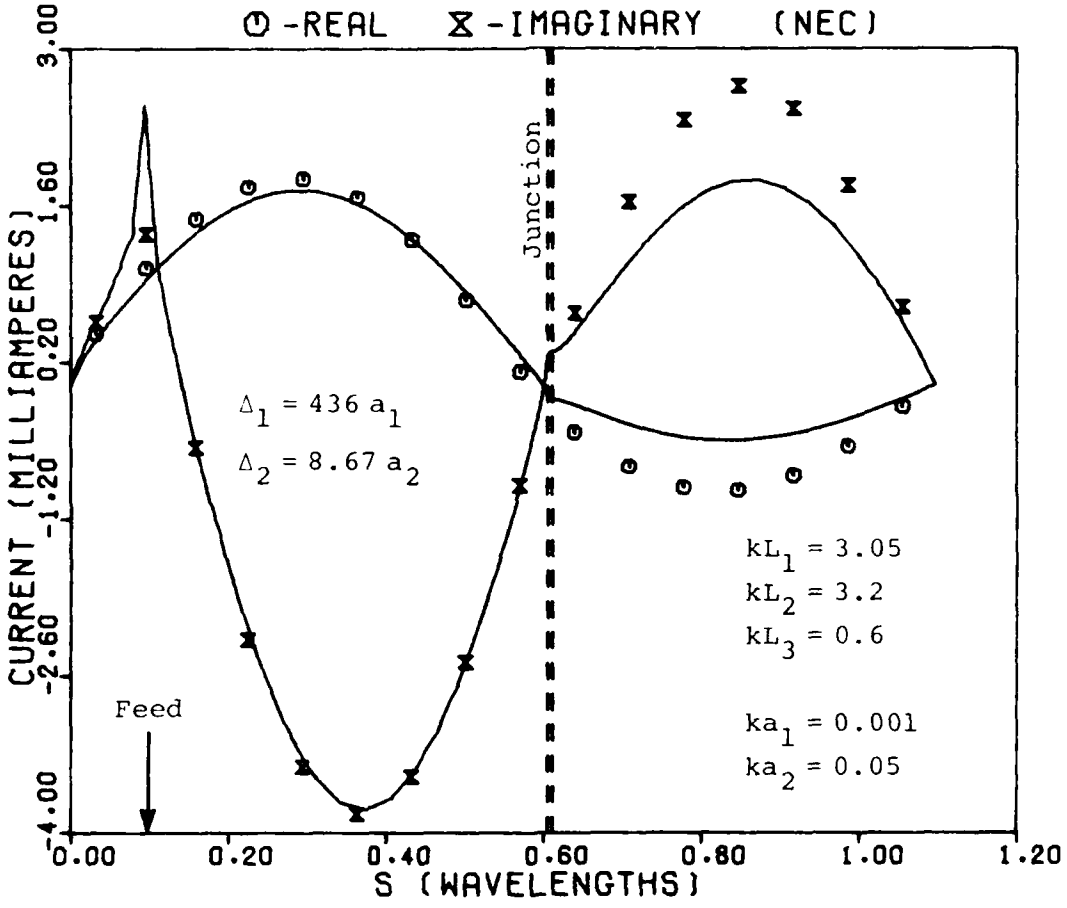

Figure 3.17. Comparison of calculated current distribution (NEC) with baseline code results for a stepped-radius antenna having a radius change of ratio 50 to 1, where the source is located on the section with the larger radius.

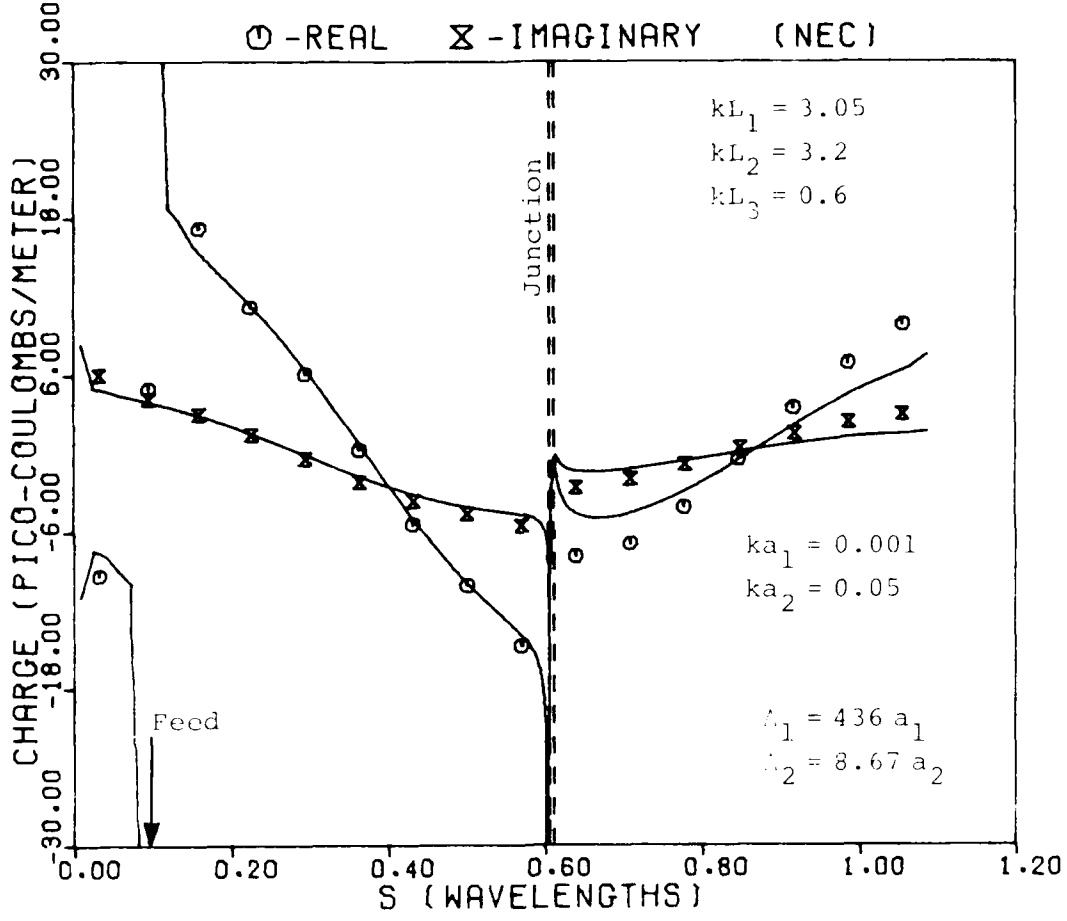

Figure 3.18. Comparison of calculated charge distribution (NEC) with baseline code results for a stepped-radius antenna having a radius change of ratio 50 to 1, where the source is located on the section with the larger radius.

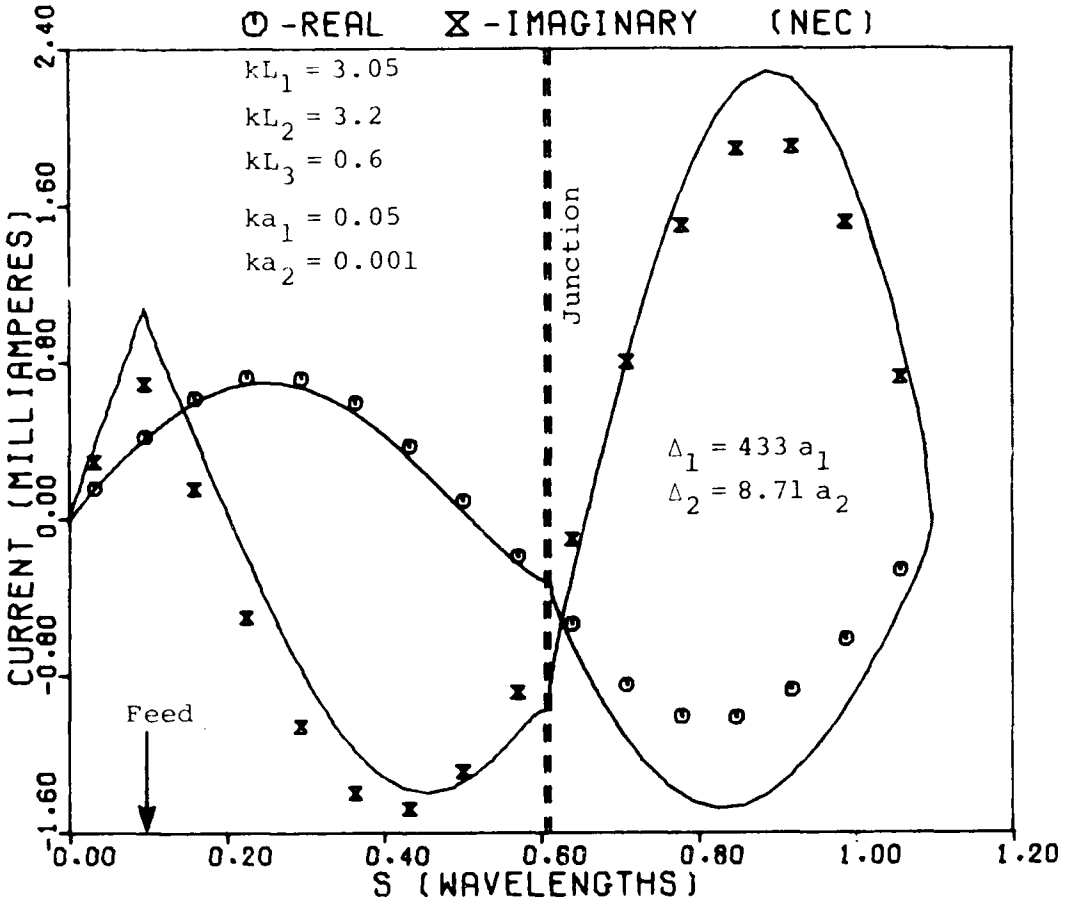

Figure 3.19. Comparison of calculated current distribution (NEC) with baseline code results for a stepped-radius antenna having a radius change of ratio 50 to 1, where the source is located on the section with the smaller radius.

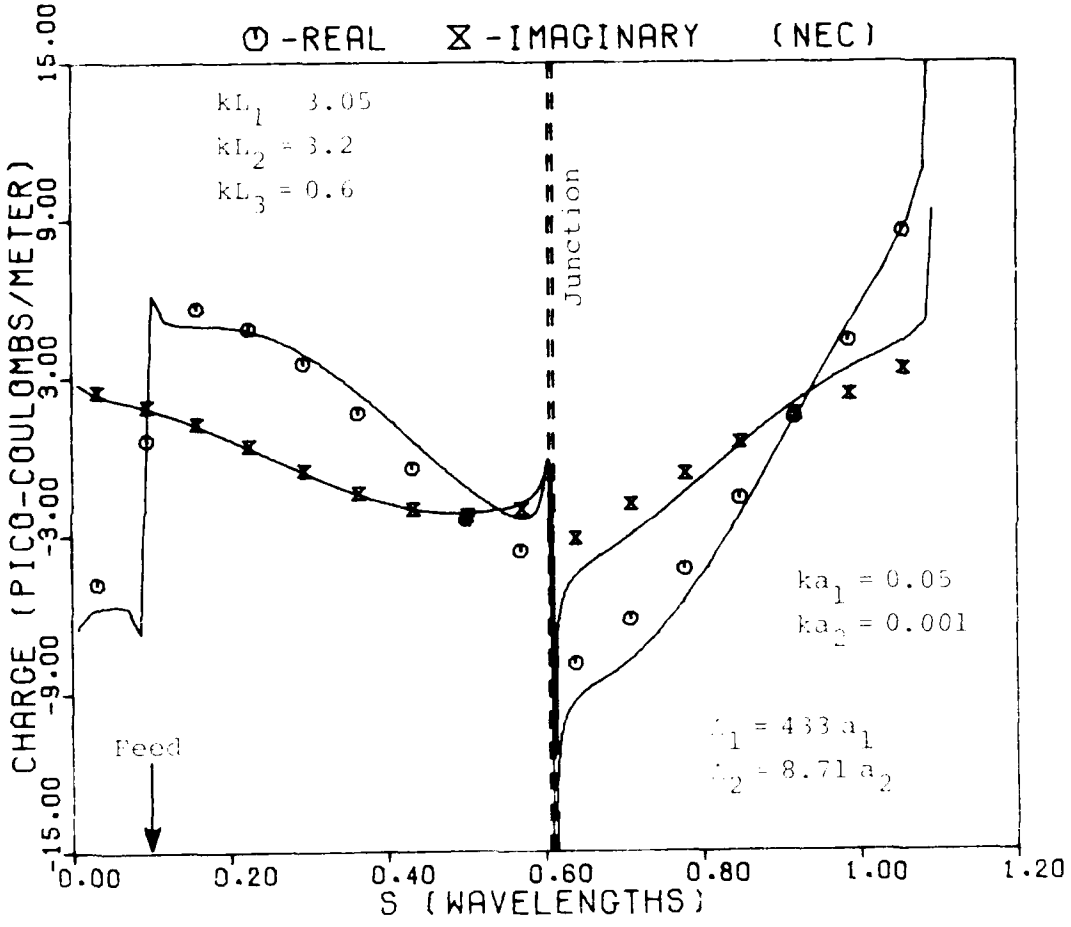

Figure 3.20. Comparison of calculated charge distribution (NEC) with baseline code results for a stepped-radius antenna having a radius change of ratio 50 to 1, where the source is located on the section with the smaller radius.

AD-A097 327 MISSISSIPPI UNIV UNIVERSITY DEPT OF ELECTRICAL ENGIN--ETC F/G 20/3
NUMERICAL PROCEDURES FOR HANDLING STEPPED-RADIUS WIRE JUNCTIONS--ETC(U)
MAR 79 A W GLISSON, D R WILTON N66001-77-C-0156

UNCLASSIFIED NL

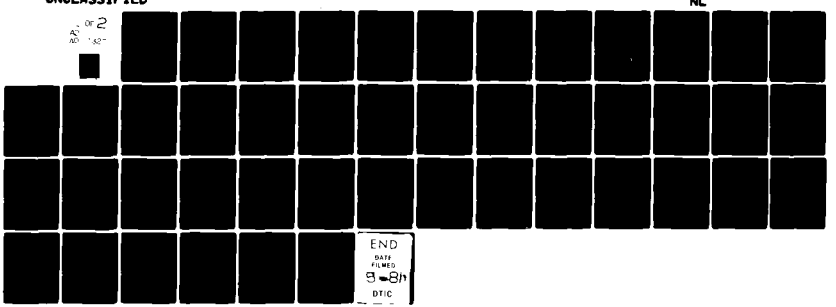

limited ourselves to such cases to illustrate the influence of the junction region primarily because it has been found that an accurate treatment of the charge is more critical near a charge maximum. To illustrate, consider Figs. 3.21 and 3.22, which show the current and charge distributions on a stepped-radius antenna structure for which the junction is located near a charge minimum (again, discounting the region in the neighborhood of the junction). The radii are the same as in Fig. 3.17 ($ka_1 = 0.001$, $ka_2 = 0.05$) so that there is a 50 to 1 change in radius at the junction. The lengths of the various wire sections are $kL_1 = 4.7$, $kL_2 = 3.2$, and $kL_3 = 0.6$. We note that although there is some difference between results calculated using NEC and those of the baseline code PECØ, the differences are much less significant than those exhibited in Figs. 3.17 through 3.20, where the same radii but different wire lengths are employed.

We have also considered cases for which the junction is placed near the feed point or near the end of the antenna. These results have generally shown the same trends as those presented in Figs. 3.1 through 3.18 except that the current distributions calculated by NEC appear to be affected slightly more than for a similar change in radius occuring away from ends or sources. The current and charge distributions for two sample cases are presented in Figs. 3.23 through 3.26. For these two cases the step change in radius is located approximately 0.1λ from the source. Observations of a number

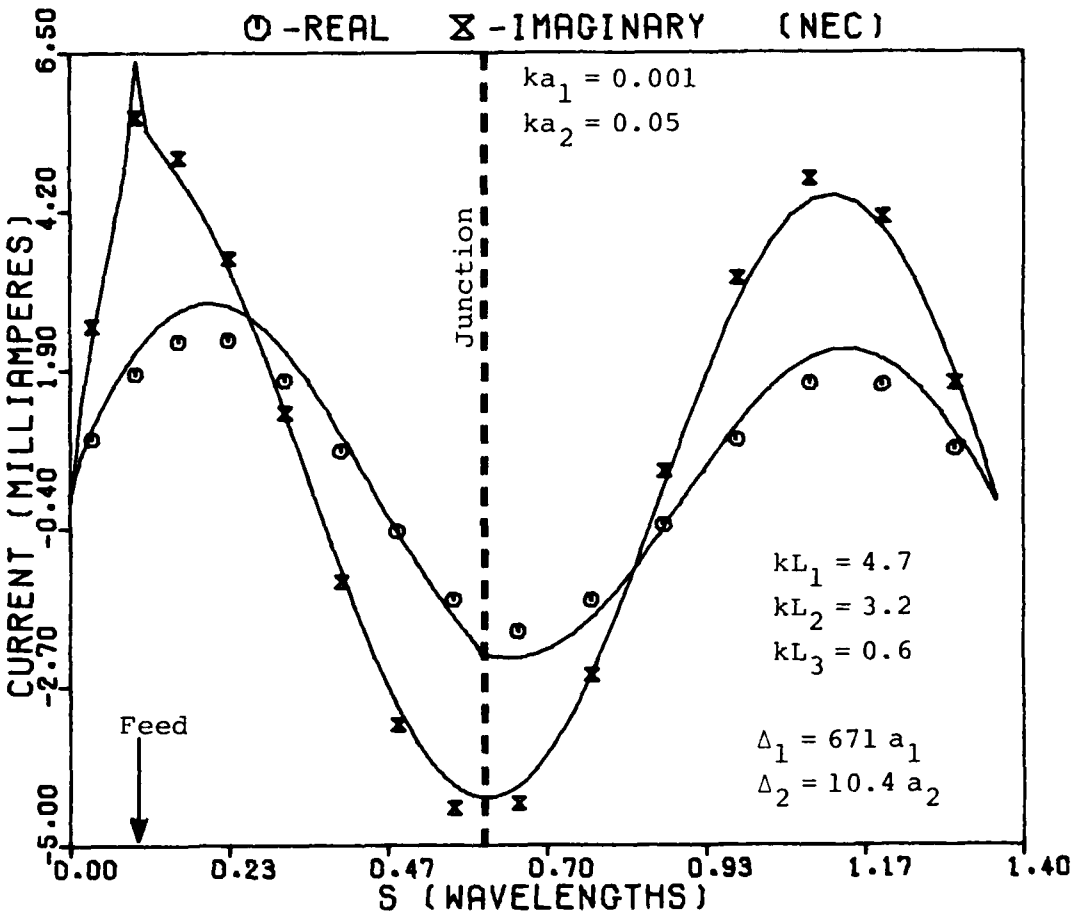

Figure 3.21. Comparison of calculated current distribution (NEC) with baseline code results for a stepped-radius antenna having a radius change of ratio 50 to 1, where the change in radius occurs near a charge minimum.

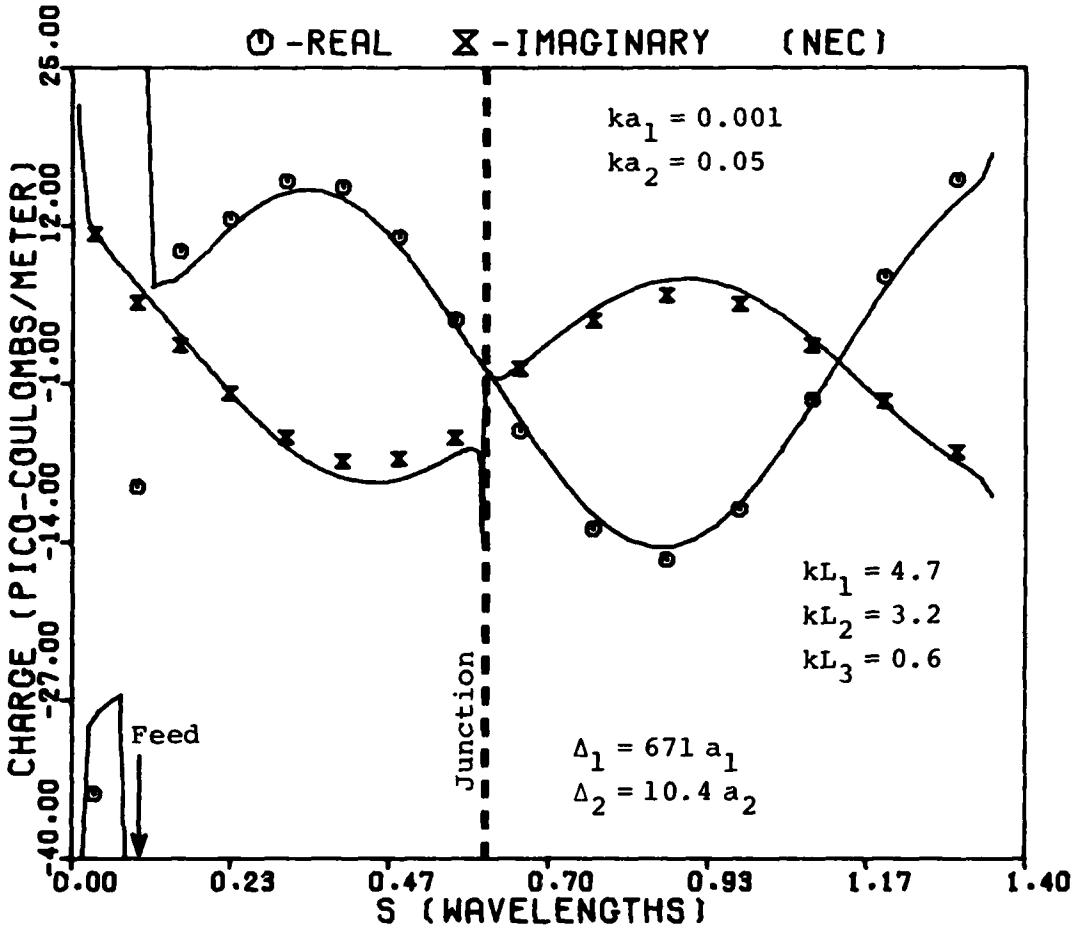

Figure 3.22. Comparison of calculated charge distribution (NEC) with baseline code results for a stepped-radius antenna having a radius change of ratio 50 to 1, where the change in radius occurs near a charge minimum.

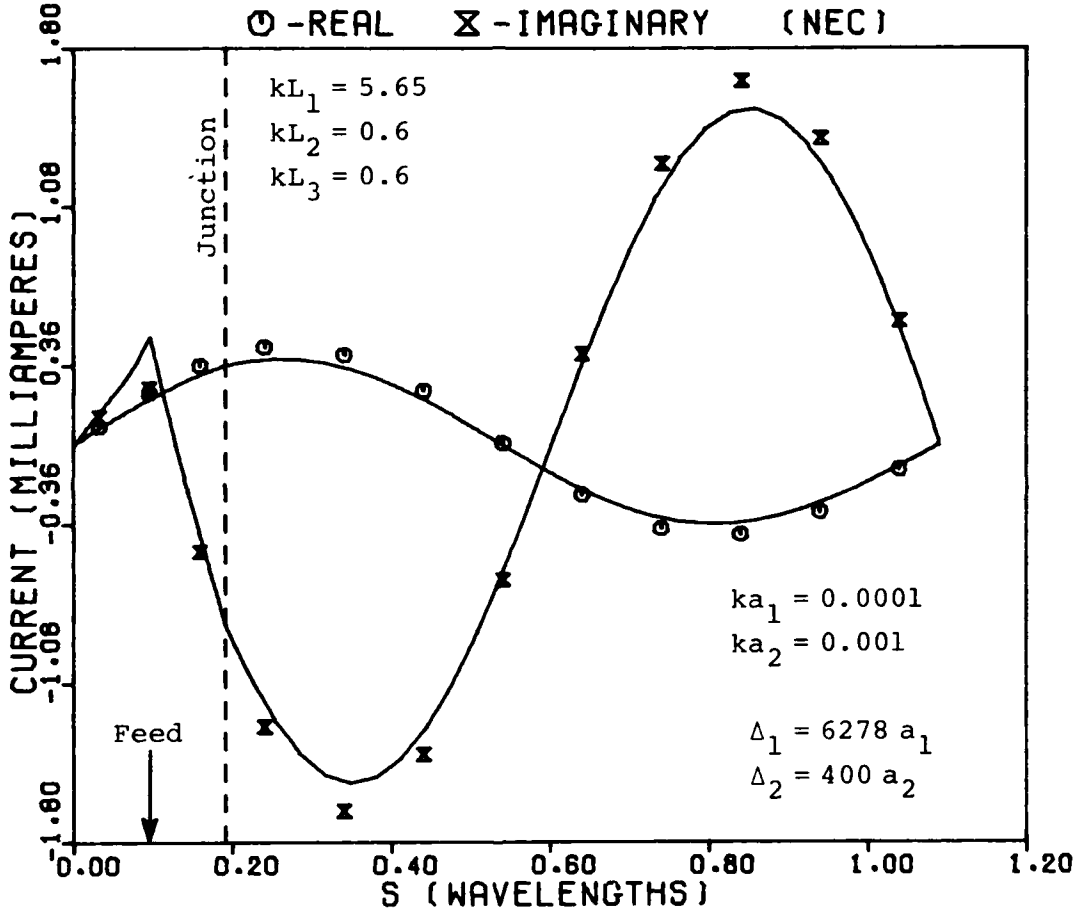

Figure 3.23. Comparison of calculated current distribution (NEC) with baseline code results for a very thin antenna having a radius change of ratio 10 to 1 approximately one-tenth wavelength away from the feed.

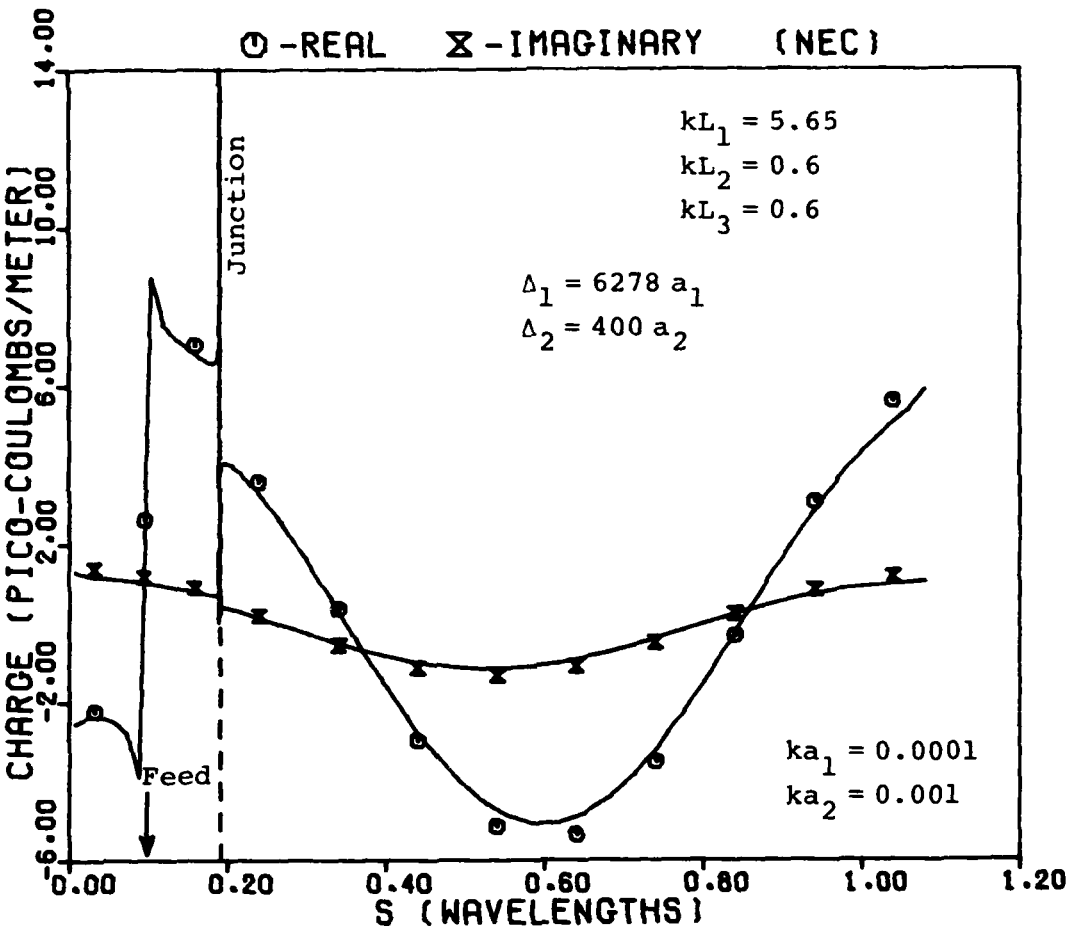

Figure 3.24. Comparison of calculated charge distribution (NEC) with baseline code results for a very thin antenna having a radius change of ratio 10 to 1 approximately one-tenth wavelength away from the feed.

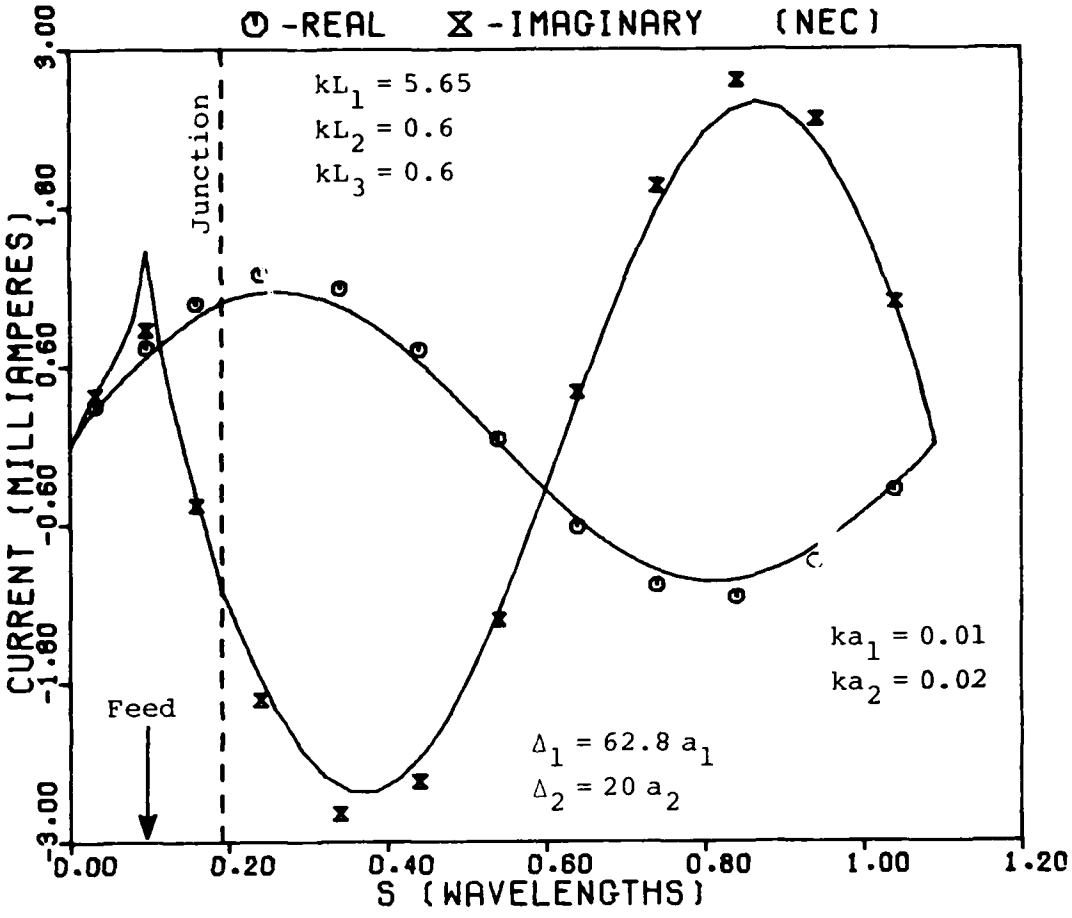

Figure 3.25. Comparison of calculated current distribution (NEC) with baseline code results for a stepped-radius antenna having a radius change of ratio 2 to 1 approximately one-tenth wavelength away from the feed.

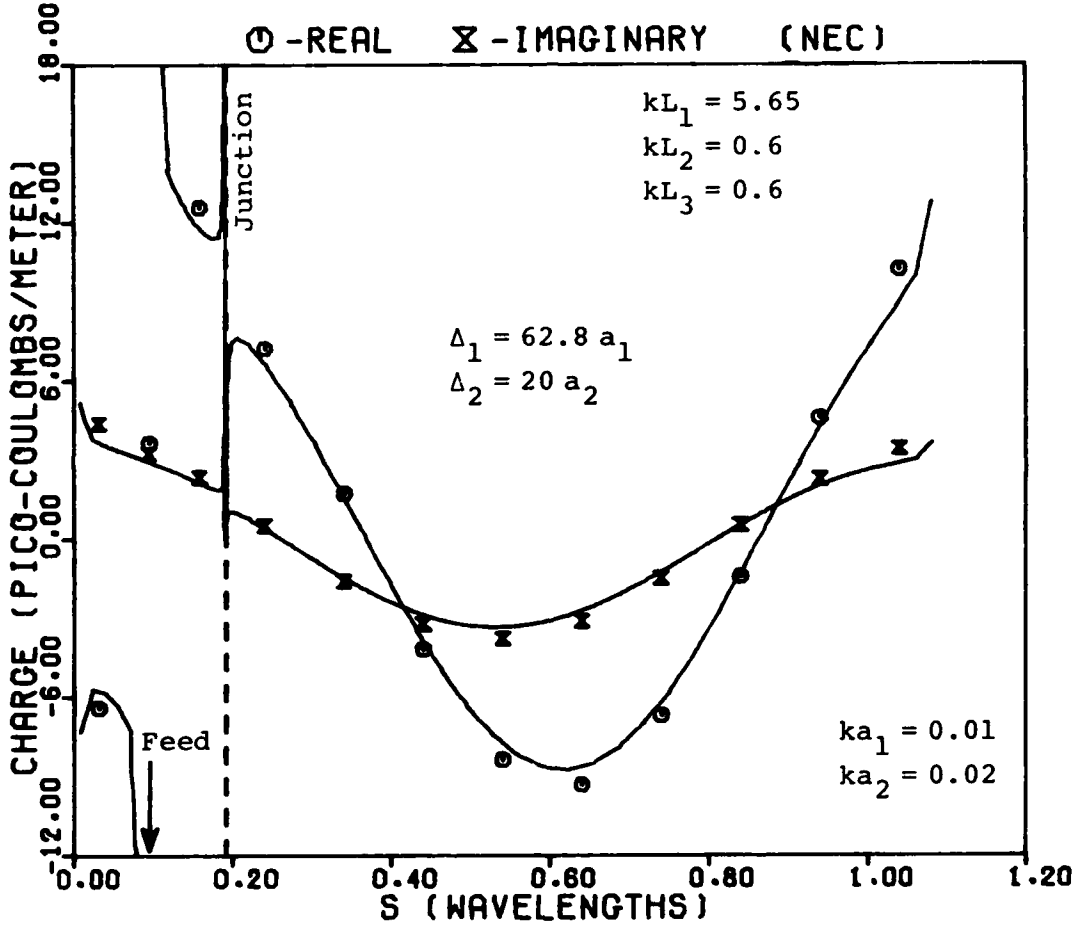

Figure 3.26. Comparison of calculated charge distribution (NEC) with baseline code results for a stepped-radius antenna having a radius change of ratio 2 to 1 approximately one-tenth wavelength away from the feed.

of cases show that, if junctions are at least 0.1λ from wire ends or sources, the error in current distributions computed by NEC is approximately the same as when the junction is placed near a charge maximum away from ends and sources for similar radii wires. Cases in which the wire with the smaller radius is fed very near the radius change are of considerable practical interest and are considered in more detail later.

Because of the large number of parameters on which accuracy depends, the data presented here is not easily summarized. Nevertheless, we attempt to reduce the data to a more compact form from which we derive a "rule of thumb" for ratios of radii which NEC can handle. To do this we consider only current distributions and compare the calculations of NEC and the baseline code PECØ. As an error criterion, we choose the maximum magnitude of the difference in current distributions calculated using NEC and PECØ, excluding the junction and feed regions. Figs. 3.27 through 3.29 depict the maximum error in the current as a function of the radius change ratio a_2/a_1, where a_1 is fixed for each figure. Separate curves are plotted for various subdomain sizes used to model the wire with NEC. The subdomain sizes indicated in the figures represent the width of the smaller of the two subdomains on each side of the junction. Excluding curves for the junction near the feed, all curves were obtained for an antenna with lengths $kL_1 = 3.05$, $kL_2 = 3.2$,

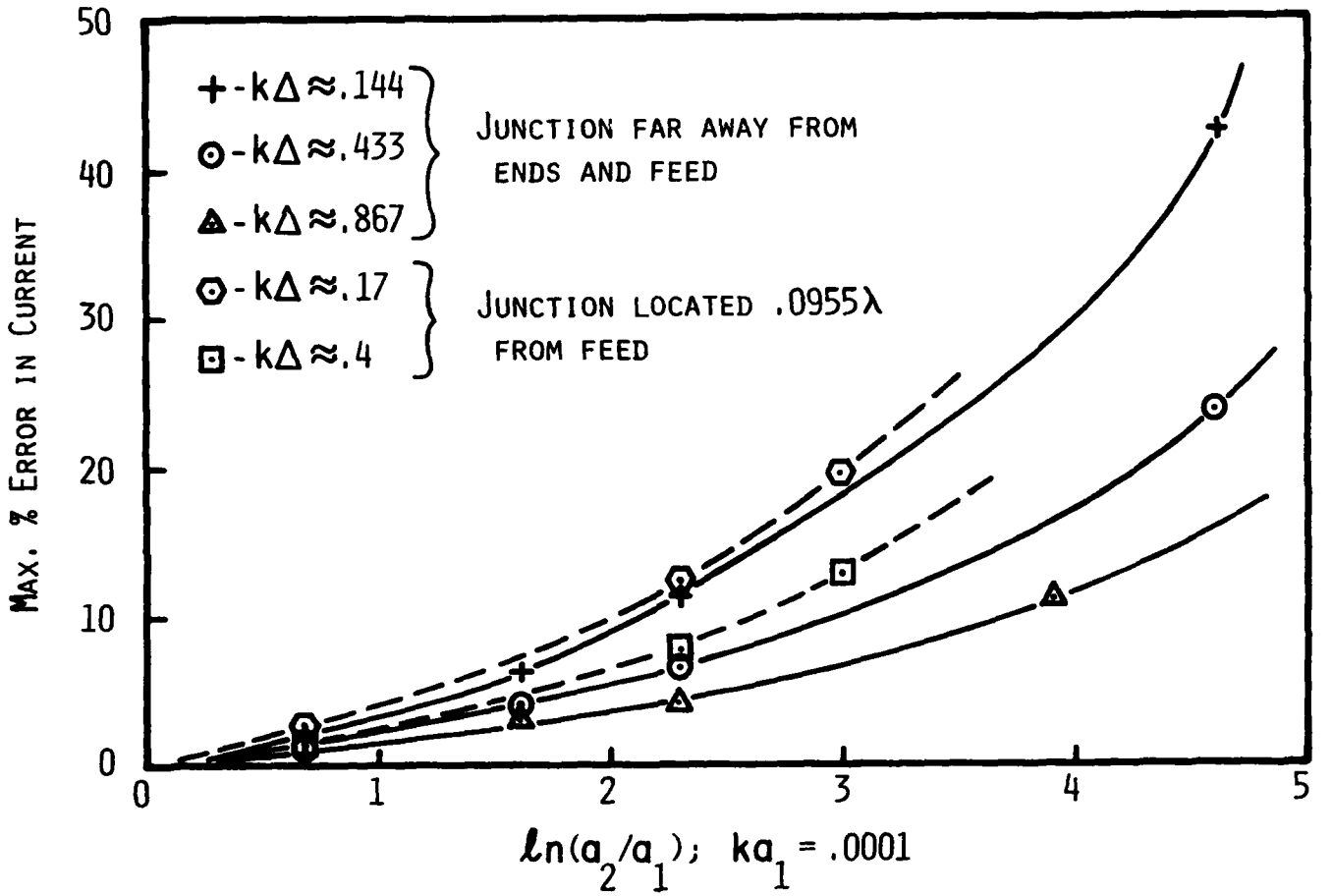

Figure 3.27. Maximum error in the current computed by NEC for a stepped-radius antenna plotted as a function of radius change ratio and subdomain size for a reference wire with radius $ka_1 = 0.0001$.

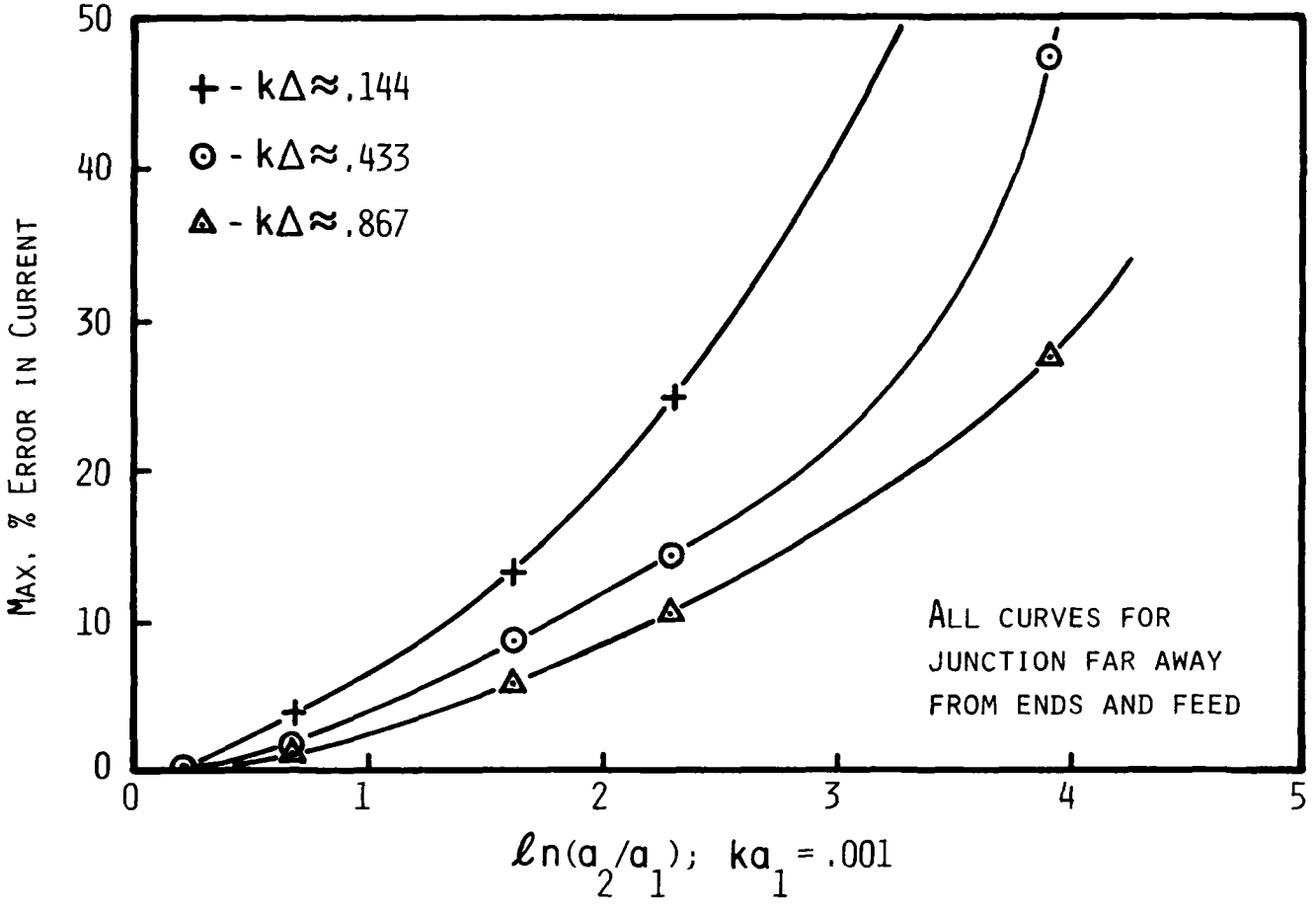

Figure 3.28. Maximum error in the current computed by NEC for a stepped-radius antenna plotted as a function of radius change ratio and subdomain size for a reference wire with radius $ka_1 = 0.001$.

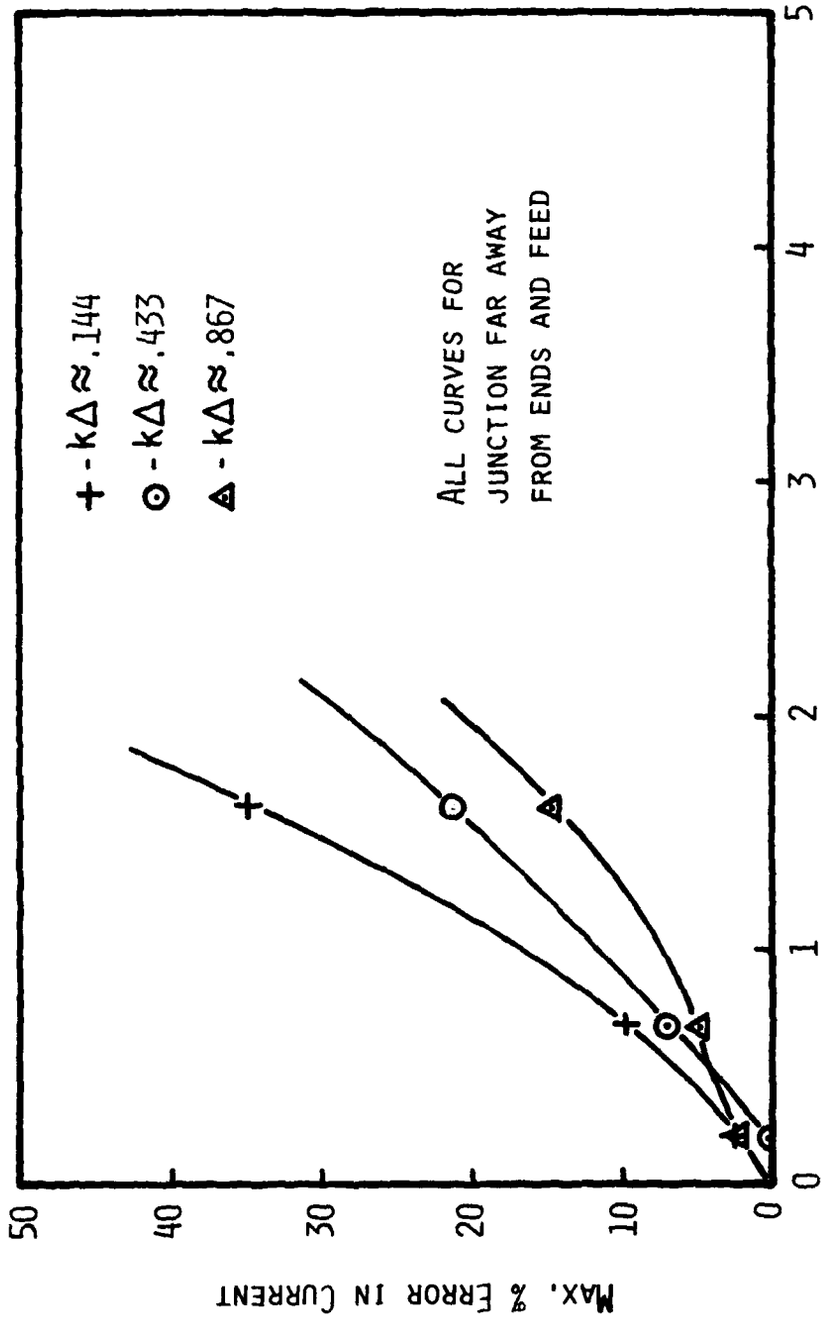

Figure 3.29. Maximum error in the current computed by NEC for a stepped-radius antenna plotted as a function of radius change ratio and subdomain size for a reference wire with radius $ka_1 = 0.01$.

and $kL_3 = 0.6$, since this results in a change maximum near the junction (which generally makes the error worse). While these figures should not be viewed as representing absolute error for all possible wire configurations, they should constitute a rough upper bound to the error. Furthermore, general trends and orders of magnitude can be deduced from the figures with some confidence.

As the figures show, the percentage of error (compared to the baseline code) in current distributions calculated with NEC appears to depend on three major factors: the dimensions in terms of wavelengths of the wire radii, the ratio of the radius change, and the distance from the junction to the nearest match point (i.e., $\Delta/2$). The distance of the junction from feed points and wire ends also appears to be a factor but of less significance. We note that in general the error decreases as the subdomain size increases, or equivalently, as the distance from the junction to the nearest match point increases, assuming, of course, that the subdomain widths remain small enough so that the current outside the junction region can be adequately modeled. Our results indicate that subdomain widths on the order of 0.14λ ($k\Delta \approx 0.867$) are generally adequate. (Note, however, that the curves corresponding to this subdomain width in Figs. 3.27 through 3.29 are more difficult to generate because interpolation of the data is required and thus the curves obtained may not be as accuarate as those obtained using smaller subdomains. Also note that

reference [11] recommends the use of subdomains of approximately 0.1λ width or less.) From the information in these figures one may obtain a general idea of the parameter ranges for which the NEC code yields acceptable results. If a specific subdomain size is chosen, say $k\Delta \simeq 0.867$, the data in Figs. 3.27-3.29 may be reduced to a more readily usable form such as Fig. 3.30. From this figure one can quickly estimate acceptable limits on the wire radii for a fixed maximum allowable error in the current. If, for example, the maximum error is specified as 10%, then for wires with the smaller radii $ka_1 = 0.01$, 0.001, and 0.0001, acceptable limits on the wires of larger radii are $ka_2 = 0.035$, 0.0089, and 0.0038, respectively. Again, we emphasize that the information summarized in this figure represents only rough upper bounds on the error of currents calculated by NEC. For many wire configurations and excitations the error in the current may possibly be larger, but is generally expected to be less significant.

One may derive a rough "rule of thumb" formula for acceptable ratios of radii (i.e., error less than 5%) by requiring that all combinations of radii fall below the straight line drawn in Figure 3.30. Thus, if the closest match point is about 0.14λ from the junction, radii ratios which satisfy the condition

$$\ell n \frac{a_2}{a_1} \leq -\frac{5}{14}[\ell n(ka_1) + 3] \qquad (3.2)$$

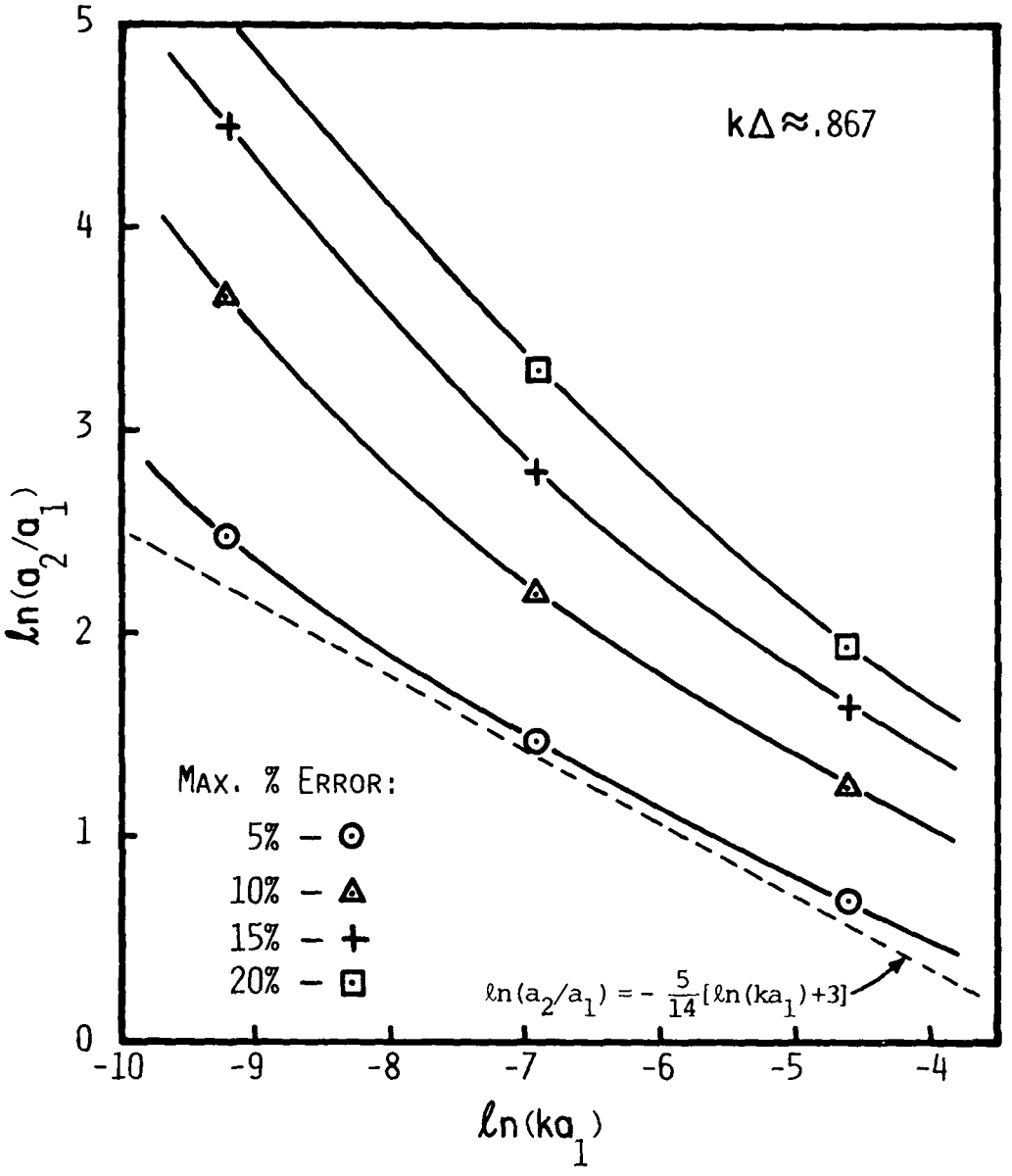

Figure 3.30. Level curves for the maximum error in the current distribution computed by NEC for various radius change ratios when subdomain size is specified to be $k\Delta \approx 0.867$.

with $a_2 \geq a_1$ can be expected to yield reasonably accurate current distributions. It is clear from the figure, that for very thin wires ($\ell n \frac{1}{ka_1} > 10$), the above estimate is probably too conservative. The equation also appears to be too conservative for thicker wires ($\ell n \frac{1}{ka_1} < 3$), but failure of the thin-wire assumptions more than likely precludes the use of NEC in this range for most applications.

The results obtained to this point apply to antennas only. We next consider very briefly two stepped-radius scatterers. Both structures are approximately one wavelength long and have a step change in radius midway between the two ends. Fig. 3.31 illustrates the current distribution excited by a normally incident plane wave when $ka_1 = 0.001$ and $ka_2 = 0.005$. For the same structure, Fig. 3.32 shows the current distribution excited by a plane wave which is incident at an angle of 45° with respect to the positive ℓ axis (see Fig. 2.1). The phase reference in each of the figures is located at $s = 0$. Results obtained with the NEC code used a subdomain width of $k\Delta \simeq 0.53$. From Fig. 3.28, we expect, for subdomains of this width and a radius change ratio of 5 to 1, a maximum error in the current calculated by NEC of about 8% or less. This is approximately the maximum error present in Figs. 3.31 and 3.32. Figs 3.33 and 3.34 show the current distributions excited by plane waves with normal and 45° incidence, respectively, for a structure with radii $ka_1 = 0.001$ and $ka_2 = 0.05$. Again, from Fig. 3.28 for a radius

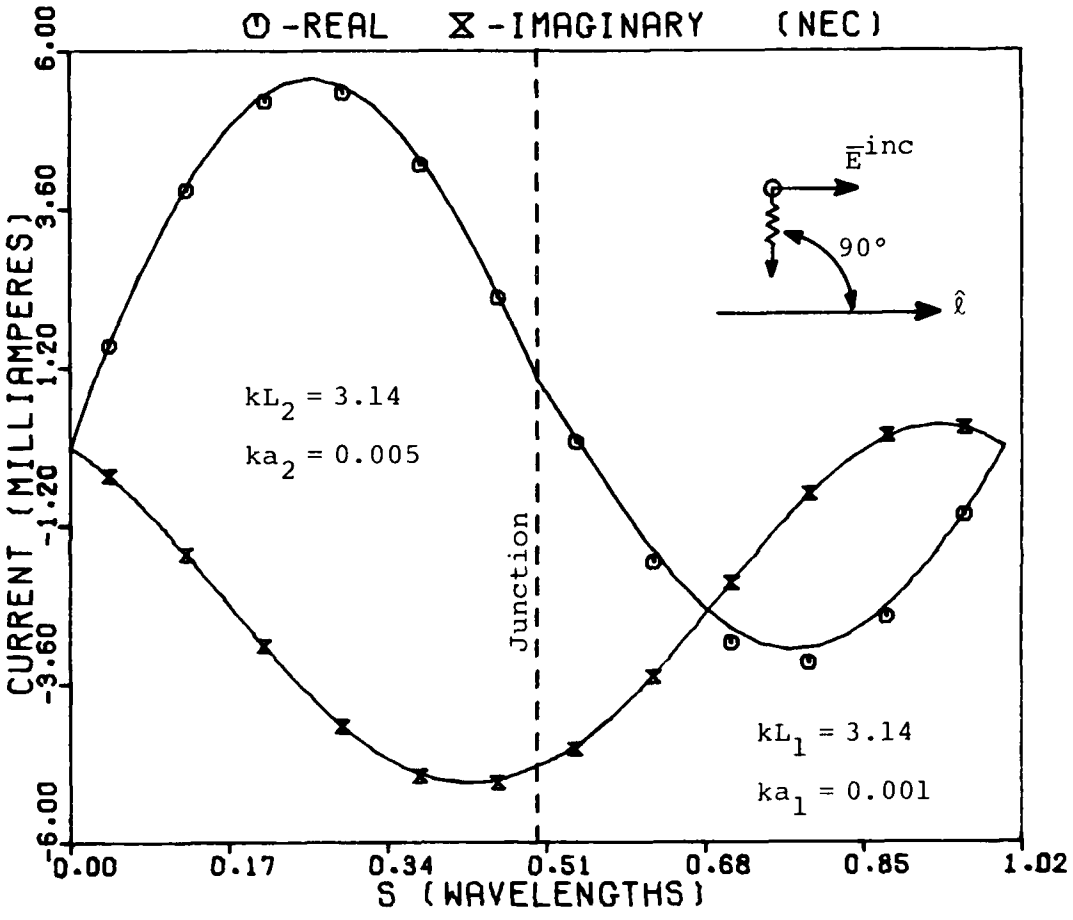

Figure 3.31. Comparison of calculated current distribution (NEC) with baseline code results for a stepped-radius scatterer excited by a normally incident plane wave and having a radius change of ratio 5 to 1.

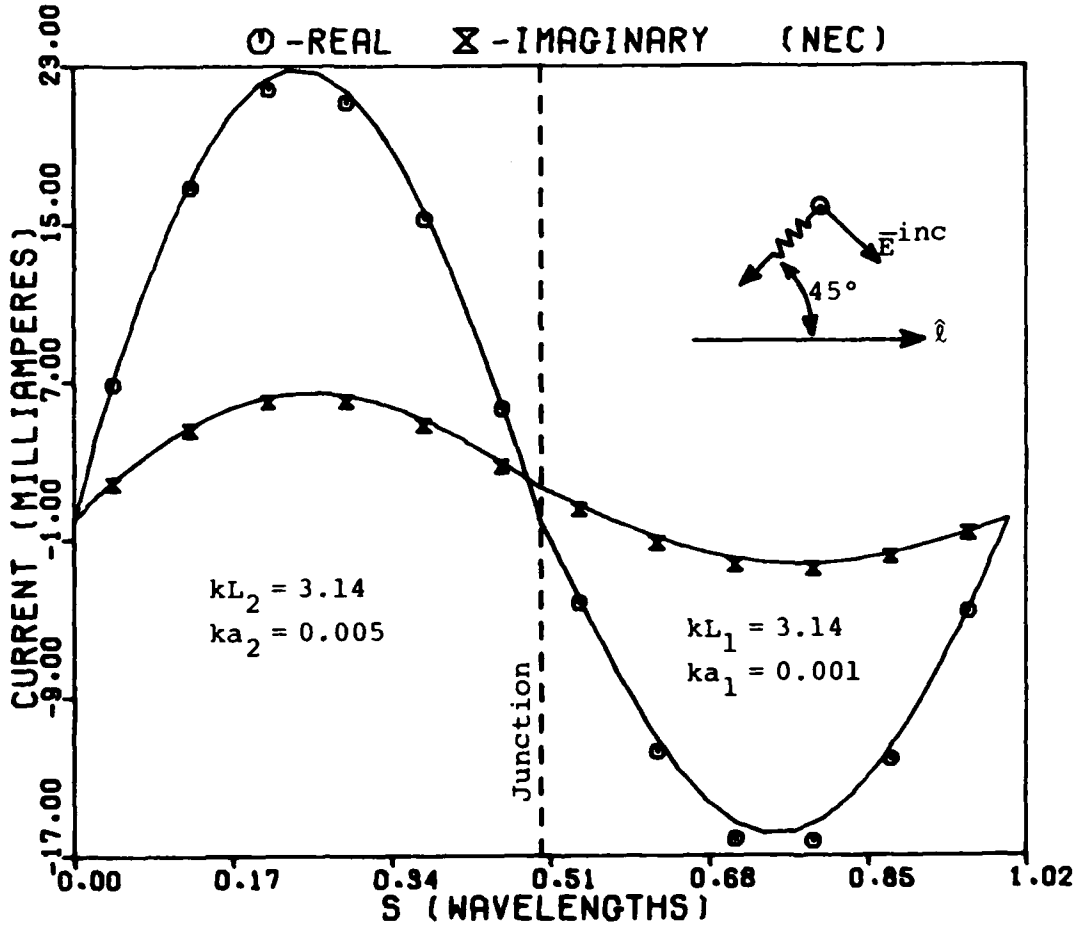

Figure 3.32. Comparison of calculated current distribution (NEC) with baseline code results for a stepped-radius scatterer excited by an obliquely incident plane wave and having a radius change of ratio 5 to 1.

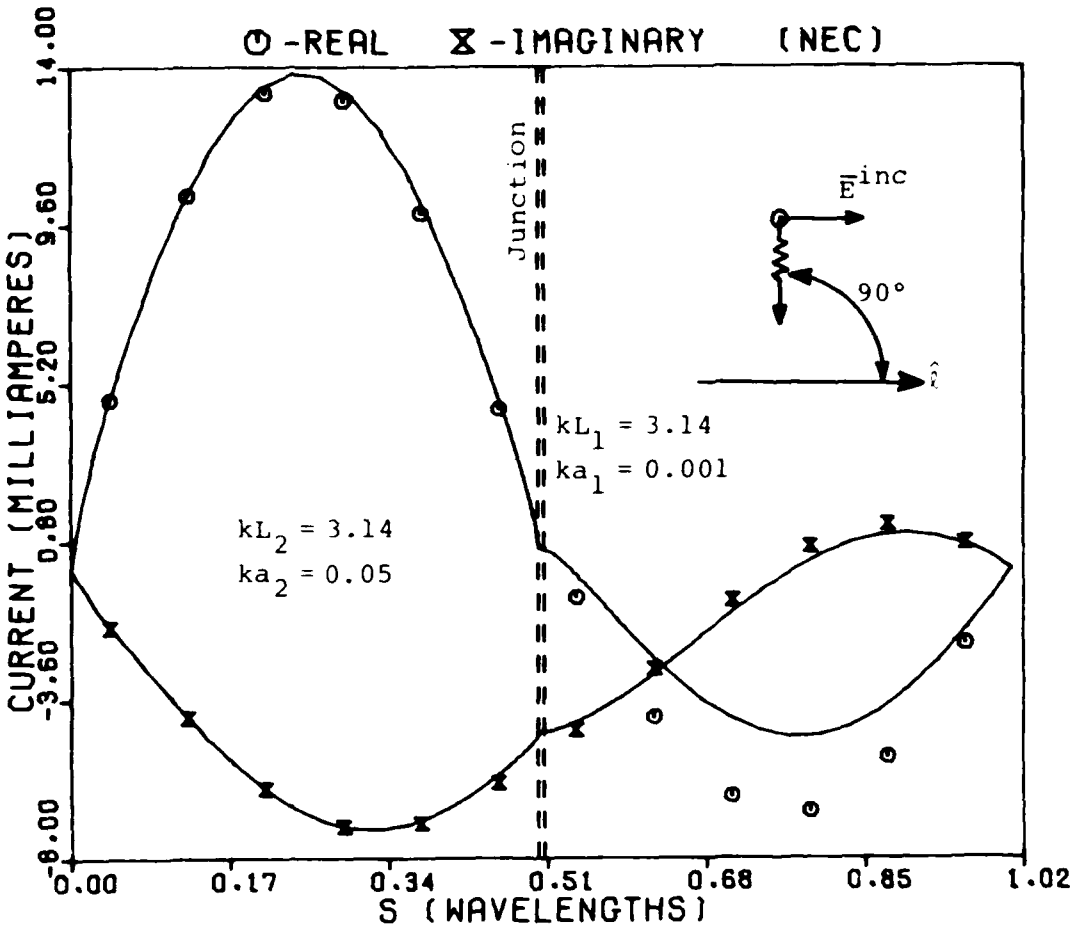

Figure 3.33. Comparison of calculated current distribution (NEC) with baseline code results for a stepped-radius scatterer excited by a normally incident plane wave and having a radius change ratio of 50 to 1.

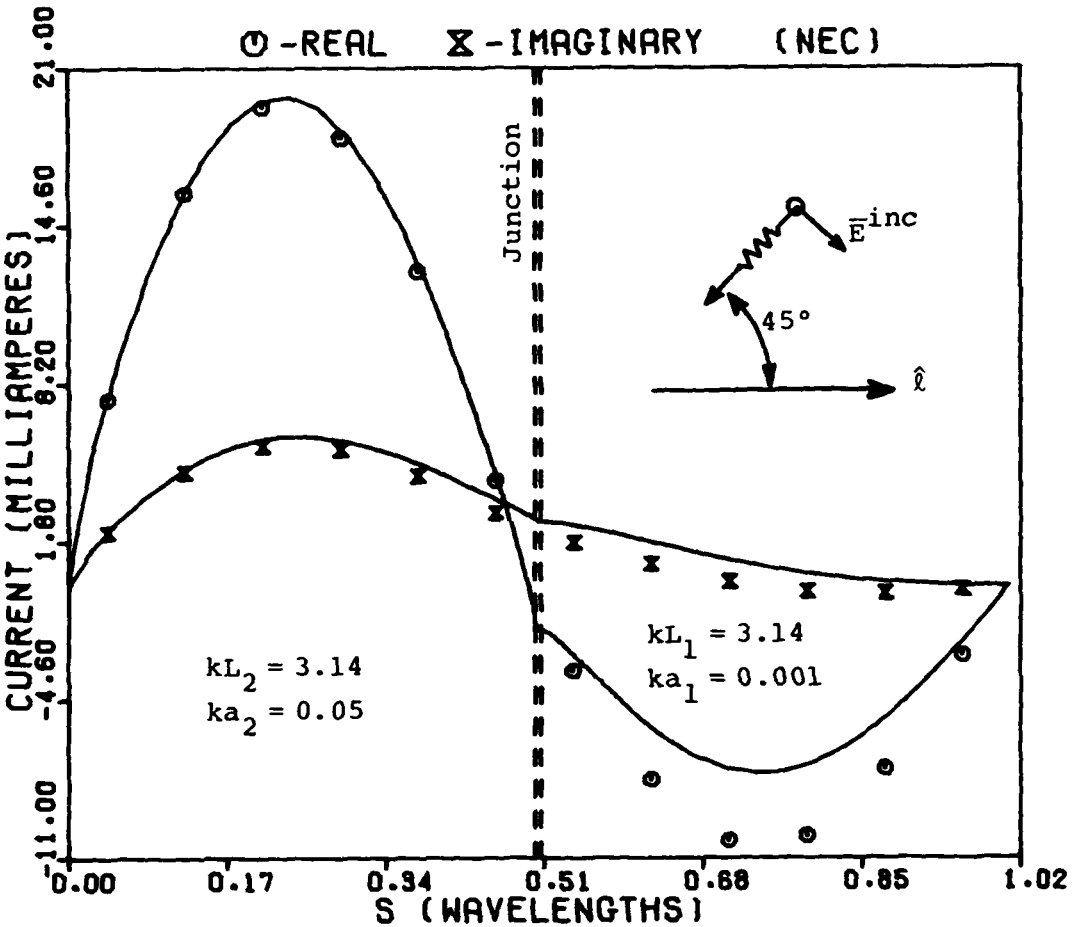

Figure 3.34. Comparison of calculated current distribution (NEC) with baseline code results for a stepped-radius scatterer excited by an obliquely incident plane wave and having a radius change of ratio 50 to 1.

change ratio of 50 to 1, we expect to find a maximum error in the current of about 45%. This predicted error corresponds well with the actual error in the currents computed by NEC in Figs. 3.33 and 3.34. In general, currents calculated with NEC for scattering structures appear to exhibit the same types and orders of error as for driven structures. This should be expected, since excitation of a scatterer can be thought of as an antenna problem with a distributed source. Furthermore, derivation of the charge jump condition does not depend on the source, except that point sources located directly at the junction are excluded.

We next study an antenna driven either in the annular junction region (see Fig. 2.1) or on the wire of smaller radius at a point very near the junction. Such a configuration approximately models, for example, a whip antenna driven against a kingpost. The baseline code PECØ is capable of treating stepped-radius structures which are driven anywhere along their length, including within the annulus region. The NEC code, on the other hand, is not presently capable of treating structures which are fed precisely at a step change in radius--because it assumes that delta gap sources are located at the center of subdomains, while all changes in radius occur at subdomain boundaries. NEC does offer an alternative point source model called the "current-slope-discontinuity voltage source" [11], which is effectively located at the boundaries between subdomains. According to [11], however, no change is radius is permitted at the point where this source model is used.

We first attempt to use NEC to simulate a stepped-radius antenna fed at the junction. For a delta gap source model, this might be accomplished by replacing the original junction with a short segment of wire of intermediate radius. Figs. 3.35 and 3.36 depict the current and charge distributions, respectively, on a 1.02λ antenna which has a step radius change in the center of the antenna and is fed in the annulus region. The wire radii are $ka_1 = 0.001$ and $ka_2 = 0.005$. NEC is used to simulate the structure by using a short segment ($k\Delta = 0.5$) of radius $ka = 0.003$ in place of the junction. We note that currents calculated with NEC are significantly in error. We attribute the error exhibited by NEC in this case partially to the differences in the two assumed models and partially due to the increased sensitivity of the current distribution to such differences because of the near half-wavelength wire elements chosen.

If the feed point is next chosen on the wire with the smaller radius and a short distance from the junction, NEC can apparently model the structure quite accurately. Figs. 3.37 and 3.38 show current and charge distributions obtained when the feed is located 0.0424λ away from the junction. The agreement with the baseline code for this case is excellent. To move the feed point closer to the junction requires a reduction in subdomain widths and hence, since the charge is then defined closer to the junction, we might expect the errors in the currents calculated by NEC to be somewhat

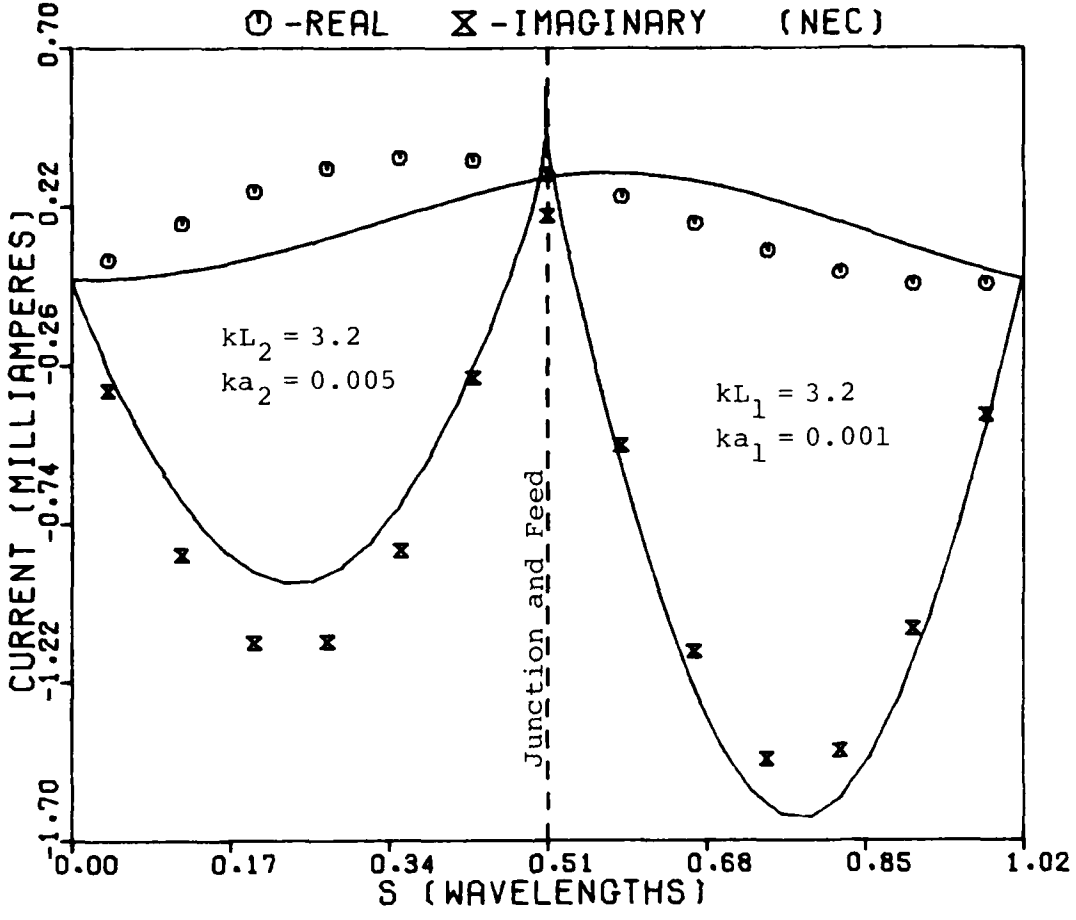

Figure 3.35. Current distribution on a stepped-radius antenna which is fed in the annulus region. For the NEC code the junction is simulated with a short wire of intermediate radius ka = 0.003.

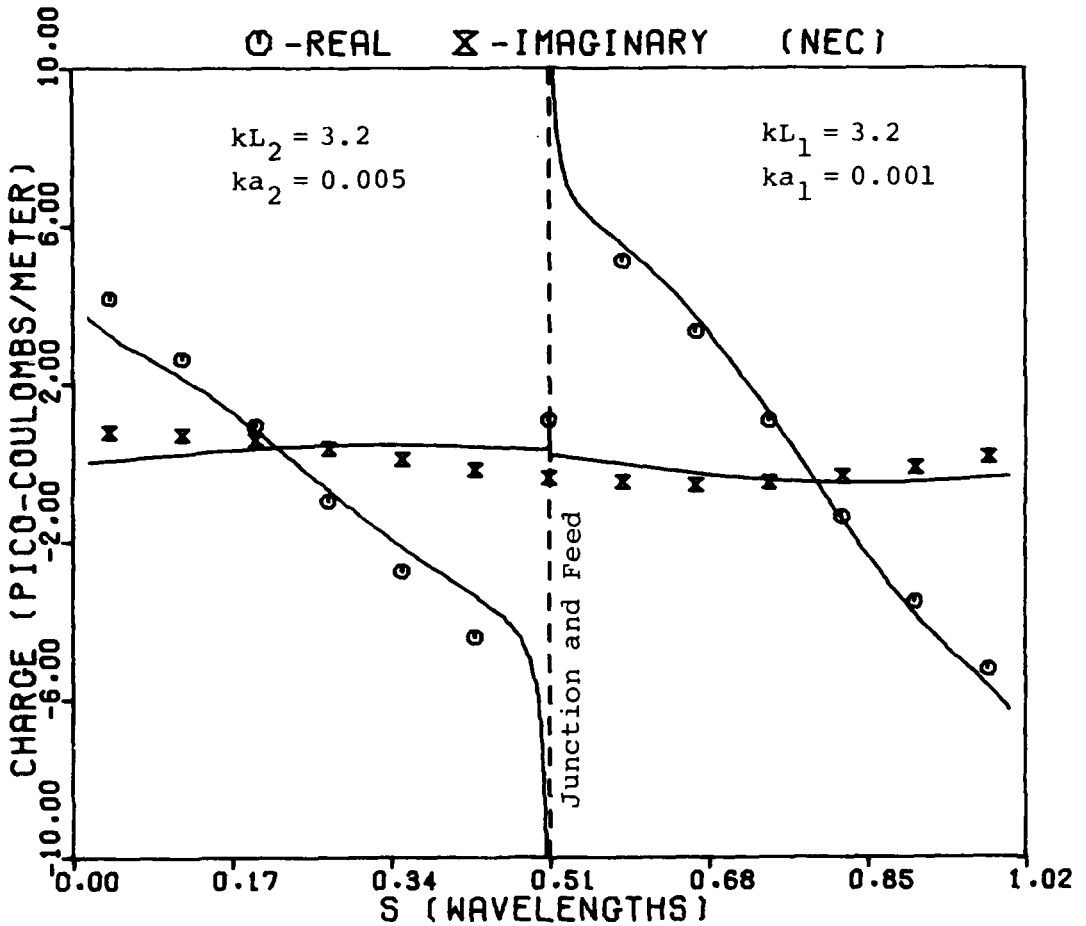

Figure 3.36. Charge distribution on a stepped radius antenna which is fed in the annulus region. For the NEC code the junction is simulated with a short wire of intermediate radius ka = 0.003.

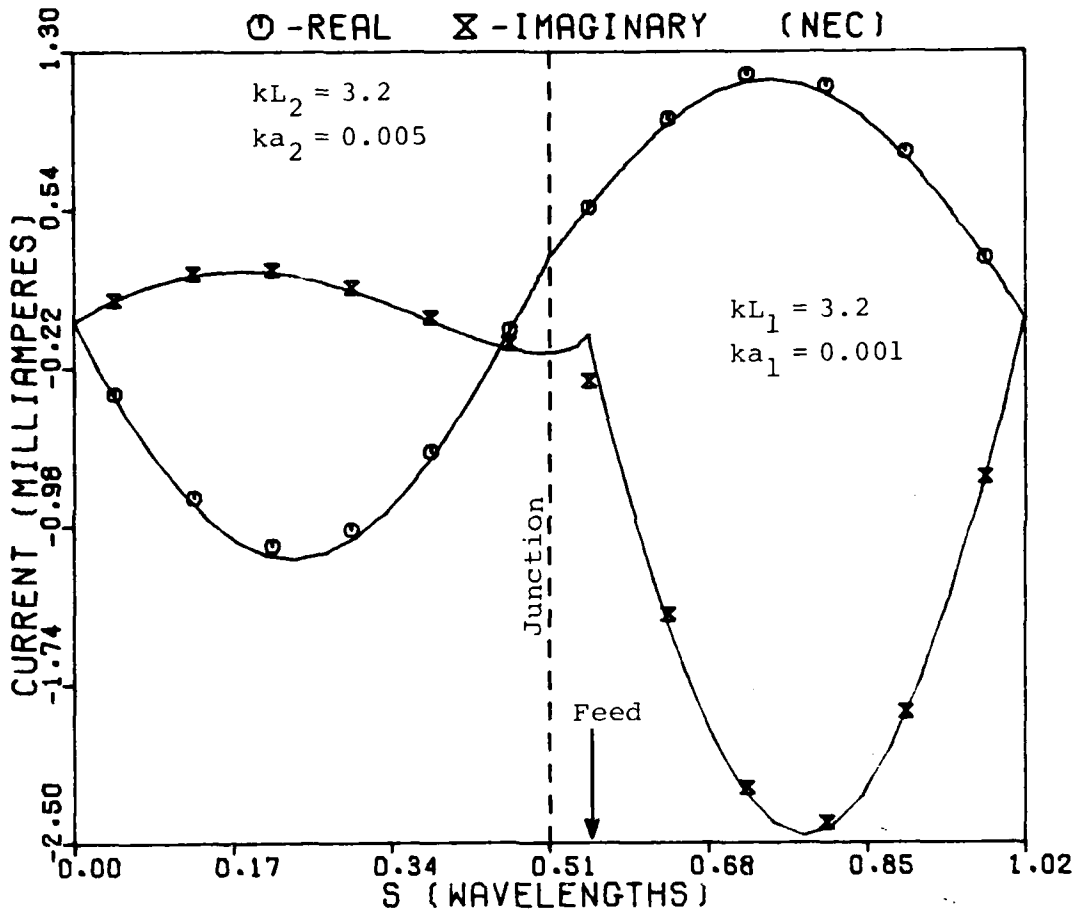

Figure 3.37. Comparison of calculated current distribution (NEC) with baseline code results for a stepped-radius antenna fed on the wire of smaller radius and near the junction.

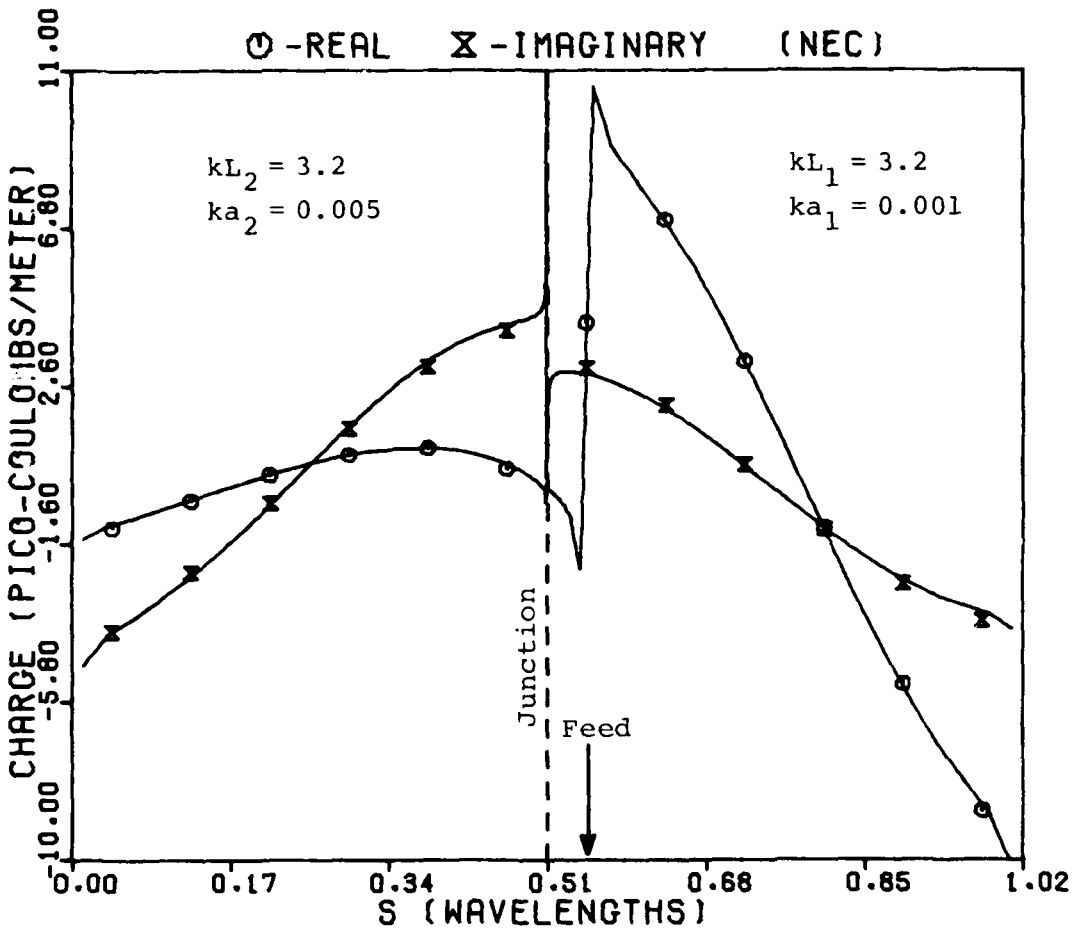

Figure 3.38. Comparison of calculated charge distribution (NEC) with baseline code results for a stepped-radius antenna fed on the wire of smaller radius and near the junction.

greater. Indeed, Figs. 3.39 and 3.40 confirm this conjecture for a feed located 0.0127λ away from the junction. Referring to Fig. 3.28 again for $k\Delta = 0.16$ and a 5 to 1 radius change ratio, we might expect a maximum error of about 14% in the current. Fig. 3.39 indicates that the currents calculated by NEC agree with the baseline code results to about 10%. A comparison of the current and charge distributions in Figs. 3.37 through 3.40 with Fig. 3.35 and 3.36 also reveals that as the feed point moves closer to the junction, the distributions approach those obtained with the baseline code for the case where the feed is placed directly in the annulus region.

Before concluding this section we note one further interesting fact regarding NEC's capability to model a source in the junction. We refer again to the case in which the source is placed in the annulus region and note that, if a radius change were allowed across the current-slope-discontinuity voltage source in NEC, this case could be modeled by NEC. If we merely ignore the warning in [11] to keep the radii on each side of the current-slope-discontinuity source model the same, the current and charge distributions of Figs. 3.41 to 3.44 are obtained. While some magnitude errors are apparent in the current distributions as calculated by NEC, the errors are within those predicted in Fig. 3.28 for junctions of the radii used in the figures. It appears, therefore, that the potential exists in NEC, possibly with

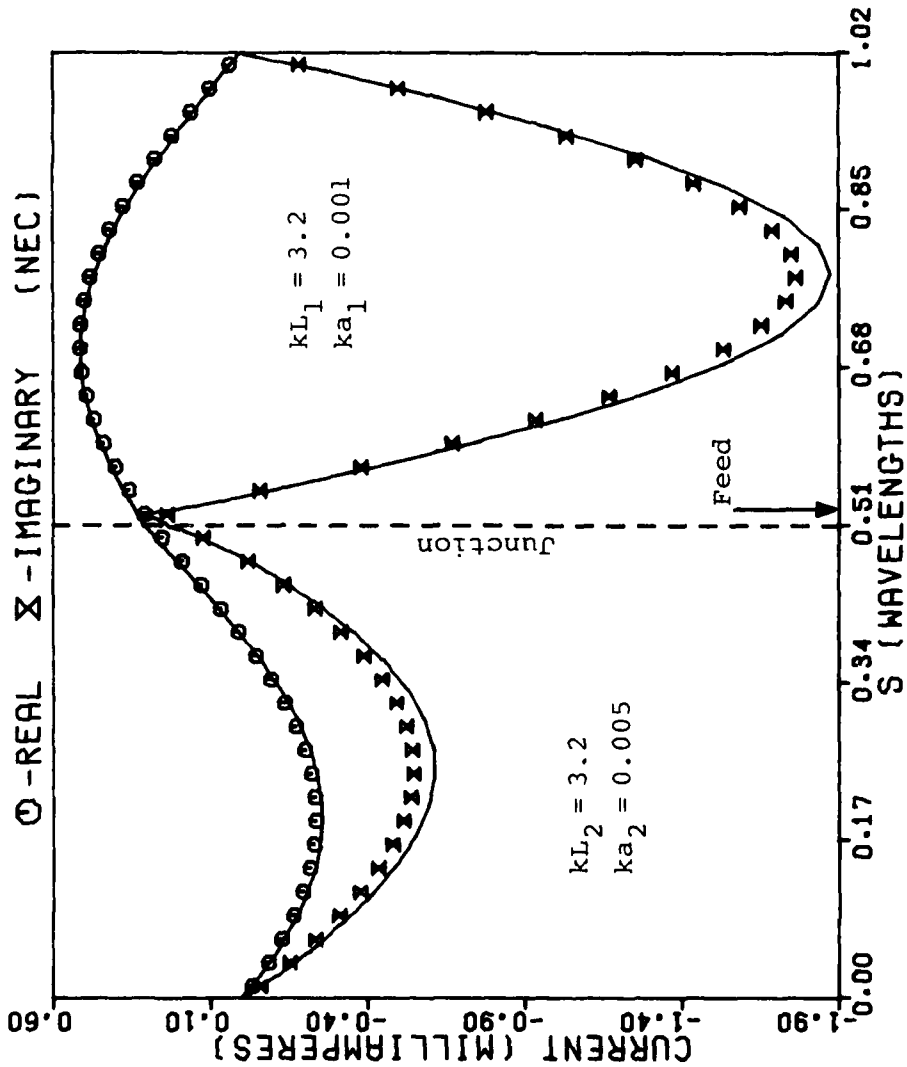

Figure 3.39. Comparison of calculated current distribution (NEC) with baseline code results for a stepped-radius antenna which is fed very near the junction region on the wire of smaller radius.

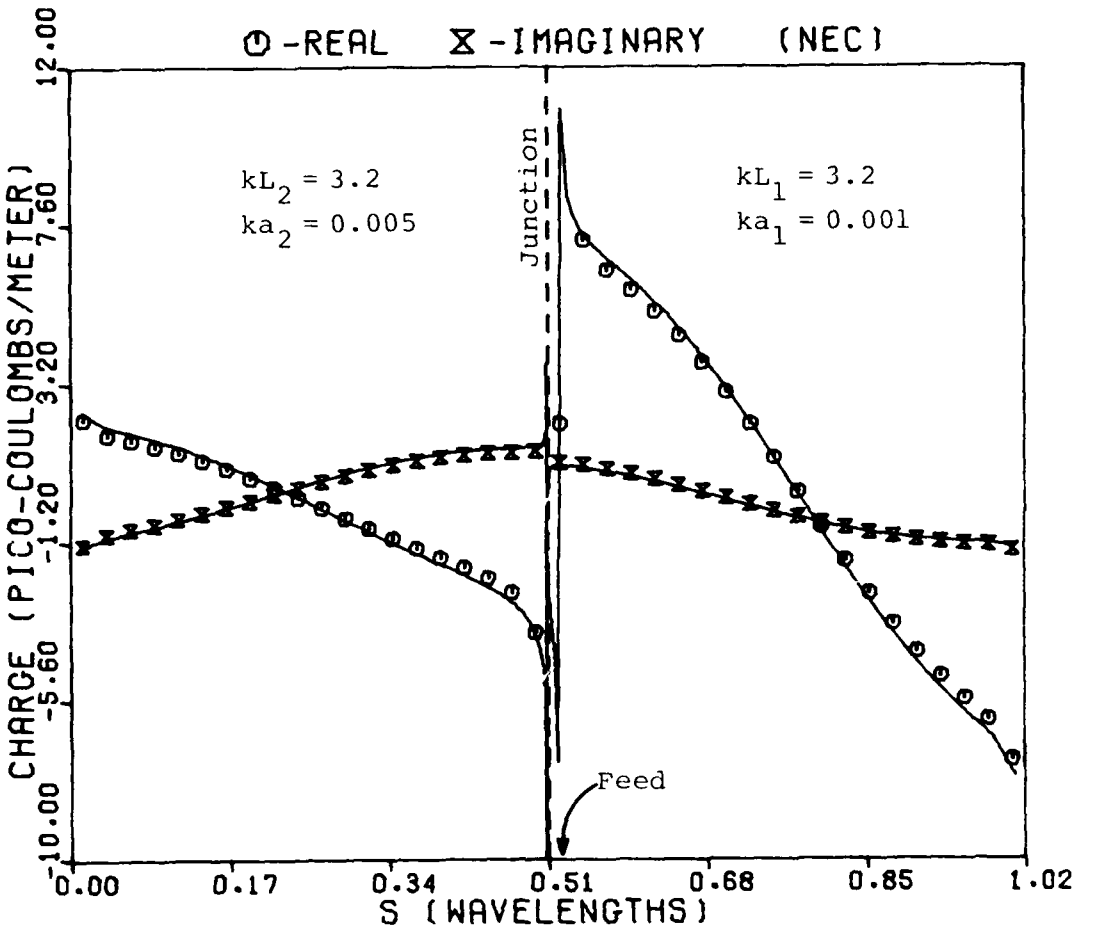

Figure 3.40. Comparison of calculated charge distribution (NEC) with baseline code results for a stepped-radius antenna which is fed very near the junction region on the wire of smaller radius.

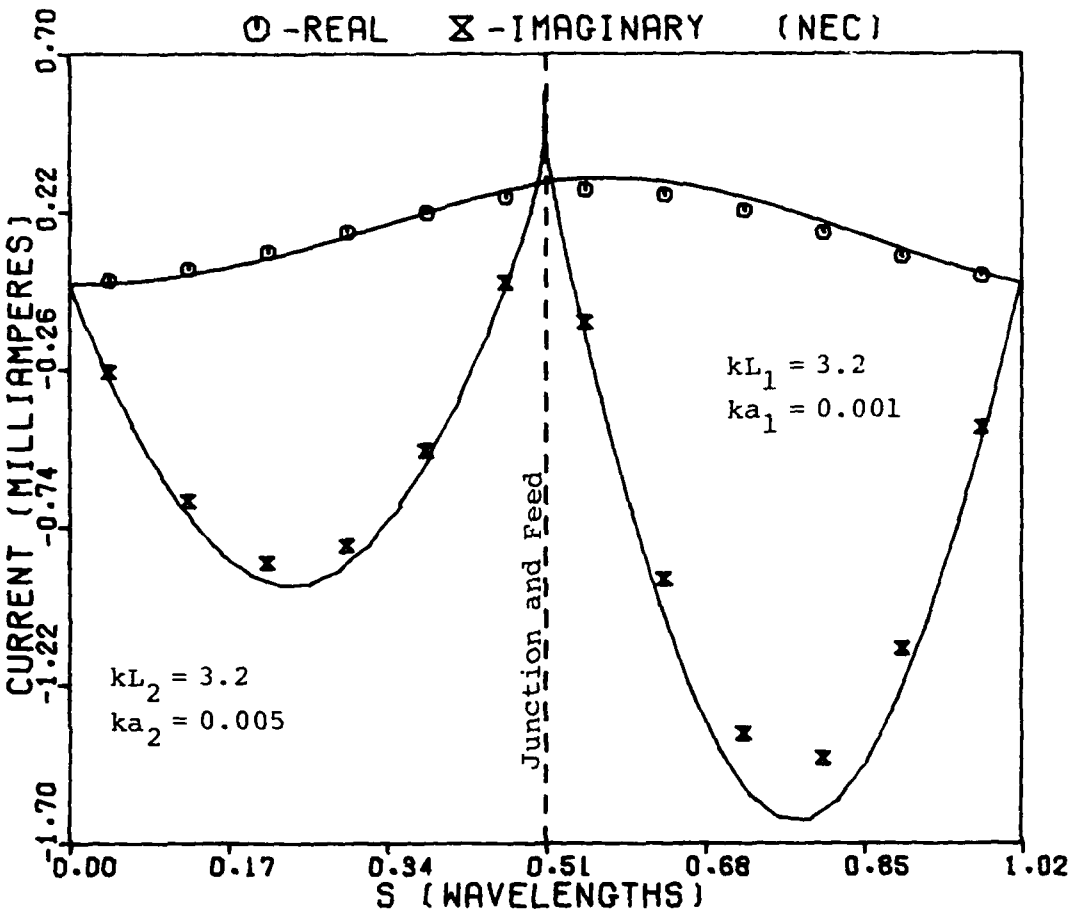

Figure 3.41. Comparison of calculated current distribution (NEC) with baseline code results for a stepped-radius antenna fed in the annulus region. The current-slope-discontinuity voltage source has been used (improperly) to obtain the results with NEC.

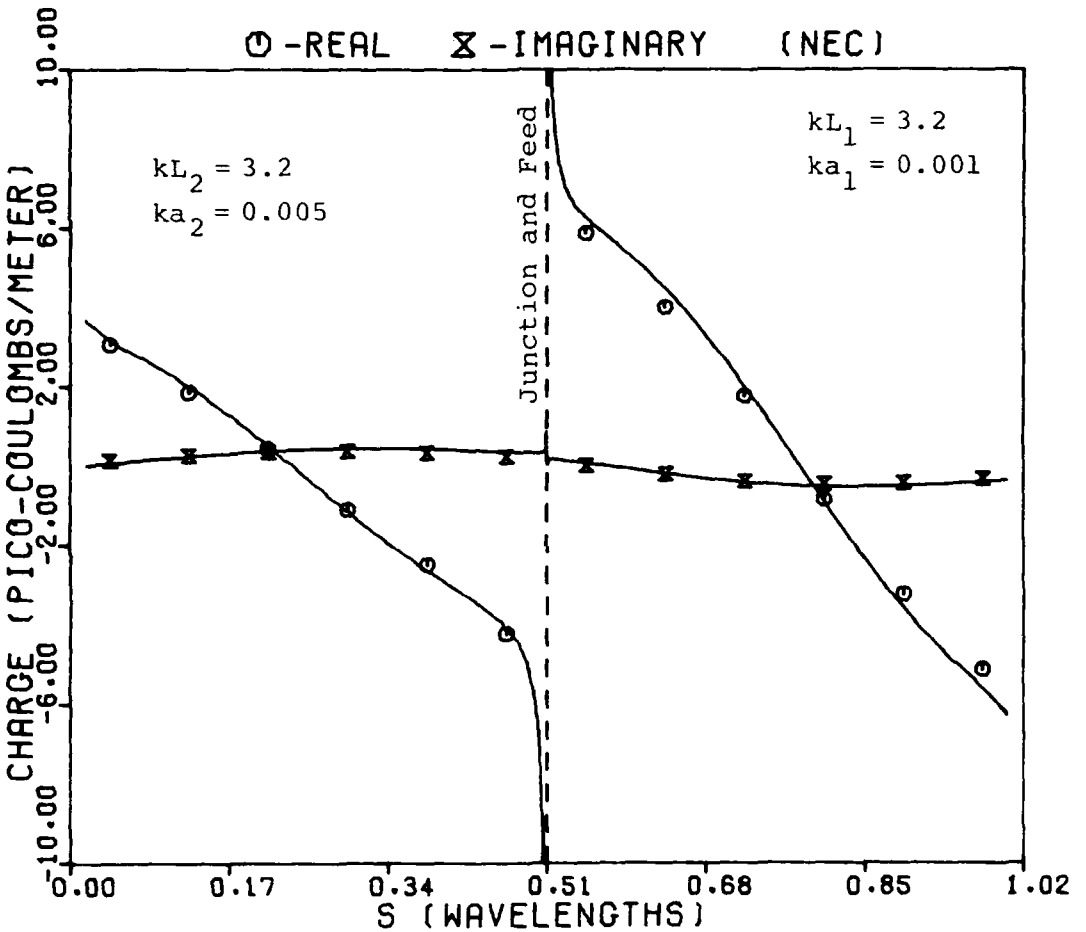

Figure 3.42. Comparison of calculated charge distribution (NEC) with baseline code results for a stepped-radius antenna fed in the annulus region. The current-slope-discontinuity voltage source has been used (improperly) to obtain the results with NEC.

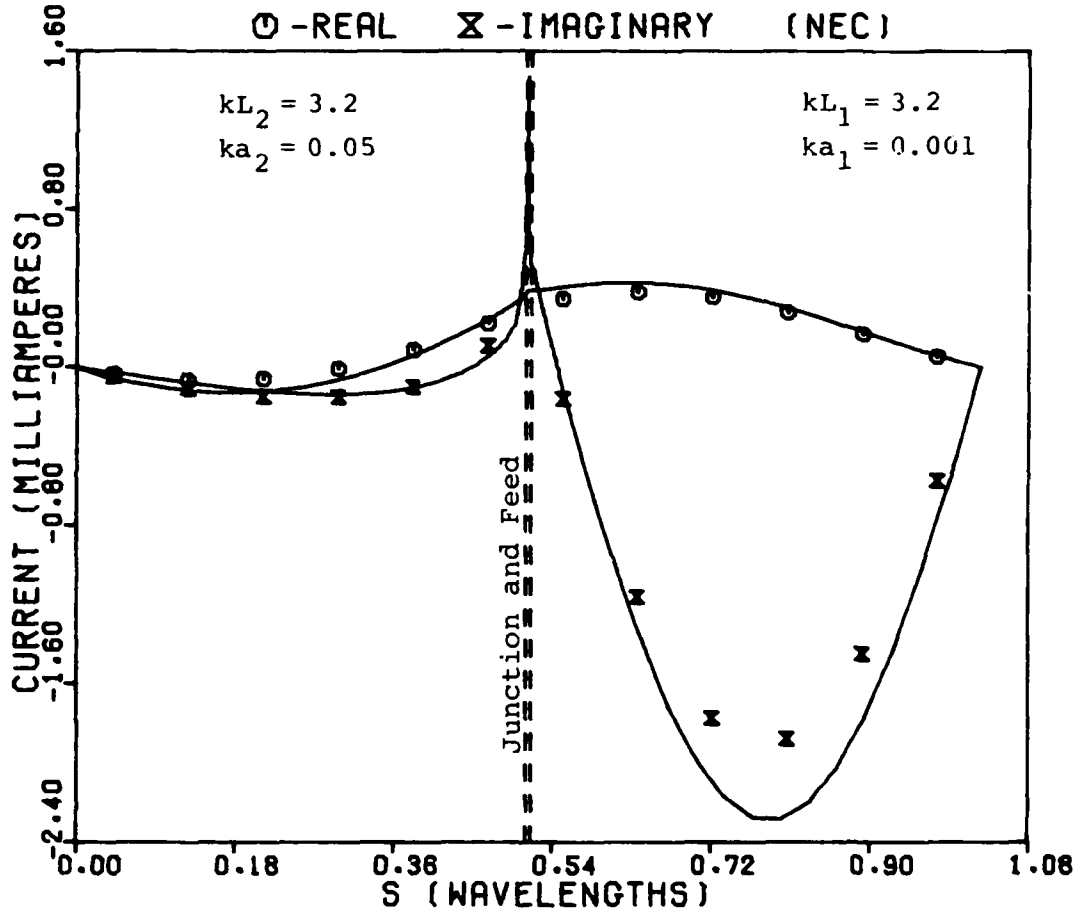

Figure 3.43. Comparison of calculated current distribution (NEC) with baseline code results for a stepped-radius antenna fed in the annulus region. The current-slope-discontinuity voltage source has been used (improperly) to obtain the results with NEC.

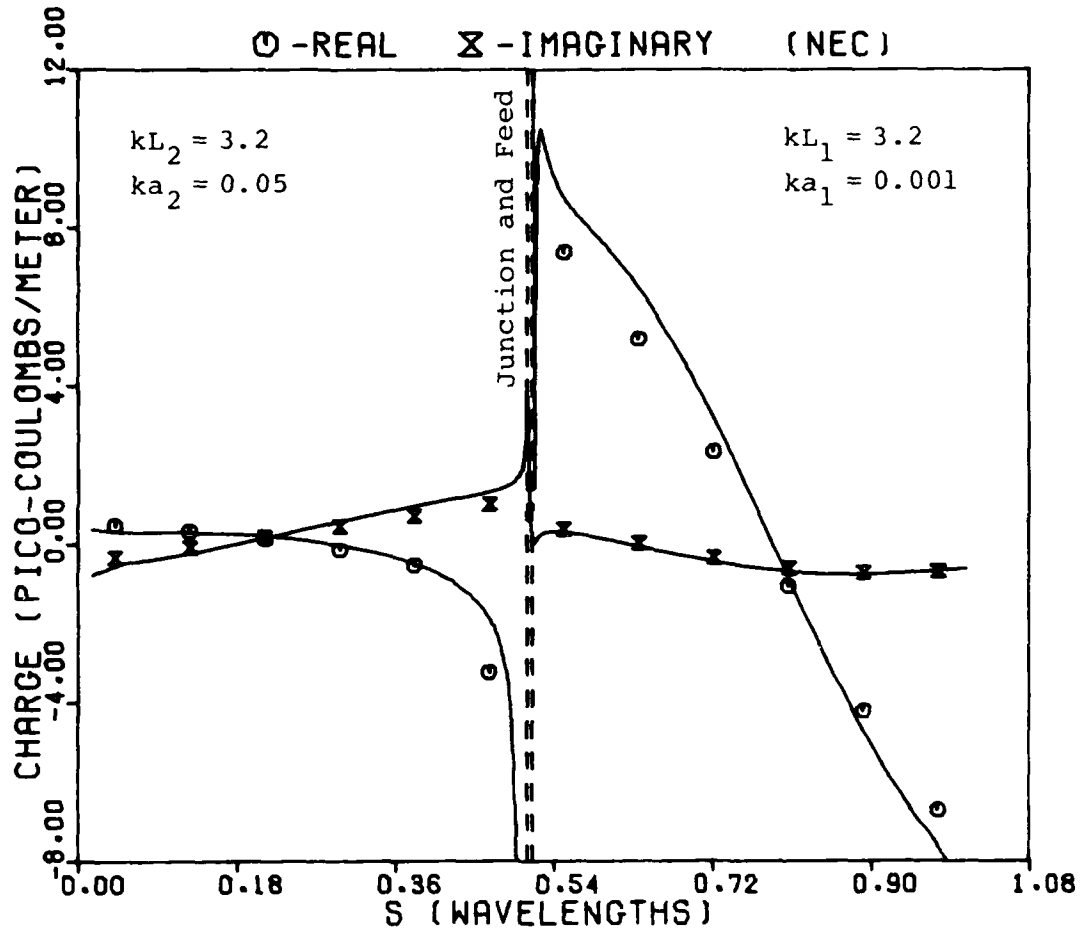

Figure 3.44. Comparison of calculated charge distribution (NEC) with baseline code results for a stepped-radius antenna fed in the annulus region. The current-slope-discontinuity voltage source has been used (improperly) to obtain the results with NEC.

some modification and/or justification of the present treatment of the current-slope-discontinuity voltage source, to accurately model structures which are fed at junctions. Alternatively, it may be possible to modify the Wu-King condition so as to incorporate a voltage source located at the junction. In the Appendix, it is argued that the Wu-King junction condition can be interpreted as a condition on continuity of scalar potential across the junction. If a voltage source is present at the junction, the condition should be modified so that the scalar potential is discontinuous by the voltage V of the source at the junction. Thus from Eqs. (A.3)and (A.4) of the Appendix we obtain

$$2\pi\varepsilon V = q_2 \left[\ell n\left(\frac{2}{ka_2}\right) - \gamma\right] - q_1 \left[\ell n\left(\frac{2}{ka_1}\right) - \gamma\right], \qquad (3.3)$$

where the positive reference potential of the source is taken to be on the wire of radius a_2. By the continuity equation, the corresponding current slopes at the junction are

$$\frac{dI_1}{ds} = -j\omega q_1 \quad ,$$

$$\frac{dI_2}{ds} = -j\omega q_2 \quad ,$$

from which a current-slope-discontinuity voltage source is obtained satisfying

$$V = \frac{j\eta}{2\pi k}\left\{\frac{dI_2}{ds}\left[\ell n\left(\frac{2}{ka_2}\right) - \gamma\right] - \frac{dI_1}{ds}\left[\ell n\left(\frac{2}{ka_1}\right) - \gamma\right]\right\}, \quad (3.4)$$

It is interesting to compare (3.4) with the present current-slope-discontinuity voltage source used in NEC when the radii on each side of the junction are the same, i.e., $a_1 = a_2 = a$. In NEC, this source condition is equivalent to

$$V = \frac{j\eta}{2\pi k}\left[\ell n\left(\frac{2d}{a}\right) - 1\right]\left\{\frac{dI_2}{ds} - \frac{dI_1}{ds}\right\}, \quad (3.5)$$

where d is the half-length of the subdomains between which the source is located, whereas (3.4) reduces to

$$V = \frac{j\eta}{2\pi k}\left[\ell n\left(\frac{2}{ka}\right) - \gamma\right]\left\{\frac{dI_2}{ds} - \frac{dI_1}{ds}\right\}. \quad (3.6)$$

It is seen that only when we choose

$$kd = e^{1-\gamma} \simeq 1.526 \quad (3.7)$$

do the above two equations agree. It is claimed in [11], however, that good results are obtained with Eq. (3.5) reqardless of the value of d. On the other hand, (3.5) does not show the logarithmic dependence on frequency evident in (3.6) which comes from (3.3) and has already been shown to

be correct in the form of Eq. (2.12). We have not managed to resolve these inconsistencies during this study--indeed, we have derived still other expressions differing from both (3.5) and (3.6) only in the form of the logarithmic terms. This should not be too surprising, however, since it is well known that in making approximations in linear antenna theory, constants associated with the terms involving logarithms of the radius cannot be uniquely fixed. We leave unresolved at this time the problem of combining the two current-slope-discontinuity conditions--one for the stepped-radius, and one for sources--into a single comprehensive condition. However, we suggest that this may be a fruitful area for further research.

SECTION IV

CONCLUSIONS AND RECOMMENDATIONS

In this report we have considered methods for treating junctions of collinear wires with dissimilar radii. A numerical technique has been presented for accurately computing current and charge distributions on a stepped-radius antenna. The method, in fact, yields the current and charge distributions in the annular junction region, permitting one to study their behavior there in detail. The technique employs a body of revolution model for the stepped-radius wire and hence treats only junctions of collinear wires. An ancillary result of this study has been the development and validation of a thin-wire theory approach which can also be used to accurately calculate current and charge distributions away from the junction region. The thin-wire approach retains the advantages of the thin-wire approximations, permits the use of the very simple pulse basis set, and does not require any condition to be enforced on the charge at the junction. Furthermore, since it has been demonstrated that no condition is required on the charge at junctions it is conjectured that the thin-wire approach is capable of accurately treating junctions of non-collinear wires of dissimilar radii and multiple wire junctions.

The Numerical Electromagnetics Code (NEC) uses basis functions which require a condition on the charge at segment boundaries. For segments of the same radii, this condition is merely that the charge be continuous from one segment to the next. When adjacent segments have different radii, however, this condition is no longer valid. To test the validity of various proposed charge "jump conditions" at a radius discontinuity both the body of revolution and the thin-wire codes have been used to calculate values of the extrapolated charge on both sides of a radius step, from which a numerical charge jump condition can be calculated. All our numerical results have verified that the analytical charge jump condition of Wu and King [7] is indeed satisfied at junctions of collinear wires. At the present time, no accurate model exists, nor does one appear feasible to develop, to verify the Wu-King condition for non-collinear or multi-wire junctions of unequal radii. However, we conjecture that the condition is also correct for these configurations. We further suggest that the thin-wire approach could be extended to these configurations and should yield charge distributions satisfying the Wu-King condition. This is because the thin-wire approach requires (approximately) continuity of scalar potential at wire junctions and this condition is also (approximately) enforced by the Wu-King condition. The authors suggest that such a test of the thin-wire theory would be useful as a check on both the validity of the thin-wire approach and on the Wu-King

junction condition for multi-wire junctions. Although the Wu-King charge jump condition is, strictly speaking, valid only at least several radii from the junction, the NEC computer code [11] explicitly enforces the condition at all wire junctions. The accuracy of the code has been studied for various locations of the step with respect to feed points and free wire ends and with respect to its location at charge minima or maxima. The results obtained by comparing the current and charge distributions calculated with NEC to those computed with the body of revolution code generally indicate satisfactory performance of NEC provided certain limitations are observed. Three primary factors have been found to influence the accuracy of results obtained with NEC: the radius of the smaller wire in terms of wavelengths, the ratio of the change in radius, and the distance from the junction to the nearest match point. Information has been presented in Section III which should enable users to determine appropriate limitations to impose on subdomain sizes and radius change ratios. Furthermore, an empirical formula is given which relates the maximum allowable radius change to the value of the smaller radius in terms of wavelengths whenever the subdomain size is restricted to about $1/7\lambda$. It may be desirable to incorporate this condition into the NEC manual and/or to have NEC print warning messages to the user whenever the condition is not met.

It is recommended that some consideration be given to attempting to combine the Wu-King type junction condition with a slope-discontinuity source condition. Both conditions on the charge discontinuity arise from considering the difference in potential between adjacent segments. Some of the cases considered in this study indicate that combining the two conditions might permit NEC to handle a source placed directly at a stepped-radius junction.

APPENDIX

In this appendix we derive the Wu-King jump condition [7] for the charge near a stepped-radius junction. The derivation given here, while less rigorous than that given in [7], is simple and yet convincing. It is shown that for thin wires the condition is equivalent to requiring that the potential be continuous across the junction.

Consider the stepped-radius antenna, Fig. 2.1, where it is assumed that the wire radii a_1 and a_2 are both electrically small (i.e., ka_1, $ka_2 << 1$). Now consider the evaluation of the scalar potential at a point Δ_1 units from the junction on the axis of the wire of radius a_1. Only the circumferentially uniform component of the charge contributes to the potential on the axis, so that ignoring the small amount of charge on the annulus region connecting the two wires of different radii at the junction, we have

$$\Phi_1 = \frac{1}{4\pi\varepsilon}\left[\int_0^{L_2+L_3} q(s')\,\frac{e^{-jkR_2}}{R_2}\,ds' + \int_{L_2+L_3}^{L_1+L_2+L_3} q(s')\,\frac{e^{-jkR_1}}{R_1}\,ds'\right], \qquad (A.1)$$

where

$$R_1^2 = (s_1 - s')^2 + a_1^2 \quad ,$$

$$R_2^2 = (s_1 - s')^2 + a_2^2 \quad ,$$

and where $s_1 = L_2 + L_3 + \Delta_1$, and Φ_1 is the scalar potential evaluated at s_1. We assume that Δ_1 is chosen such that

$$\max (ka_1, ka_2) << k\Delta_1 << 1. \qquad (A.2)$$

Thus, while our observation point is located several radii from the junction, it is still near the junction electrically. Such a point can always be found provided the wire radii are sufficiently small. Obviously, most of the contribution to the integrals in (A.1) comes from the neighborhood of the point $s' = s_1$ if a_1 is small. This permits three approximations: (1) Since $q(s')$ is relatively slowly varying in the neighborhood of $s' = s_1$, we approximate it as a constant (recall that we are sufficiently far removed from the junction to be out of the region where edge effects dominate); thus $q(s) \simeq q(s_1) = q_1$. (2) For a_2 sufficiently small, the first integral in (A.1) can be neglected compared to the second. (3) Finally, since most of the contribution to the second integral comes from the neighborhood of $s' = s_1$, the limits of integration are unimportant and may be extended to

infinity in both directions. While these approximations are somewhat gross, a more rigorous analysis leads to the same result as that below at considerable expense in simplicity. With the above approximations, (A.1) becomes

$$\Phi_1 \simeq \frac{q_1}{4\pi\epsilon} \int_{-\infty}^{\infty} \frac{e^{-jkR_1}}{R_1} \, ds'$$

$$= \frac{q_1}{4j\epsilon} H_0^{(2)}(ka_1)$$

$$\simeq \frac{-q_1}{2\pi\epsilon} \left(\ell n \frac{ka_1}{2} + \gamma\right)$$

$$= \frac{q_1}{2\pi\epsilon} \left(\ell n \frac{2}{ka_1} - \gamma\right) , \qquad (A.3)$$

where $\gamma \cong 0.5772$ is Euler's constant and the small agument approximation of the Hankel function, $H_0^{(2)}(x) \simeq -\frac{2j}{\pi}(\ell n\frac{x}{2} + \gamma)$, has been used.

Now evaluate the potential at a point $s = s_2$ a distance Δ_2 from the junction on the wire of radius a_2. Assume Δ_2 also satisfies (A.2). Then by similar reasoning as before, the potential $\Phi(s_2) = \Phi_2$ is approximately

$$\Phi_2 \simeq \frac{q_2}{2\pi\epsilon} \left(\ell n \frac{2}{ka_2} - \gamma\right) . \qquad (A.4)$$

Since the potential is a smoothly varying quantity and since both observation points are at small (electrical) distances from the junction, the potentials in (A.3) and (A.4) are

approximately equal. Equating them yields the Wu-King condition [7],

$$q_1 \left(\ell n \frac{2}{ka_1} - \gamma\right) = q_2 \left(\ell n \frac{2}{ka_2} - \gamma\right). \qquad (A.5)$$

Thus we see that the Wu-King condition may be interpreted as arising from the continuity of scalar potential at the junction. We hasten to point out, however, that the latter condition is always true, even when the wires become thick so that the Wu-King condition no longer holds. Furthermore, the Wu-King condition merely relates the behavior of the charge near the junction, (recall Eq. (A.2)) but ignores the detailed behavior of the charge in the junction region itself.

If is also interesting to note that the Wu-King condition is also easily derivable from the discussion of Schelkunoff and Friis [18], who determine the current on either side of stepped-radius junction. They also determine the behavior of the current at the junction by enforcing continuity of current and scalar potential there.

ACKNOWLEDGMENT

The authors wish to express their gratitude to Professor Chalmers M. Butler for his helpful suggestions and moral support during the course of this work.

REFERENCES

[1] A. J. Poggio and E. K. Miller, "Integral Equation Solutions of Three-Dimensional Scattering Problems," in Computer Techniques for Electromagnetics, R. Mittra, Ed., Oxford: Pergamon, 1973, Chapter 4.

[2] E. K. Miller, R. M. Bevensee, A. J. Poggio, L. Adams, F. J. Deadrick and J. A. Landt, "An Evaluation of Computer Programs Using Integral Equations for the Electromagnetic Analysis of Thin Wire Structures," AFWL EMP Interaction Note 177, p. 104, March 1974.

[3] F. M. Tesche, "Numerical Considerations for the Calculation of Currents Induced on Intersecting Wires Using the Pocklington Integro-Differential Equation," AFWL EMP Interaction Note 150, p. 27, January 1974.

[4] C. D. Taylor, "Electromagnetic Scattering from Arbitrary Configurations of Wires," IEEE Trans. Antennas Propagation, vol. AP-17, no. 5, pp. 662-663, September 1969.

[5] C. M. Butler, "Currents Induced in a Pair of Skew-Crossed Wires," IEEE Trans. Antennas Propagation, vol. AP-20, no. 6, pp. 731-736, November 1972.

[6] R. W. P. King and T. T. Wu, "Analysis of Crossed Wires in a Plane-Wave Field," AFWL Interaction Note 216, July 1974.

[7] T. T. Wu and R. W. P. King, "The Tapered Antenna and Its Application to the Junction Problem for Thin Wires," IEEE Trans. Antennas Propagation, vol. AP-24, no. 1, pp. 42-45, January 1976.

[8] C. M. Butler, B. M. Duff, R. W. P. King, E. K. Yung, and S. Singarayar, "Theoretical and Experimental Investigations of Thin-Wire Structures: Junction Conditions, Currents, and Charges," AFWL Interaction Note 238, February 1975.

[9] W. L. Curtis, "Charge Distribution on a Dipole with a Stepped Change in Radius," 1976 AP-S International Symposium Digest, Amherst, Massachusetts, pp. 189-192, October 1976.

[10] B. M. Duff, "Charge Condition at the Junction of Unequal Radii Wires," Part I of Final Report, AFOSR Grant 75-2862, University of Mississippi, University, Mississippi, February 1978.

[11] G. J. Burke and A. J. Poggio, "Numerical Electromagnetics Code (NEC) - Method of Moments," Technical Document 116, AFWL-TR-76-320, prepared for Naval Electronic Systems Command, Naval Ocean Systems Center, San Diego, California, July 1977.

[12] R. F. Harrington, Field Computation by Moment Methods. New York: Macmillan, 1968.

[13] A. W. Glisson, "On the Development of Numerical Techniques for Treating Arbitrarily-Shaped Surfaces," Ph.D. dissertation, University of Mississippi, University, Mississippi, June 1978.

[14] A. W. Glisson and D. R. Wilton, "Simple and Efficient Numerical Techniques for Treating Bodies of Revolution," Technical Report for RADC Post-Doctoral Program, GIT Contract No. GIT7-E-21655, University of Mississippi, University, Mississippi, November 1978.

[15] D. S. Jones, The Theory of Electromagnetism. New York: Pergamon, 1964, pp. 567-568.

[16] B. M. Duff, private communication.

[17] C. D. Taylor and D. R. Wilton, "The Extended Boundary Condition Solution of the Dipole Antenna of Revolution," IEEE Trans. Antennas Propagation, vol. AP-20, no. 6, pp. 772-776, November 1972.

[18] S. A. Schelkunoff and H. T. Friis, Antennas: Theory and Practice. New York: Wiley, 1952, Chapter 8.

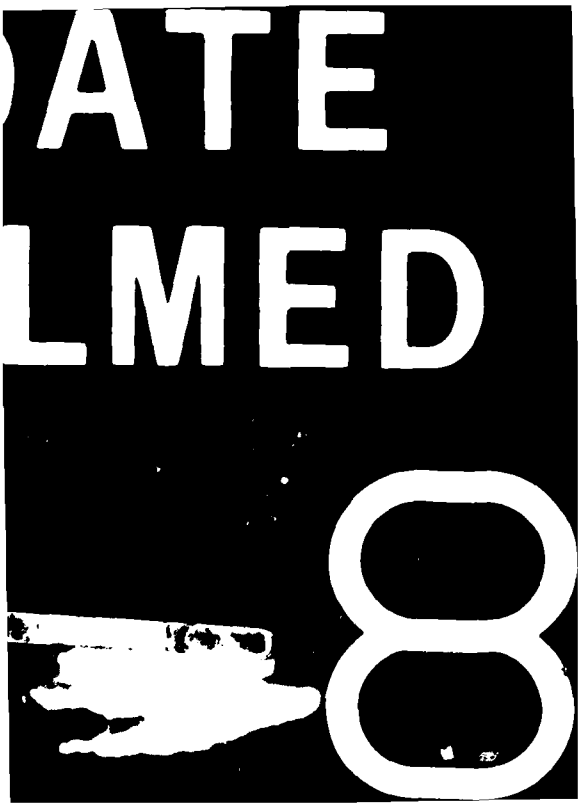
ATE
LMED
8